TALLINNA TEHNIKAÜLIKOOL
TALLINN UNIVERSITY OF TECHNOLOGY

Department of Materials and Environmental Technology

FIELD MEASUREMENTS AND SIMULATIONS OF HYGROTHERMAL PERFORMANCE OF CROSS LAMINATED TIMBER EXTERNAL WALLS

RISTKIHTLIIMPUIDUST VÄLISSEINTE VÄLIMÕÕTMISED JA HÜGROTERMILISE JÕUDLUSE MODELLEERIMINE

MASTER THESIS

Student:	Laura Cukkere
Student code:	KVEM177311
Supervisor:	Villu Kukk, Early Stage Researcher
Co-supervisor:	Prof. Jaan Kers, Head of Laboratory of Wood Technology

Tallinn, 2019

AUTHOR'S DECLARATION

Hereby I declare, that I have written this thesis independently.
No academic degree has been applied for based on this material. All works, major viewpoints and data of the other authors used in this thesis have been referenced.

"....." 2019

Author: .....
/signature /

Thesis is in accordance with terms and requirements

"....." 2019

Supervisor: .....
/signature/

Co-supervisor: .....
/signature/

Accepted for defence

"....."..... 2019 .

Chairman of theses defence commission: .....
/name and signature/

Department of Materials and Environmental Technology

THESIS TASK

Student: Laura Cukkere KVEM177311

Study programme: KVEM 12/15 Technology of Wood, Plastic and Textiles

Main speciality: Wood technology

Supervisor(s): Early Stage Researcher Villu Kukk, Tel: 6202402, villu.kukk@taltech.ee

Co-supervisor: Professor Jaan Kers, Tel: 6202910, jaan.kers@taltech.ee

Thesis topic:

(in English) Field measurements and simulations of hygrothermal performance of cross laminated timber external walls

(in Estonian) Ristkihtliimpuidust välisseinte välimõõtmised ja hügrotermilise jõudluse modelleerimine

Thesis main objectives:

1) To evaluate the impact of built-in moisture, insulation type and location of the building envelope to the hygrothemral performance of CLT wall assemblies in cold climate conditions with warm summers and snowy winters.
2) To create validated simulation models for further investigation to evaluate the risk of mould growth in CLT wall assemblies.

Thesis tasks and time schedule:

No	Task description	Deadline
1.	Literature review and introduction	25.02.2019
2.	Description of method	11.03.2019
3.	Creation of simulation models, validation	22.04.2019
4.	Description and discussion of results	06.05.2019
5.	Complete work	27.05.2019

Language: English **Deadline for submission of thesis:** "....."....."....."2019

Student: Laura Cukkere ..... "....."....."....."2019

/signature/

Supervisor: Villu Kukk	…….	“…….”.....2019
	/signature/	
Co-supervisor: Jaan Kers	…….	“…….”.....2019
	/signature/	

Terms of thesis closed defence and/or restricted access conditions to be formulated on the reverse side

CONTENTS

PREFACE 8
List of abbreviations and symbols 9
1 INTRODUCTION 10
1.1 CLT as a product 10
1.1.1 Composition 10
1.1.2 Raw material 11
1.1.3 Manufacturing and technologies 11
1.2 Hygrothermal properties 15
1.2.1 Thermal conductivity 15
1.2.2 Moisture transmission 16
1.2.3 Air permeability 19
1.3 Fields of application 19
1.3.1 Buildings 20
1.3.2 Minimum requirements and design for NZEB 21
1.4 Problem statement and objectives 23
2 Method 25
2.1 Field measurements 25
2.1.1 Specimens 25
2.1.2 Equipment 33
2.1.3 Conditions 35
2.2 Hygrothermal modelling 38
2.2.1 2D simulation 39
2.2.2 Indoor and outdoor pressure difference 40
2.2.3 Evaluation criteria 42
3 Results 44
3.1 Test walls insulated with mineral wool (EW-1) 44
3.1.1 Field measurements and simulation of Northern side walls with initial MC of 13% (EW 1.1_N) 44
3.1.2 Field measurements and simulation of Northern side walls with initial MC of 25% (EW 1.2_N) 48

3.1.3 Field measurements and simulation of Southern side walls with initial MC of 13% (EW 1.1_S) 52
3.1.4 Field measurements and simulation of Southern side walls with initial MC of 25% (EW 1.2_S) 55
3.2 Test walls insulated with cellulose (EW-2) 59
3.2.1 Field measurements and simulation of Northern side walls with initial MC of 13% (EW 2.1_N) 59
3.2.2 Field measurements and simulation of Northern side walls with initial MC of 25% (EW 2.2_N) 62
3.2.3 Field measurements and simulation of Southern side walls with initial MC of 13% (EW 2.1_S) 65
3.2.4 Field measurements and simulation of Southern side walls with initial MC of 25% (EW 2.2_S) 69
3.3 Test walls insulated with PIR (EW-3) 72
3.3.1 Field measurements and simulation of Northern side walls with initial MC of 13% (EW 3.1_N) 72
3.3.2 Field measurements and simulation of Northern side walls with initial MC of 25% (EW 3.2_N) 75
3.3.3 Field measurements and simulation of Southern side walls with initial MC of 13% (EW 3.1_S) 78
3.3.4 Field measurements and simulation of Southern side walls with initial MC of 25% (EW 3.2_S) 82
4 Discussion 85
4.1 Field measurements 85
4.2 Simulations 89
4.3 Improvement of flaws 91
Conclusion 92
Summary 93
Kokkuvõte 94
LIST OF REFERENCES 96
APPENDICES 99
Appendix 1 – Graphs of MC change in walls 100

Appendix 2 – Tables of differences 102
Appendix 3 – List of terms 104

PREFACE

This research is done as a part of a larger scale project investigating hygrothermal properties of Cross Laminated Timber (CLT) panels in external wall assemblies, done in Tallinn University of Technology (TalTech), Estonia. During the research the author was assisted by Early Stage Researcher Villu Kukk and professor Jaan Kers, by a generous share of knowledge and time.

The main aim of the research was to investigate the hygrothermal performance in CLT wall assemblies, by comparing walls with 3 different insulation types, different initial moisture contents of CLT and location either on Southern or Northern façade. By gaining field measurements, there were made computer simulation models of each wall, where the calculation results were compared with measured data and the model was calibrated accordingly. Measurements gave four parameters to analyse – temperature (T), partial pressure (P_v), relative humidity (RH) and heat flux (q). Temperature and relative humidity in certain arrangement gives favourable conditions for mould growth. As the risk of mould growth is briefly analysed in the discussion part, these are only presumptions which need to be further investigated, by considering material sensitivity classes and exposure time.

The first part of the thesis is a literature review, where the CLT is introduced as a material and is described its production process, followed by hygrothermal properties, where there are analysed thermal conductivity, moisture transmission and air permeability of plain wood and CLT as crucial factors influencing hygrothermal performance of whole wall assembly. A brief introduction of requirements for Nearly Zero Energy Building (NZEB) are given, mentioning how the CLT can be applied there and what insulation types can be used. In the end of this chapter, the main objectives and hypothesis of this thesis are given.

Paragraph of Method describes used specimens, equipment, wall types and conditions of field measurements, followed by a short description of hygrothermal modelling. In results there are described final results of field measurements and calculated data of all wall types and all parameters, giving a brief comparison of average differences between calculated and measured results.

Discussion part gives an insight of which wall types and which locations in the wall assembly are the most crucial, how these results relate to other studies, reasons for differences in calculated results and how a possible improvement of future research can be done.

Conclusion summarizes the whole research and points out the answers on proposed research questions.

Keywords: CLT, Hygrothermal modelling, Mould growth, Field measurements

List of abbreviations and symbols

Symbols

d – thickness	m
P_v – water vapour partial pressure	Pa
q – Heat flux	[Wm^2K]
R – Thermal resistance	[m^2K/W]
RH – Relative humidity	[%]
T – Temperature	[°C]
U – Heat transfer coefficient (thermal transmittance)	W/m^2K
λ – Thermal conductivity	[W/mK]
μ – Water vapour resistance factor	[-]
ρ – Density	[kg/m^3]

Abbreviations

1C-PUR – One component polyurethane

CLT – Cross laminated timber

(E)MC – (Equilibrium) moisture content

EW – External wall

FSP – Fibre saturation point

NZEB – Nearly zero energy building

W_p - Short-term absorbability

W_{pl} - Long-term absorbability

UF – Urea formaldehyde

PVAc – Polyvinyl acetate

PIR - Polyisocyanurate

EPI – Emulsion polymer isocyanate

MUF – Melamine urea formaldehyde

Ave. diff. – Average difference

Std. d. – Standard deviation

1 INTRODUCTION

As the CLT is still a comparatively new building material in the industry, there a lot of fields to be investigated and tested. One of them is its behaviour in terms of moisture affection, where the current supply of researches done concerning moisture affection to CLT wall assemblies is not enough, and this hopefully would be a useful research paper to describe this topic.
In the first part of this paper there is given a literature review of relevant topics and aims of this research, in chapter of method there are described specimens, conditions and hygrothermal modelling. In the final parts there is given an analysis of results, discussion and a conclusion. Additional appendices are attached to provide a better understanding of the experiment.

1.1 CLT as a product

1.1.1 Composition

Cross laminated timber *(CLT)* is a laminated solid wood product for structural load–bearing use, consisting of three, five or seven layers glued together crosswise (orthogonally) *(Figure 1).* Due to cross lamination, the properties of CLT compared to single wood board or a frame are improved. CLT main mechanical properties are good bending and shear strength. By cross lamination there is improved dimensional stability, which allows prefabrication of long and wide floor slabs and single storey walls.
Performance of CLT in bending is very much affected by the grade of the outer layers and their strength and stiffness, thus CLT can be customized for different kinds of uses. As a strength graded timber must be used for panel production, commonly C24 grade is used for homogenous lay-up and in “combined CLT” C16/C18 grades are used for transverse layers (Ansell, 2015). According to European standard EN 16351, wood based panels fulfilling requirements for use in service class 2 or 3 can be used, built up of at least 3 orthogonally bonded layers (at least 2 of them timber layers) and may have additional layers bonded parallel to grain (Estonian Centre for Standardisation, 2015).

This makes CLT a cost-competitive and sustainable wood-based solution which can complement or replace such currently used materials as concrete, masonry or steel, and can be a great addition to well-known light frame wooden structures.

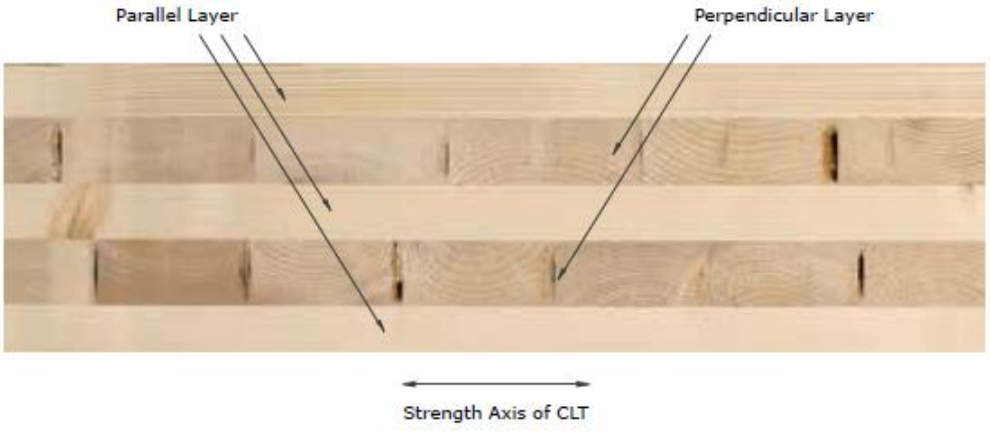

Figure 1. Cross section of CLT. (Karacabeyli & Douglas, 2013)

1.1.2 Raw material

CLT is mostly made of softwood and the main species used is Norway spruce (Picea abies). Other species used are Scots Pine (Pinus sylsvestris), European Larch (Larix decidua), Douglas Fir (Pseudotsuga menziesii) and Swiss Stone Pine. Species are carefully arranged according to standards and requirements, often having better looking boards in outer layers. Use of hardwoods is also possible, however its use is still under research and development. (Ansell, 2015) In order to comply with European standard CLT has to be made of coniferous species or poplar (Estonian Centre for Standardisation, 2015).

Wood stores CO_2, which is a major advantage compared to other building materials, especially concrete, which instead of storing carbon, makes a great amount of emissions while being produced, transported and installed. Timber materials are often a good choice also in terms of using a local material, specifically for Northern Europe, in this way encouraging local economy and reducing transportation costs.

1.1.3 Manufacturing and technologies

Manufacturing of CLT panels is usually done by the following steps:

1) Board selection
2) Board grouping
3) Board planning

4) Board or layer cutting to length
5) Adhesive application
6) Panel lay-up & pressing
7) Product cutting
8) Surface machining
9) Marking & packaging

The key of success for a full production is lumber quality and control of adhesive bond manufacture. Assembly process of one panel can take 15-60 minutes, depending on equipment and adhesive used. (Karacabeyli and Douglas, 2013)

Boards used in production usually have *MC* of 12 % ± 3 %, which prevents dimensional variations and surface cracking (Karacabeyli and Douglas, 2013). However, a little vertical shrinkage of around 3mm per storey, when used in multi-storey buildings, have been observed (Espinoza *et al.*, 2016). It is recommended that the max difference of *MC* between adjacent pieces to be joined together does not exceed 5 %. The temperature in manufacturing rooms may also affect some parameters of CLT panel during open assembly curing time. That is why it is recommended for it to be around 15 °C.

Board thickness varies from 4 mm veneers to 80 mm boards, however European standard sets different requirements - timber layers of 6-45 mm, except 60 mm for the inner layer of three-layered CLT (Estonian Centre for Standardisation, 2015). Due to shear stresses between CLT layers, a minimum width of four times the thickness is recommended.

Boards are graded in two major categories - construction grade and appearance grade – where the latter one is used in outer layers of CLT providing specific visual characteristics. Grouping of lumbers is done according to MC level and visual characteristics. All panels in mayor strength direction will be required to have the same mechanical properties. Besides that, according to European standard each timber layer shall be made of boards of one strength class. (Estonian Centre for Standardisation, 2015)

Prior to applying adhesives, planning is done in order to activate the wood and to reduce oxidation for improved gluing effectiveness. Adhesive application should be done shortly after planning. There are two main types of adhesives currently used in manufacturing – melamine-urea-formaldehyde (MUF) and one component polyurethane adhesives (1K-PUR) – both of them being nearly colourless. Polyurethane adhesives (1K-PUR) are free from formaldehyde and due to swelling on curing, provide some internal pressure during bonding. The other adhesive, melamine-urea-formaldehyde (MUF), provides gap-filling properties and has a better

performance at higher temperatures. Parameters that have to be controlled during manufacturing are the applied quantity of adhesive, bonding pressure and curing procedures in order to keep good quality of material. These previously mentioned adhesive types are both approved by European standard, however there is another type of adhesive permitted – emulsion polymer isocyanate (EPI), which is not that commonly used. (Karacabeyli and Douglas, 2013)

Boards are finger jointed in order to obtain greater lengths and quality of timber. The position of finger joints can be edgewise (fingers visible on the face) or flatwise (higher visual quality and increased airtightness), *see Figure 2*.

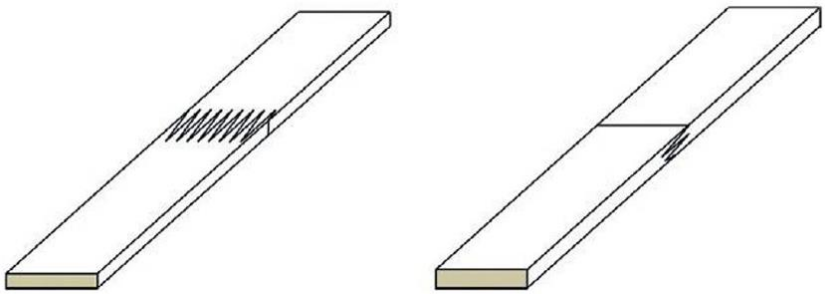

Figure 2. Edgewise (left) and flatwise finger joints. (Brander, 2013)

Boards are then laid up side by side to be glued and pressed. Distance between boards cannot exceed 6mm to comply with European standard. However, for some manufacturers there is an intermediate stage of board edge-gluing, where they are glued by sides of each board into single lamellas. This has advantages such as lower pressure in bonding to adjacent panels and smaller board width to thickness ratios, but at the same time increasing production costs. Besides gluing, nails or wooden dowels can also be used to attach the layers, which also meets European standards.

Lay-up of layers can be made homogenous where one layer follows another one layer orthogonally or can be made in symmetrical build up, where two layers have the same direction, but the structure is symmetrical, *see Figure 3,* which provides specific structural capacities.

Pressing of layers is a critical point of manufacturing, which accounts for proper bound development and CLT quality. There are two types of pressing - hydraulic press and vacuum press. Bonding pressure is required to overcome roughness of the surface or warp/twist and achieve a complete wetting of the surface with adhesive. Hydraulic press is the most expensive and mostly used by bigger producers. With this method thicker lamellas can be used and an edge pressure can also be applied (to bond gaps in outer surfaces). Vacuum pressing is used by smaller producers, where boards are often placed manually and adhesive applied by a machine.

On the contrary to hydraulic pressing, with this method curved or shaped CLT elements can be made.

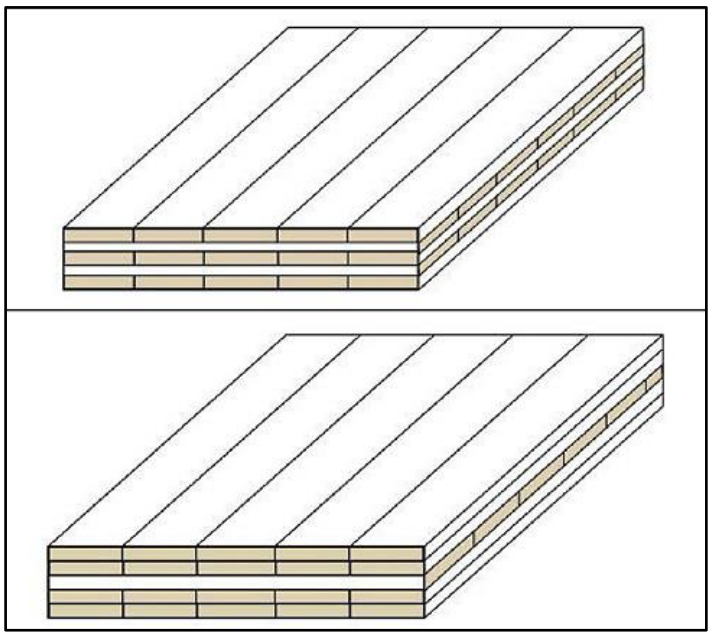

Figure 3. Lay-up of CLT. Upper – homogenous lay-up, bottom – five-layered symmetrical layer with double outer layers. (Brander, 2013)

After sanding CLT is moved to Computer Numerical Control (CNC) machines, where precise openings for windows, doors and service channels can be cut.

One of the advantages of CLT production is an efficient material use, where there are also used small boards from outer layers of a log which would be otherwise rejected. In this way now the use of the whole log is efficient. For CLT production there can be used also a lower quality juvenile wood which is usually less desired in the wood industry, bringing it to the inner layers of CLT, leaving higher quality boards for outer layers. However, according to European Standard, no reused timber or wood based panels can be used for CLT production. (Estonian Centre for Standardisation, 2015)

Panels can be produced in lengths up to 22 m, with a width up to 3.5 m according to manufacturer's data *(KLH, Arcwood, Binderholz, StoraEnso).* Dimensions, however, are often limited because of transportation limits. Thickness depends on a number of glued boards, with a 7-ply CLT it makes up to 400 mm thickness. According to European standard, the overall thickness of CLT can be up to 500 mm, with a max deviation ± 2 mm or 2 % of nominal thickness

(Estonian Centre for Standardisation, 2015). An advantage of CLT panels is that there can be cut very precise holes and openings using CNC machines.

CLT has been found to be in compliance with European labelling programs in terms of Volatile organic compound (VOC) emissions (Bucur, 2011). What is more, thinking of future of CLT constructions, the panels are also recyclable.

1.2 Hygrothermal properties

Hygrothermal properties of wood are referred as heat, air and moisture transport in material. Moisture content, oxygen supply, temperature in certain arrangement is the environment for development of wood degrading organisms (Lebow and White, 2007). That is why a knowledge is required of how each of the parameters are mutually related in order to achieve conditions where wood degradation can be avoided.

1.2.1 Thermal conductivity

Thermal conductivity λ,[W/mK], also called lambda value is a material property that states its steady-state ability to conduct heat. In other words, the value indicating a material's insulating capacity – the lower the value, better the material holds the heat. Thermal resistance R [m2K/W] is an inverse value of thermal conductivity (R=1/U), describing heat conductivity of a material per unit thickness. Thermal transmittance parameter is used to describe the insulating capacity of a building envelope, for example, external wall structure.

According to Glass and Zelinka (2010). thermal conductivity of plain softwoods varies from 0.09 to 0.17 W/mK, depending on their moisture content. By increasing wood's moisture content, density and temperature, thermal conductivity even increases. For example, according to AlSayegh (2012), for a dry CLT panel ($\rho \sim 340$ kg/m3), made of spruce wood, a measured thermal conductivity was 0.103-0.104 W/mK, which is lower than for regular CLT *c*oming from a factory. According to manufacturer specifications *(StoraEnso, KLH, Binderholz)*, thermal conductivity of CLT panels ranges from 0.11-0.13 W/mK.

Although the CLT differs from a plain wood with an adhesive layer in between the lamellas, several authors (Raji *et al.*, 2009; AlSayegh, 2012; Byttebier, 2018) have mentioned that glue does not have any effect on thermal conductivity. As the thickness of adhesive layer is only around 0.1mm, compared to the thickness of 10-14 cm of the whole CLT panel, the adhesive thermal properties are very insignificant (Byttebier, 2018).

1.2.2 Moisture transmission

Wood is a hygroscopic material, where it gains or releases moisture like a sponge, depending on the surrounding environment. These processes are classified as either adsorption or desorption *(Figure 4).* Adsorption is a process, in which moisture is added or absorbed in a material until steady state is reached, whereas desorption is when moisture is released back into the air. While adsorbing or desorbing water, the wood is in a hygroscopic range, where these processes cause either swelling or shrinkage of wood and may affect mechanical performance. It is easier for wood to gain moisture than to lose it, which also affects the drying process of the whole assembly (Byttebier, 2018).

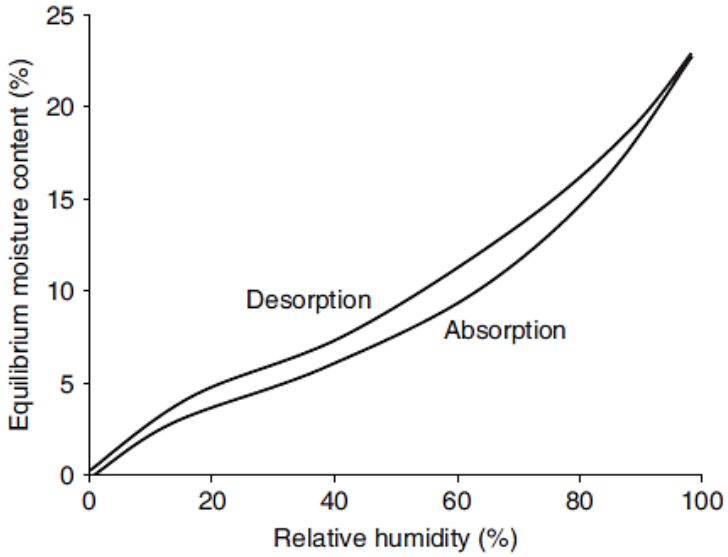

Figure 4. Sorption curve resulting from the average adsorption and desorption isotherms for six species of wood at 40°C (Domone and Illston, 2010)

Wood cells contain free and bound water. The free water is held in cell lumen and the bond water is located in the cell walls. Moisture content of wood is affected by the surrounding environment, especially the relative humidity. In general, as the air is more moist, wood gets more wet as well; however there is a point where the cell walls are completely saturated as a bound water, and there is no free water in cell lumen, which is called fibre saturation point *(FSP).* For wood, the *FSP* is typically at around 30 % *MC* (*Wood and Moisture | The Wood Database*). Relative humidity affects *MC* of wood only until the *FSP* is reached; afterwards, when the water is also in the cell lumen, the *MC* is not affected. The capillary (free) water has no dimensional impact on wood (Zillig, 2009).

Similar to thermal conductivity, the mass of glue lines between layers of CLT is insignificant towards the total panel weight, which makes it negligible in terms of water adsorption (Byttebier, 2018).

On a surface of a large CLT panel, there may be variations in MC, as it is more affected by the surrounding environment, while the inner layers of CLT may respond to MC changes slower (Gagnon, Pirvu and FPInnovations (Institute), 2011).

Moisture content, where wood neither gains nor loses the water as long as the temperature and relative humidity of surroundings are not changed, is called equilibrium moisture content *(EMC)*. By raising the RH, the EMC of wood also increases, although the relation is not linear. A visual illustration of this relation can be seen in *Figure 5,* where above 85 % of RH, the line goes up more rapidly, which means the wood swells more. Isotherm stops at around 27 % of EMC, as that is almost the FSP, where the cell walls are saturated and the wood stops swelling.

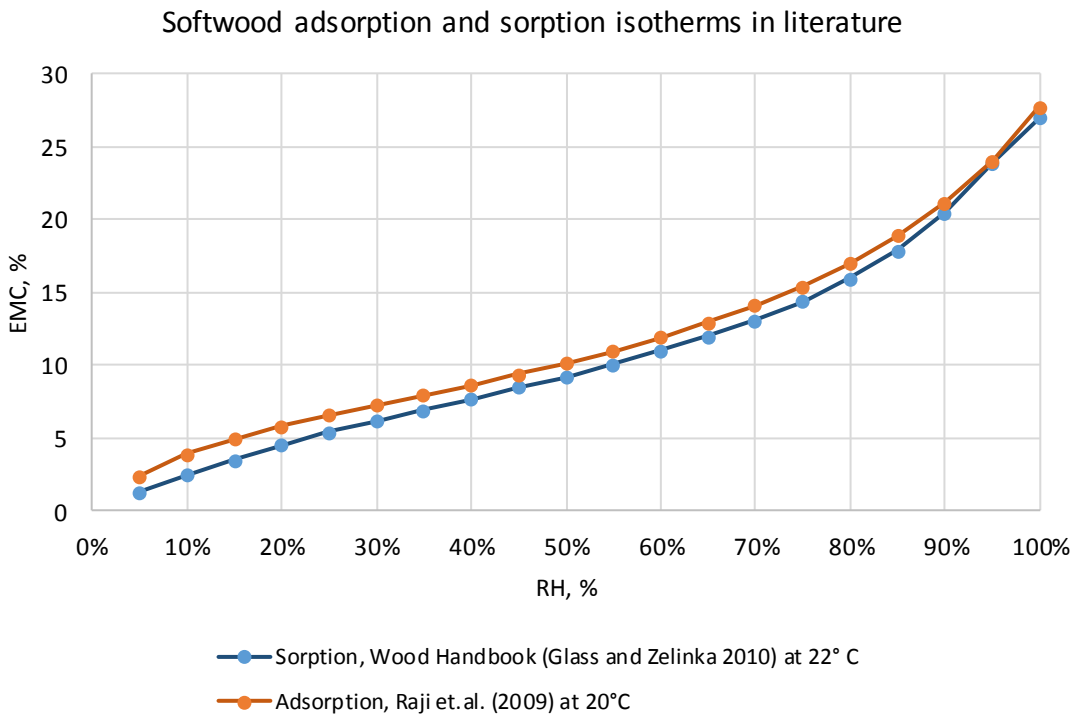

Figure 5. Softwood adsorption and sorption isotherms at ambient temperatures in literature (based on AlSayegh 2012)

A moisture movement in up to 95 % *RH* is considered as water vapour transmission, which is called a diffusion, where water vapour under a pressure gradient moves from highly concentrated to low concentrated zones to achieve equilibrium. To describe diffusion there is a parameter of vapour permanence or vapour resistance, where the first is the materials ability to let through the air or vapour and accordingly resistance is ability to resist air or vapour flow through the material. (Byttebier, 2018)

The vapour diffusion resistance of a material decreases by increasing the moisture flow. When RH reaches above 95 % *RH* it is considered a liquid water transport, where the moisture movement through the material is affected by condensation (AlSayegh, 2012). Due to hydraulic pressure by the water and the negative suction pressure, moisture transport is faster (ISO 15148, 2002).

Vapour permeability in wood is higher in a longitudinal direction. Similarly, wood also absorbs moisture faster parallel to grain. That is why when considering CLT position in building, the longitudinal surface should not be exposed (AlSayegh, 2012).

A relation for vapour resistance to *RH* for plain wood and CLT panels in tangential and radial direction is shown in *Figure 6.* By increasing RH, a material's permeability increases and resistance decreases, as they are inverse values. In *Figure 6* it can be noticed that the vapour resistance for a CLT, or wood with adhesive layers, is lower than for a plain spruce wood, which might mean that the addition of adhesive layers decreases the resistance to vapour diffusion. By higher RH, the results from CLT and plain wood even out.

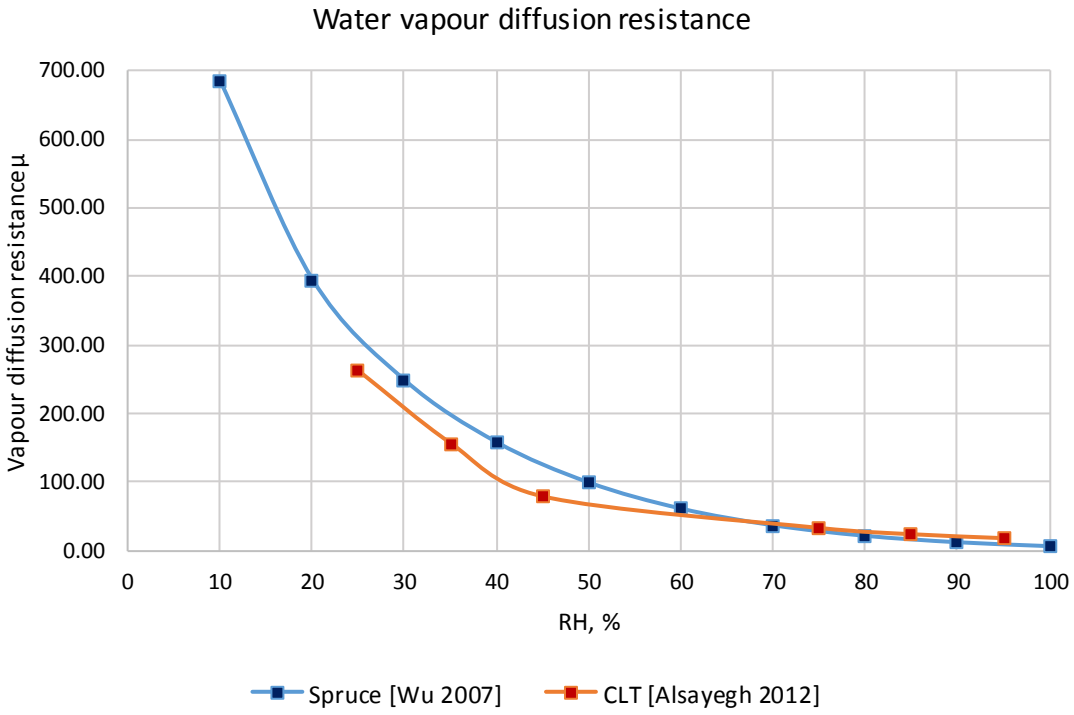

Figure 6. Vapour diffusion resistance in literature (based on Byttebier, 2018)

However, there are different opinions of adhesive presence hindering the vapour transmission or not. Volkmer *et al.* (2012) states that for a high RH, vapour diffusion resistance of PUR adhesive is larger than for other adhesives *(UF, PVAc,, EPI, MUF)*, but the resistance value is rather unrelated to *MC* of wood. At the same time, several sources (Raji *et al.*, 2009; Sonderegger *et al.*, 2010) mention that the presence of an adhesive layer slows down the water transport, where the glue is acting as a seal, reducing the diffusion of moisture.

1.2.3 Air permeability

Air permeability can refer to air flow through the specimen at different pressure differentials across the specimen. The performance of the material can be described in air permeance *(kg/m^{2}Pa s).* (AlSayegh, 2012)

Apart from causing a negative effect on acoustical performance, fire safety and thermal comfort, air movement through a material also causes a movement of moisture and heat. Accordingly, the breathability of a material can affect its thermal performance. If the building envelope is not airtight, it also might not meet the energy requirements.

Wu (2007) held measurements of various materials, including a spruce, where he concluded that spruce at large thickness in dry conditions can be considered airtight. As CLT is mostly made of spruce, also a composed panel of spruce boards and adhesives, where the panel thickness is around 100-140mm, can be considered airtight (Byttebier, 2018). Other experiments have found that adhesives only decrease permeability, however, again, the properties of adhesives compared to high thickness CLT board are almost insignificant (Raji *et al.*, 2009).

Nevertheless, attention must be paid to panel quality itself and the joints between the boards. In low-quality panels, there might be cracks even on the boards themselves, which obviously can be a cause of air movement through material. Louwet and Van Tricht (2017) held a test of permeability of 3-, 5-, and 7-layered panels, where the CLT panels were initially airtight. After the oven-drying, the results showed that the CLT panel remained impermeable, but the air tightness decreased, which was most likely caused by wider gaps between the boards after the drying, because the wood shrinks and gaps between boards increase. This means that the joint quality and the glue continuity is important to consider for overall CLT panel airtightness properties. What is more, no less important is to properly seal the joints between the panels also on site, when installing elements in a building.

1.3 Fields of application

As CLT is called the building material of the 21st century and has obviously gained popularity in constructions for various purposes, more and more examples of successful buildings are discovered. There are several benefits of using CLT, but one of the most important is being environmentally friendly, which is an emerging issue nowadays. CLT is also preferred due to health comfort and the pleasant internal atmosphere it provides to its users in CLT buildings.

1.3.1 Buildings

CLT can be a light-weight replacement of steel and concrete for mid-rise and high-rise building structures *(Figure 7).* The light weight factor, reducing the building weight by 60-70 %, may be also helpful in seismic zones, where it can easily absorb the impact of sudden shifts. What is more, lighter panels give opportunity to use smaller foundations, which accordingly means a use of smaller cranes, in this way also reducing construction costs.

Figure 7. Proposal of 12-storey building of CLT panels, Portland, USA. (www.dezeen.com, 2017)

Easy handling during construction and high level of prefabrication leads to fast project completion. To ensure a smooth delivery and installation, elements have to be delivered in the correct sequence in order to be able to install elements directly from lorry to a place in the building. After installation, services, ceilings, wall finishes, insulation and cladding are fixed to CLT panels, usually using screws, which are also quicker and easier to fix compared to concrete structures. Usage of CLT provides also increased safety, less demand of skilled workers on site, less distribution to the surrounding environment and less waste, as the material is prefabricated and requires less installation work on site.

Outer layers of CLT in walls are usually parallel to gravity loads in order to maximize a vertical load capacity of the wall. Likewise, in floor and roof systems outer layers run parallel to mayor span direction. At the same time, thanks to cross lamination, there will always be laminations which resist load in the perpendicular direction as well. To resist lateral loads from wind and earthquakes, CLT structures are made in wall and floor systems as shear walls and diaphragms.

At the same time, no less important factors are proper fastener installation, shear strength of CLT panel initials and connections.

Connections play an important role to maintain good properties of construction – strength, stiffness, stability, ductility. Consequently, this requires detailed attention by designers to design proper solutions before the actual construction starts. Traditional systems of connections are dowels, wood screws and nails, however, there can be used joints where panels are connected themselves, using tongue and groove joints, and additionally fixed by metal screws and brackets. CLT can be jointed to any other material – light wood frame, heavy timber, steel and concrete (Van De Kuilen *et al.*, 2011).

A well-known high-rise residential building using a combination of CLT panels, glulam and light weight frame is the 53m-tall Treet in Bergen, Norway. However, *CLT* is also known in Estonia, where the first net zero energy building was built in Põlva in the year 2013, using CLT as its main construction material (Reinberg *et al.*, 2013).

As the CLT panels provide some level of thermal insulation themselves, as mentioned in paragraph 1.2.1, heat is stored during the day and released during night-time. This means also lowering use of energy to cool or heat up the building.

However, wood is a hygroscopic material and it is very much affected by moisture and water content both inside the structure and in surrounding environment. So are the CLT panels, however, they absorb and dry out the water much slower than light frame constructions. A key to a sustainable and durable construction is to reduce wetting and to promote drying.

1.3.2 Minimum requirements and design for NZEB

According to Minimum requirements for energy performance (2018) a nearly zero-energy building *(NZEB)* is characterized as a building that is built according to best possible construction practice, which uses energy efficient solutions and renewable energy technologies and whose total energy performance indicator meets class A requirements.

According to European directive on the energy performance of buildings (2010), by December 31st of 2020, all new buildings shall be NZEB (energy class A) and after 31 December 2018, new buildings occupied and owned by public authorities are NZEB. This makes architects and designers aware of demands to follow when designing a building envelope for residential, public, educational, health care buildings and offices. However, historical, religious, short-term usage, industrial buildings with no living premises and buildings with area up to 50m^2 are not required to comply with these minimum energy performance requirements. (Republic of Estonia Ministry of Economic Affairs and Communications, 2015)

The current limit values for energy performance for NZEB are listed in *Table 1*.

Table 1. Limit values for energy efficiency figures for NZEB (Republic of Estonia Ministry of Economic Affairs and Communications, 2018)

No	Building type	Limit value for energy efficiency figure, kWh/m2a)
1	Small house with heated surface <120m²	145
2	Small house with a heated surface of 120-220 m² and a terraced house	120
3	Small house with heated surface> 220 m²	100
4	Apartment building	105
5	Barracks	170
6	Office building	100
7	Accommodation building	145
8	Commercial building	130
9	Public building	135
10	Commercial building and terminal	160
11	Education building, Pre-school child care institution building	100
12	A treatment building	100
13	Warehouse	65
14	Industrial building	110
15	High energy building	820

When talking about the building envelopes, estimated thermal transmittance values for NZEB vary in a range of 0.08 – 0.14 W/m2K, depending on architectural design and other energy performance measures. The values have been estimated in different regions, including Estonia, Southern Canada, Finland and for overall European climate. (Arumägi and Kalamees, 2016; Asaee, Ugursal and Beausoleil-Morrison, 2019; D'Agostino and Parker, 2019; Sankelo *et al.*, 2019)

However, as the CLT panels alone do not meet the energy requirements for buildings, additional thermal insulation has to be added in order to improve the thermal resistance of whole construction. For example, the thermal transmittance *(U)* for CLT alone *(d=100 mm, λ=0.12 w/mK)* is 1.2 W/m^{2}K, whereas, when adding a 300 mm of a mineral wool *(λ=0.037 W/mK),* the overall thermal transmittance is decreased to 0.11 W/m^{2}K, which is about 10 times lower and is sufficient to meet the energy requirements as it is in the range of estimated values mentioned before.

There are several types of insulation which can be used with CLT. As mineral wool is often a more preferred material, there are other types such as polyisocyanurate (PIR), expanded polyurethane (EPS) or extruded polystyrene (XPS).

Mineral wool is used the most often, considering aspects such as good thermal conductivity *(λ=0.037 W/mK)*, average price category and good performance in a wall construction as the water vapour resistance is very low *(μ =1)* and it allows the wall construction materials to dry out. According to *Vitanen et al.* (2011) it is medium resistant to mould growth.

Foil-faced polyisocyanurate insulation is expected to act similar to XPS. As PIR, XPS and EPS are not natural insulation materials and the water vapour resistance is very high (*μ=104)*, they are not acting too well when in contact with wood if it has higher moisture content, simply because it does not let it dry out well. That is why it should be used only when wood is dried out (McClung *et al.*, 2014). Nevertheless, PIR insulation is classified as resistant to mould growth (Viitanen, Ojanen and Peuhkuri, 2011), although the adjoining wooden surface is still in a high risk of mould growth. A benefit of using PIR may be that the insulation layer in construction can be decreased, as the thermal conductivity is very low *(0.022 W/mK)* and the necessary thermal transmittance can be achieved with using less insulation than, for example, mineral wool.

It is possible to use also a cellulose insulation, which, however, is more sensitive to mould risk (Viitanen, Ojanen and Peuhkuri, 2011) than mineral wool or PIR. As the thermal conductivity is slightly higher than mineral wool *(0.039 W/mK)*, it requires an even thicker layer of insulation in a wall construction. However, a benefit of using cellulose insulation may be that similarly as mineral wool, it allows the wood to dry out (μ=2.05), but still holds the moisture better in terms of buffering the water vapour throughout the insulation, instead of letting it all through and allowing it to accumulate in one point of wall construction.

Nevertheless, in all cases of insulation type, a well-ventilated cladding system is important.

1.4 Problem statement and objectives

Moisture affection to CLT wall assemblies is crucial in terms of a possible mould growth risk and affection to properties of adjoining materials in a wall structure, especially insulation, which should provide a dry out of CLT panel.

Moisture from weathering – rain, snow, humidity – affecting the CLT panel during construction and installation period is called exceed moisture. This may be caused by improper covering of panels and installation during high humidity conditions, so that the panel installed is actually wet, having exceed moisture and *MC* is higher than required. That accordingly affects the

insulation properties and thermal conductivity of the wall in general, by the increase of moisture content, proportionally increasing the thermal conductivity of insulation, respectively, lowering the insulation heat keeping capacity (Karamanos, Hadiarakou and Papadopoulos, 2008; Sandberg, 2009). As CLT is still new material in the market, it's applications still need to be tested and analysed. There have been done similar studies using CLT in an external wall structure, however, this research is considering 3 different insulation types in the same conditions and the computer simulation model will provide a platform for further analysis also in different conditions.

Considering these issues, the main problem this research addresses is the insufficient information about hygrothermal performance of CLT concerning risk of mould growth. Two main objectives of this thesis are given below:

1) To evaluate the impact of built-in moisture, insulation type and location of the building envelope to the hygrothemral performance of CLT wall assemblies in cold climate conditions with warm summers and snowy winters.
2) To create validated simulation models for further investigation to evaluate the risk of mould growth in CLT wall assemblies.

Considering these aspects, the author has established a hypothesis:

1. Wall assemblies with *CLT* panels of high built-in moisture, with a low vapour-permeable insulation and located in the Northern direction have a greater risk of mould growth.

In order to answer the proposed problem, achieve objectives and confirm or discuss the hypothesis, an experimental work was done, using CLT wall assemblies with different insulation types, initial MC and placement in building. Based on filed measurements there were created simulation models using Delphin software. However, the final conclusions of mould growth risk can be done only after the experiment is fully carried out, using a mathematical mould growth model, considering material sensitivity classes and time of exposure.

2 METHOD

Experimental part of this thesis was started in January 2018 and the field measurements were held until March 2019. As in the whole experiment there are installed and tested six types of wall assemblies, a scope in this thesis is made only on three types of them, *described in paragraph 2.1.1.*

The study is focusing on moisture behaviour through parameters of temperature, partial pressure of water vapour and relative humidity between each material layer in wall assembly and heat flux through whole wall section. The results provide a conclusion of affection of initial MC of CLT to wall structure and possible threat of mould growth on material surfaces.

At the same time, a computer simulation was done to compare the results gained from installed sensors in wall assemblies to calculated, simulation-made results and enable to do simulations with new parameters.

2.1 Field measurements

2.1.1 Specimens

The main specimens of the experiment are CLT panels consisting of five crosswise laminated layers *(Figure 8).* Panels were made of spruce (Picea) boards and produced in Estonia by Arcwood (Peetri Puit OÜ), using one of the most common adhesives – 1C-PUR. Panels had average dimensions of 850x850x100mm, with an average initial weight of 34.28 kg.

Figure 8. Example of bonded CLT panel (http://hybrid-build.co/wp-content/uploads/2013/03/CLT2.jpg)

As mentioned before, there were tested three types of walls, where the only variable material was the insulation – mineral wool, cellulose insulation and PIR (polyisocyanurate). Description of three wall assembly types and their structure is given below *(Figures 9-11).*

1) EW-1

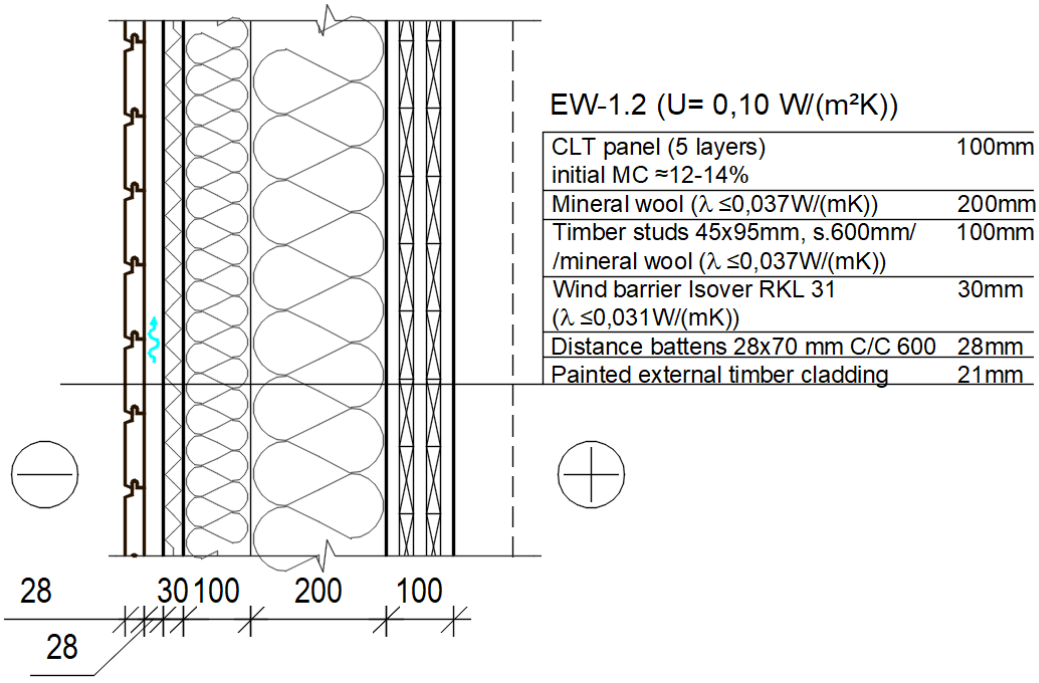

Figure 9. Wall type EW-1.2 (Technical drawing by V.Kukk, adjusted by author)

Structure:

- **CLT panel**, outer layers made of C24 quality timber, MC 12-14% or 25-27%
- **Mineral wool insulation**, λ ≤ 0.037 W/(mK) (Knauf, Classic 037, multipurpose use), short-term absorbability, $W_p \leq 1$ kg/m^2, long-term absorbability, $W_{pl} \leq 3$ kg/m^2, diffusion resistance factor μ = 1.
- **Wooden studs / mineral wool** (same type)
- **Wind barrier** Isover RKL 31, λ ≤ 0.031 W/(mK), air permeability <30 * 10E-6 m³ / msPa, the product is not hygroscopic (the product does not bind to humidity)
- Distance battens
- Painted facade cladding

2) EW-2

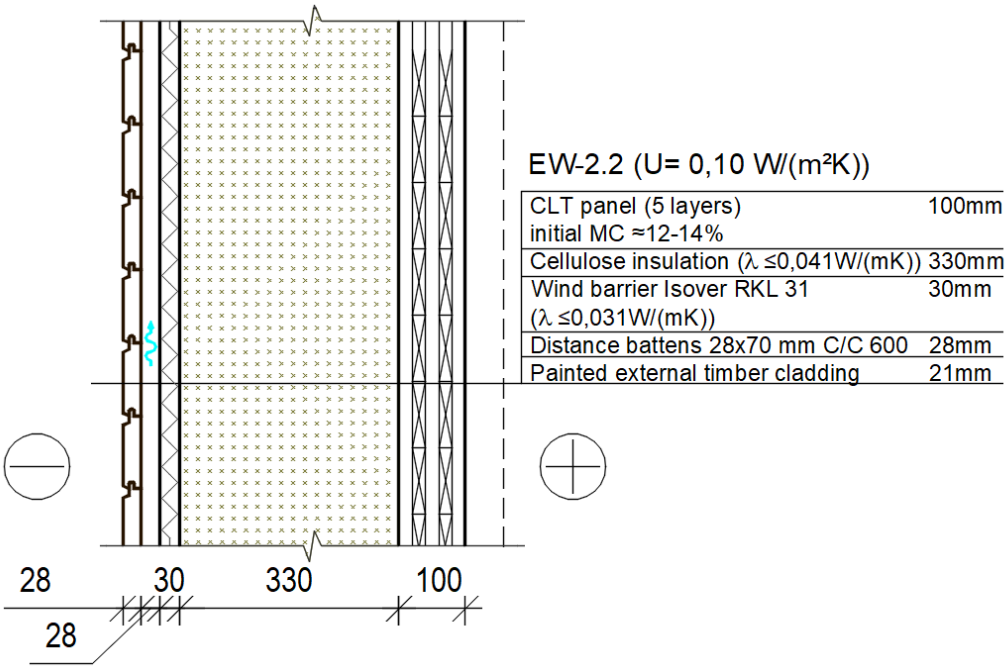

Figure 10. Wall type EW-2.2 (Technical drawing by V.Kukk, adjusted by author)

Structure:

- **CLT panel**, outer layers made of C24 quality timber, MC 12-14 % or 25-27 %
- **Cellulose insulation** (Werro wool), λ ≤ 0.041 W/(mK), wind resistance coefficient 37 kPa s/m^2
- **Wind barrier** Isover RKL 31, λ ≤ 0.031 W/(mK), air permeability <30 * 10E-6 m³ / msPa, the product is not hygroscopic (the product does not bind to humidity)
- Distance battens
- Painted facade cladding

3) EW-3

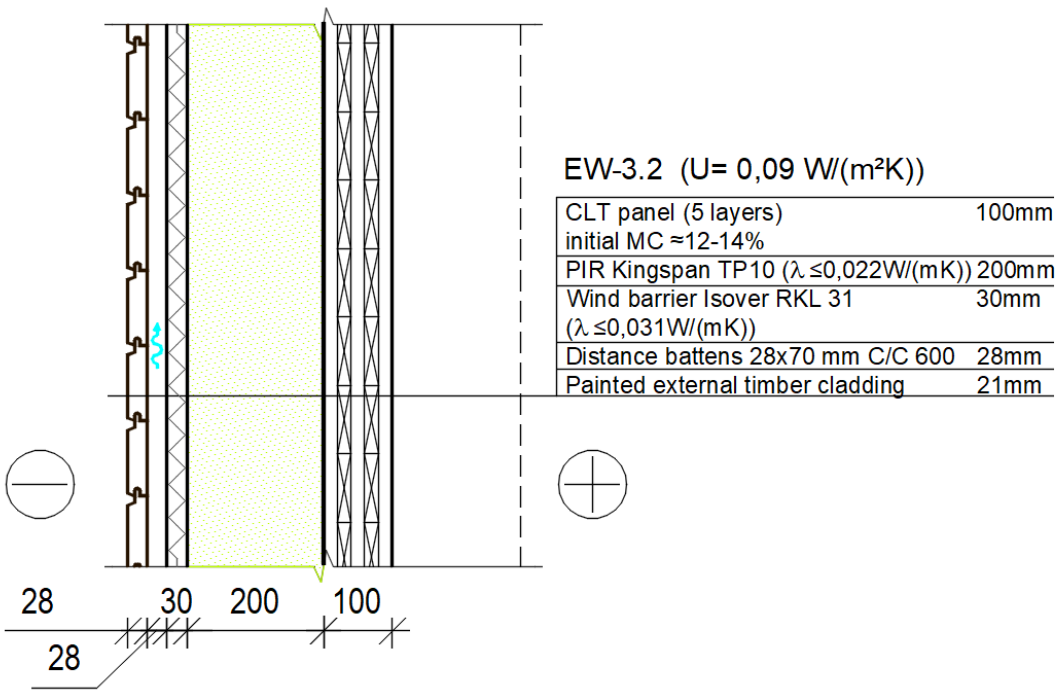

Figure 11. Wall type EW-3.2 (Technical drawing by V.Kukk, adjusted by author)

Structure:

- **CLT panel**, outer layers made of C24 quality timber, MC 12-14 % or 25-27 %
- **Polyurethane foam insulation** (Kingspan TP10, λ ≤ 0.022 W/(mK). Core made of high performance rigid thermoset polyisocyanurate (PIR) insulant, facing made of low emissivity composite foil. Water vapour resistance ≥100 MN.s/g.
- **Wind barrier** Isover RKL 31, λ ≤ 0.031 W/(mK), air permeability <30 * 10E-6 m³ / msPa, the product is not hygroscopic (the product does not bind to humidity)
- Distance battens
- Painted facade cladding

Besides the different wall constructions, for each wall type there were used two kinds of CLT panels with different MC. That is why some of panels were moisturised on purpose in order to see the difference of different MC affection to the same wall construction.

First MC of panels used were with an initial MC, when received from manufacturer, which varied between 11-14 %. In order to gain the other MC, some panels were wetted (soaked) by putting them in a self-made pool, located outdoors to gain MC of 25-27 %. However, before any wetting, all the panels were weighted to calculate what mass has to be achieved in order to get the desired MC of 25-27 %. Panels gained the desired MC approximately in a month *(Table 2)*. A graphical visualization of moisture gain can be seen in *Appendix 1.*

Table 2. Moisture content change in a time interval and initial MC for the dry panels

Wall No	Panel No	Initial MC, %	Final MC, %	Days	Interval
EW 1.1 N (wet)	P13	14.18	26.15	24	13.11-6.10
EW 2.1 N (wet)	P18	13.51	25.39	24	13.11-6.11
EW 3.1 N (wet)	P15	14.76	25.28	24	13.11-6.12
EW 1.2 N (dry)	P24	13.57	-	-	-
EW 2.2 N (dry)	P23	14.66	-	-	-
EW 3.2 N (dry)	P22	14.46	-	-	-
EW 1.1 S (wet)	P17	13.72	26.10	30	13.11-12.12
EW 2.1 S (wet)	P16	14.83	26.40	24	13.11-6.12
EW 3.1 S (wet)	P14	14.31	25.80	24	13.11-6.12
EW 1.2 S (dry)	P19	13.23	-	-	-
EW 2.2 S (dry)	P8	12.73	-	-	-
EW 3.2 S (dry)	P6	13.37	-	-	-

The pool was made to moisturize half of the panels as a simple construction of plywood board frame, placed on the asphalt outdoors. Then the plastic was put in to make a ground surface of pool and the water was added. *(Figure 12)*

To prevent a dry-out of moisture from narrow sides of panel, a Blower proof liquid brush (mastics) *(Figure 13),* polymer-based paste – was painted on narrow side surfaces of CLT panels, forming a flexible, permanent, continuous airtight seal layer in order to block the drying out in these directions. Damp diffusion resistance factor - $\mu = 35967$.

Figure 12. Pool for wetting the CLT panels (Adeniyi, 2019)

Figure 13. Blower proof liquid brush (mastics). (Author's photo)

After the CLT panels were ready for installation, the wall assemblies were constructed according to planned structures and prepared for installation – adding the moisture resistant plywood frame and sealing the edges of materials (around the frame). Meanwhile, there were also installed the sensors both in the materials and in between the material surfaces *(Figure 14).*

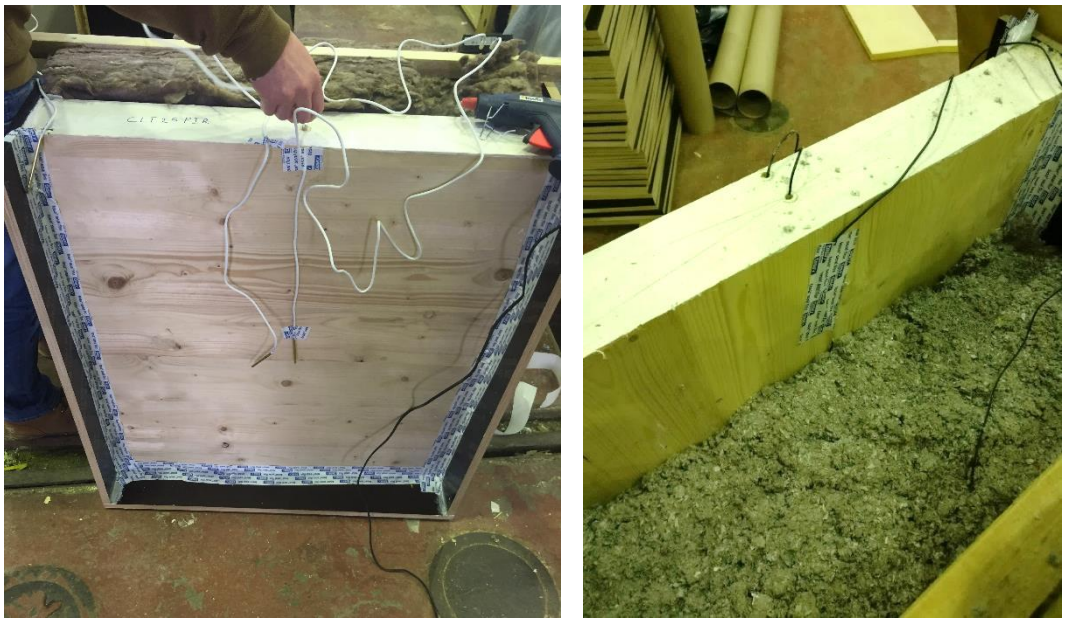

Figure 14. Left – Temperature and relative humidity sensors and airtight tape to seal around the edges of CLT. Right - sensor installation in CLT and in cellulose insulation. (Author's photos)

The constructed wall assemblies were installed in a frame of NZEB building. The plan of house is showed as *Figure 15.*

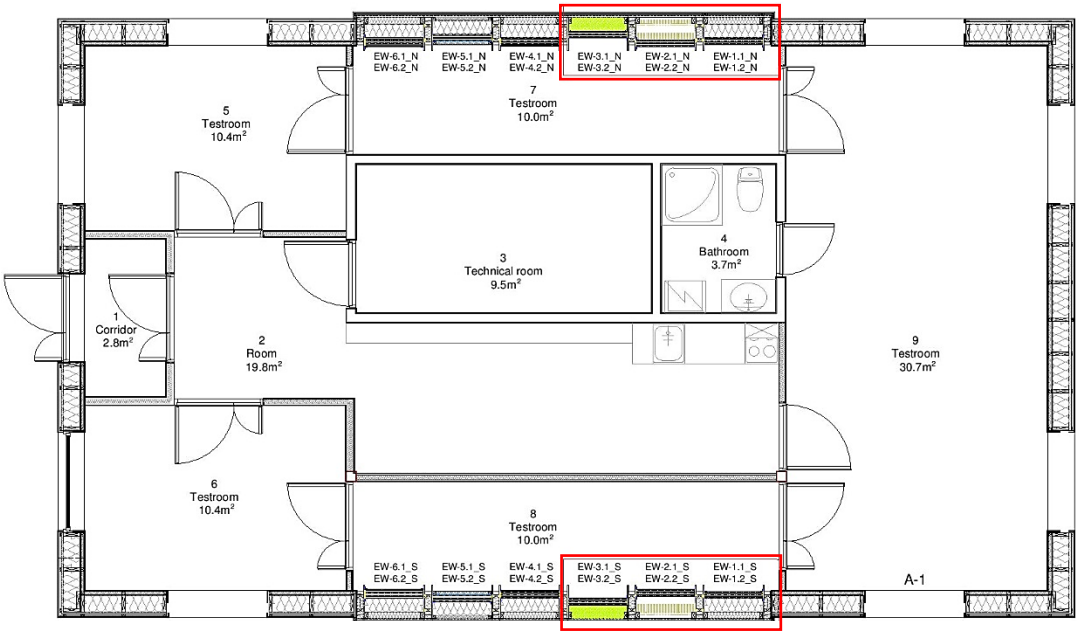

Figure 15. Plan of the NZEB (investigated wall types marked with red rectangle). (Technical drawing by V.Kukk, adjusted by author)

Layout of wall assemblies from inside and from outside showed in *Figures 16 and 17.*

Figure 16. Placement of wall assemblies from inside (Author's photo)

Figure 17. Placement of wall assemblies from outside (Author's photo)

2.1.2 Equipment

In the experiment there were certain parameters to be measured for specimen properties and during their performance in the field measurements. For measuring the weight of CLT panels, there were used **scales** (KERN DE 150K20D Weighting range Max 60/150 kg, readout, d=20/50 g) and for MC measurements there was used an electronic **moisture meter** (GANN HYDROTEST LG 3).

For field measurements there were used three types sensors to measure temperature (T°,C), relative humidity (RH, %) and heat flux (W/m^2).

- For **surface temperatures** there was used digital temperature sensor DS18B20 (Uniflex), accuracy of ±0.5 °C from -10 ° to 85 °C. *(Figure 14, left)*
- For temperature and relative humidity – Omnisense A-1, accuracy of ±0.3 °C from 0 ° to 60 °C (t sensor) and ±2.0 % from 0 % to 100 % (RH sensor). *(Figure 14, right)*
- For heat flux - Hukseflux HFP01, uncertainty of calibration ±3 % (k = 2). *(Figure 19)*

Sensors were marked in a certain system. Explanation given below.

HF/t&RH/ts_L/S1, where:

- **HF/t&RH/ts** – measured quantity (HF- heat flux, t&RH- temperature and relative humidity, ts- surface temperature)
- **L/S1** – location of the sensor (L stands for layer number where sensor is placed, S1 means inner surface or S2 – outer surface)

In each wall there were placed sensors – on surfaces, between the layers and one inside the CLT panel, *see Figure 18.* The placement of a sensor on a CLT surface is showed in *Figure 19.*

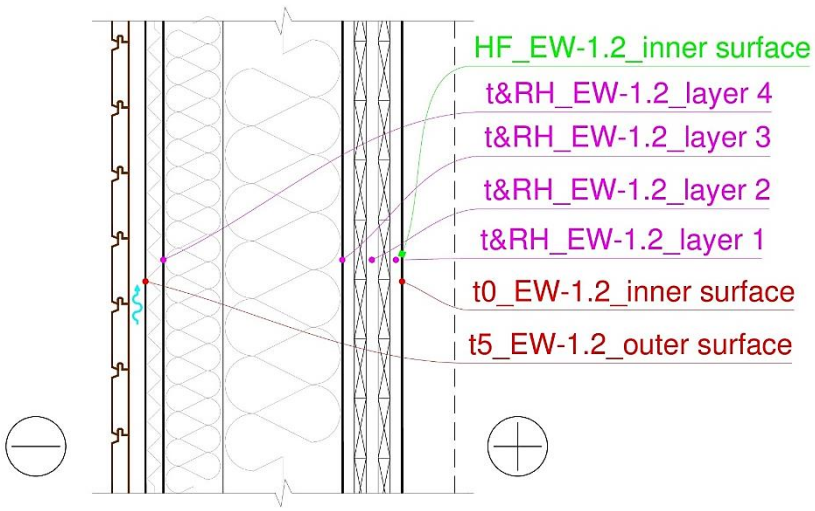

Figure 18. Example of sensor placement in a wall assembly (EW 1.2) (Technical drawing by V.Kukk, adjusted by author)

Figure 19. Placement of the heat flux and surface temperature sensors on the inner surface of the test wall (Author's photo)

2.1.3 Conditions

Wall assemblies were installed in NZEB building, located in TalTech campus in Tallinn, Estonia. *(Figure 20)* Each type of walls was exposed both on North and South facades.

Figure 20. NZEB building in TalTech campus, Tallinn, Estonia (Author's photo)

The internal environment of house is quite constant - 21° C (24° C in summer), RH in winter is 30-40 % and up to 60 % in summer. As the experiment was first held for one year, it was experiencing external environment of Estonian climate conditions through all four seasons. Graphical illustrations of relative humidity and temperature changes inside and outside the test room are shown in *Figures 21 and 22 (Test room 7, North)* and in *Figures 23 and 24 (Test room 8, South)* for a period of 13 months, where the outdoor RH is measured by local weather station in Tallinn-Harku and the outdoor temperature measured on outer surface of wind barrier.

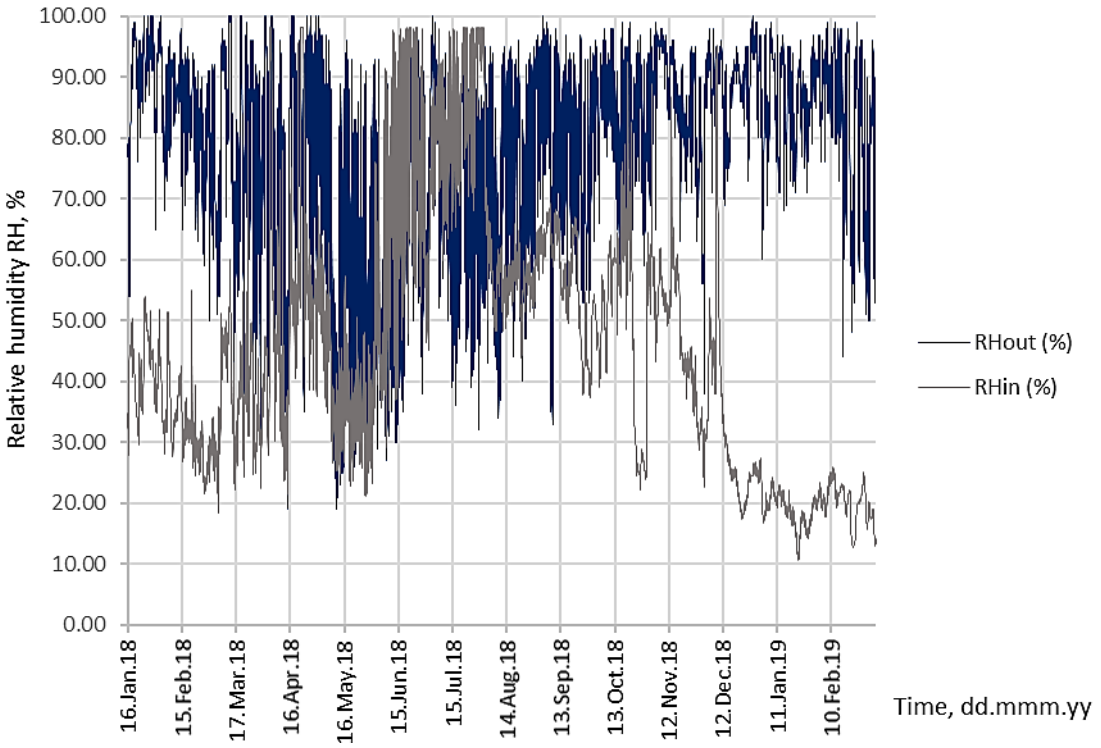

Figure 21. Boundary conditions, indoor and outdoor relative humidity in test room No7 (North). (Author's illustration)

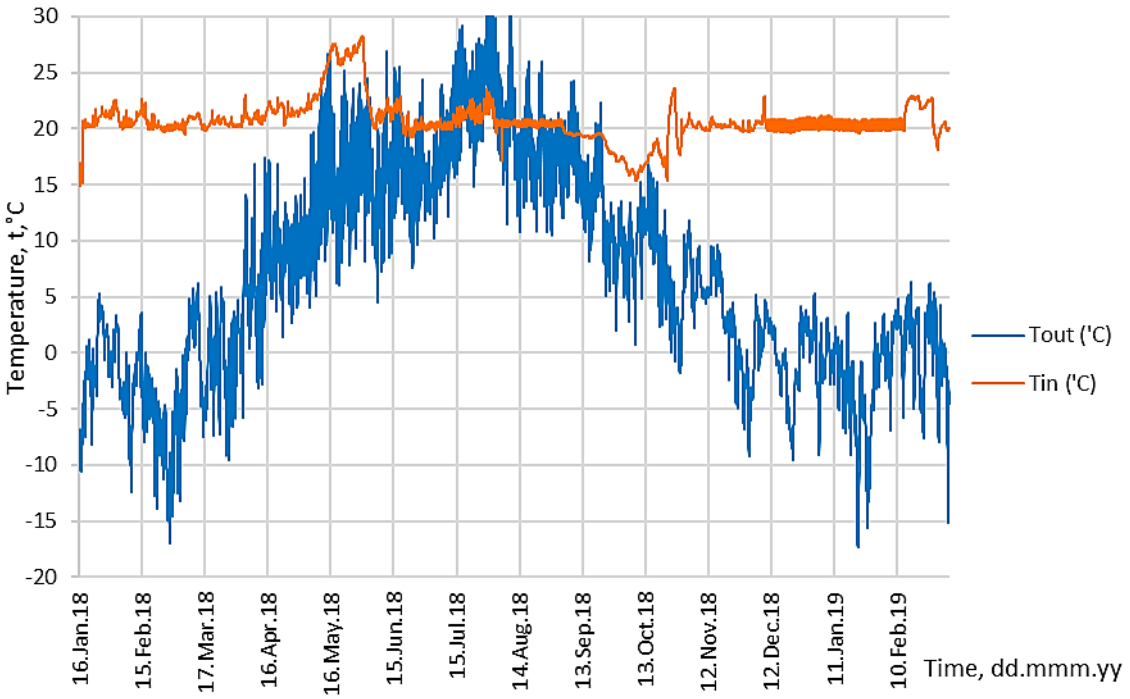

Figure 22. Boundary conditions, indoor and outdoor temperature in test room No7 (North). (Author's illustration)

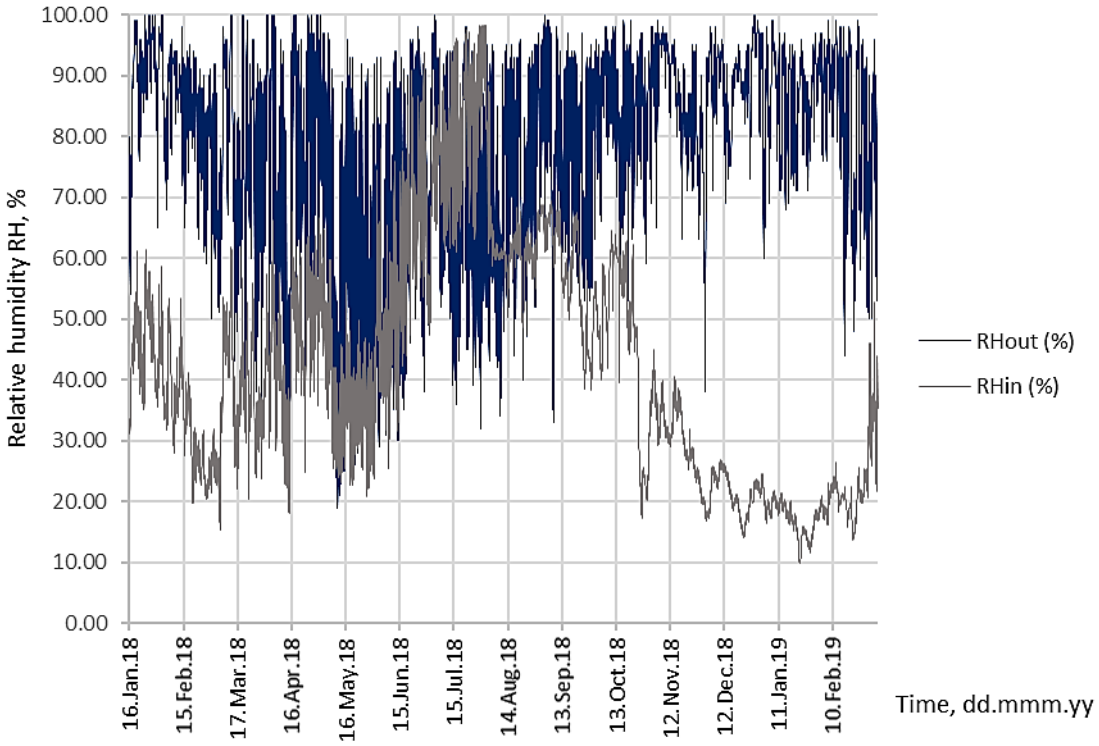

Figure 23. Boundary conditions, indoor and outdoor relative humidity in test room No8 (South). (Author's illustration)

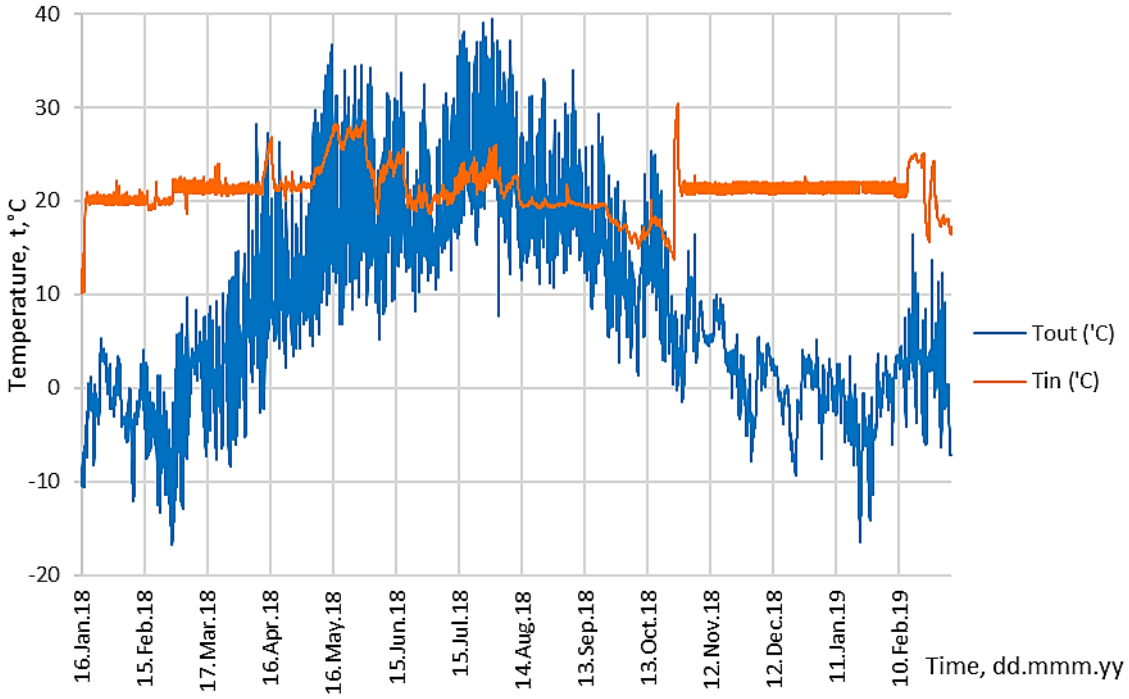

Figure 24. Boundary conditions, indoor and outdoor temperature in test room No8 (South). (Author's illustration)

2.2 Hygrothermal modelling

In order to analyse the data, there were gained results from computer modelling program Delphin 5.9.4, which were afterwards calibrated by the actual results, collected from sensors concerning the same parameters – temperature, relative humidity and heat flux. Partial pressure data was also gained by modelling, however the actual partial pressure data was calculated manually using measured data of temperature and relative humidity.

Delphin is a simulation program for the coupled heat, moisture, and water transport in porous building materials to analyse moisture movements, temperature, relative humidity and other parameters both inside the structure and on the top surfaces (boundaries). Interior surface of the modelled walls had thermal resistance R_{SI} of 0.125 m^2K/W and water vapour diffusion resistance of $3 \cdot 10^{-8}$ s/m. For exterior surface the thermal resistance R_{SE} was 0.04 m^2K/W and water vapour resistance of $2 \cdot 10^{-7}$ s/m. For each material of the wall there were inserted their properties, shown in *Table 3*. A schematic illustration of what data is inserted and analysed and final outputs are shown in *Figure 25*.

The program provides a graph and the numerical data, which can be exported to Microsoft Excel where it can be further analysed.

Table 3. Properties of materials used in calculation model

Material	Thickness, d, mm	Bulk density, ρ, kg/m³	Thermal conductivity, Λ, W/(mK)	Water vapour resistance factor, μ	Water uptake coefficient, Kg/(m²s⁵)	Moisture storage capacity, RH 80%, m³/m³
Spruce (CLT)	100	418.8	0.11	474.725	0.0132732	$6.26 \cdot 10^{-2}$
Mineral wool insulation	300/200	37.0	0.035 (0.037)	1.0	0.00	$6.78 \cdot 10^{-5}$
Mineral wool wind barrier	30	100.0	0.033 (0.031)	1.0	0.00	$6.78 \cdot 10^{-5}$
Cellulose insulation	330	65.0	0.039	2.05	0.562862	$6.33 \cdot 10^{-3}$
PIR Kingspan insulation	200	38.0	0.022	104.0	0.0001	$1.1 \cdot 10^{-3}$

** In brackets indicated initial value before adjusting*

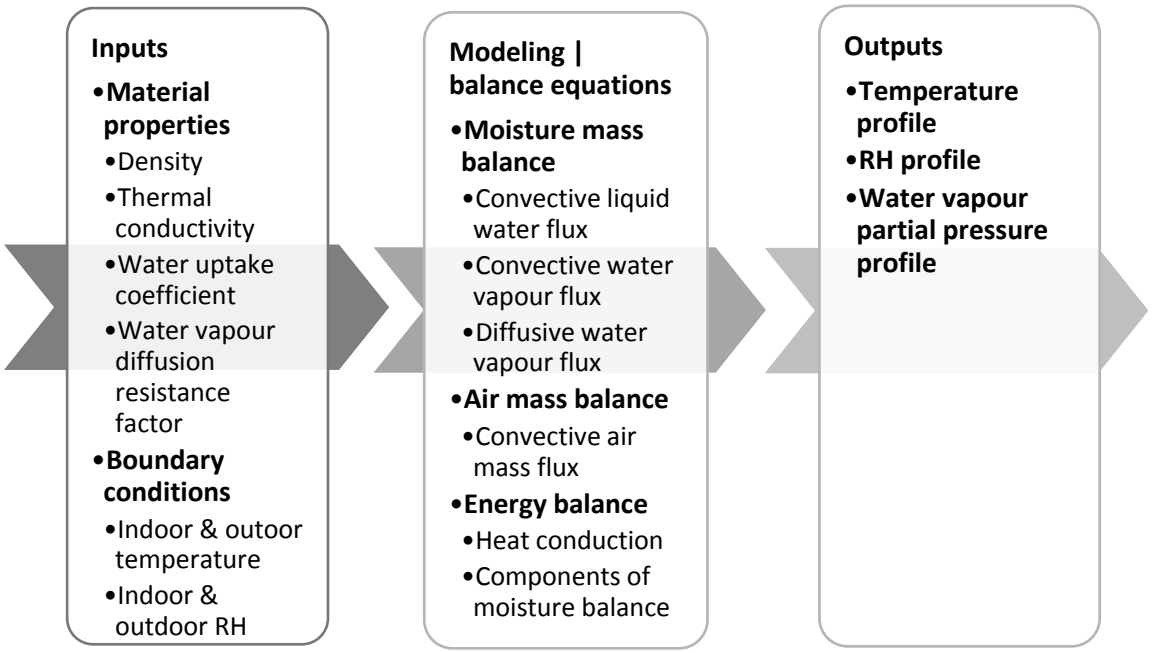

Figure 25. Scheme of data input, equations and outputs in modelling (Author's illustration)

2.2.1 2D simulation

As the 1D simulation did not give satisfying results, the wall structures were changed in 2D, adding an air gap, which was also an influential part of result change. For 2D modelling there was used a Delphin 6 version *(Figure 26).*

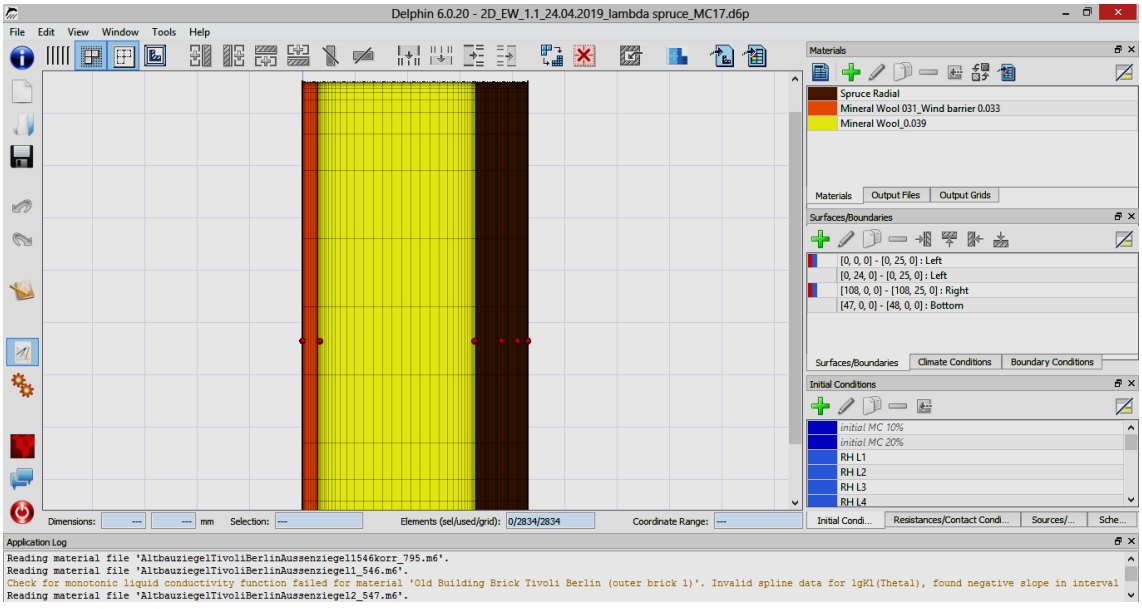

Figure 26. Screenshot of Delphin 6 simulation program.

2.2.2 Indoor and outdoor pressure difference

When considering the general air movement through wall assemblies, an intense ventilation may create an underpressure in the test rooms, which accordingly causes a pressure difference from indoors to outdoors. As the pressure is different, it tends to even the value between inside and outside, which then causes air movements through wall assemblies. A high pressure difference causes an air flow, which accordingly creates convectional moisture transport (moisture movement by air), which explains why values of RH in location 3 behaves similar to indoor environment. Calculation model, however considers only moisture diffusion (movement caused by vapour pressure through material cellular structure) from indoor to outdoor environment.

In order to assure an assumption of pressure difference between indoor and outdoor environment, which caused high differences between measured and calculated data of partial pressure and RH, there were held measurements for indoor and outdoor pressure differences. A schematic drawing and a picture of measurement points is visible in *Figures 27* and *28*.

In the graph of results *(Figure 29)*, there are showed measurements in 4 points, 2 of them in test room 7 and 2 in test room 8. In each room there is one measurement point in the upper level – in the middle of upper wall assemblies -, and one in lower level – in the middle of lower wall assemblies. Upper measurement point (MP) in test room 7 was held for a longer period of time, only after 10 days the rest of measurement points were added.

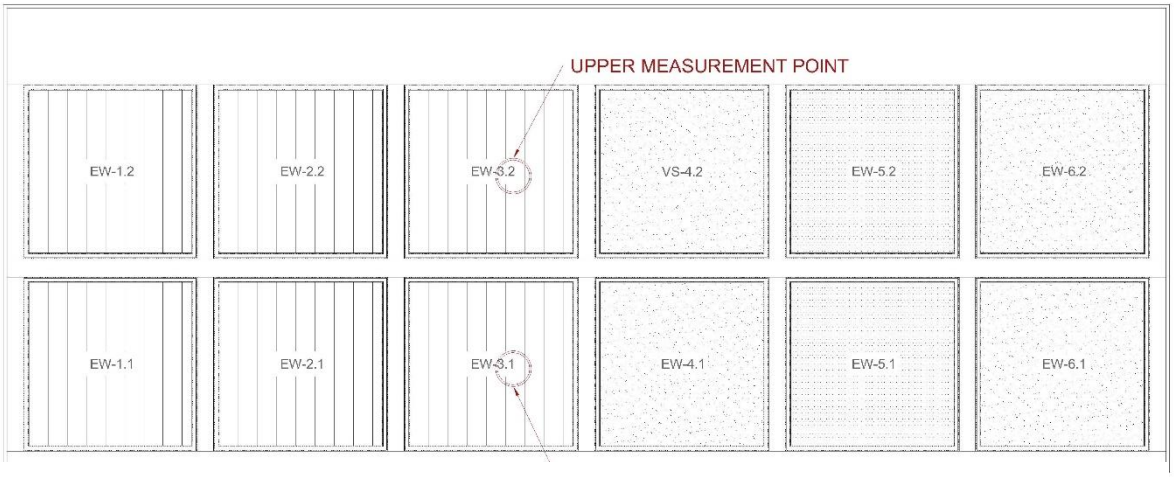

Figure 27. Scheme of measurement point placement in test room. (Technical drawing by V.Kukk, adjusted by author)

Figure 28. Picture of measurement point placement in test room. (Author's photo)

At first the measurements were held for 5 days, to see if there is an actual pressure difference. When the assumption was confirmed (average difference 19.6 Pa), the air flow rate was decreased on November 18th, by reducing both inlet and outlet of air, which already caused a decreased pressure difference and an average value of -9.3 Pa, where a higher pressure was in the test room.

On 22nd of November, when the other measurement points were added, the difference was still high, so the openings (inlet and outlet) were closed, in that case there was be no air flow at all.

As it is seen in the graph, from the final stage from 23rd of November until 2nd of December, the differences are decreased a little, but are still high. When looking at the average values, the smallest pressure difference is in the test room 7, the upper MP, and the biggest differences are in the test room 8, the upper MP.

As the differences are still high, the ventilation has to be stopped not only in test rooms, but also in the whole test house, as the air still travels through some small openings. The goal is to reach a difference of -5 Pa, which would be acceptable in order to even the measured and calculated results. As the pressure difference for entire measurement period is unknown, for modelling it was decided to use as a constant pressure difference of -20 Pa.

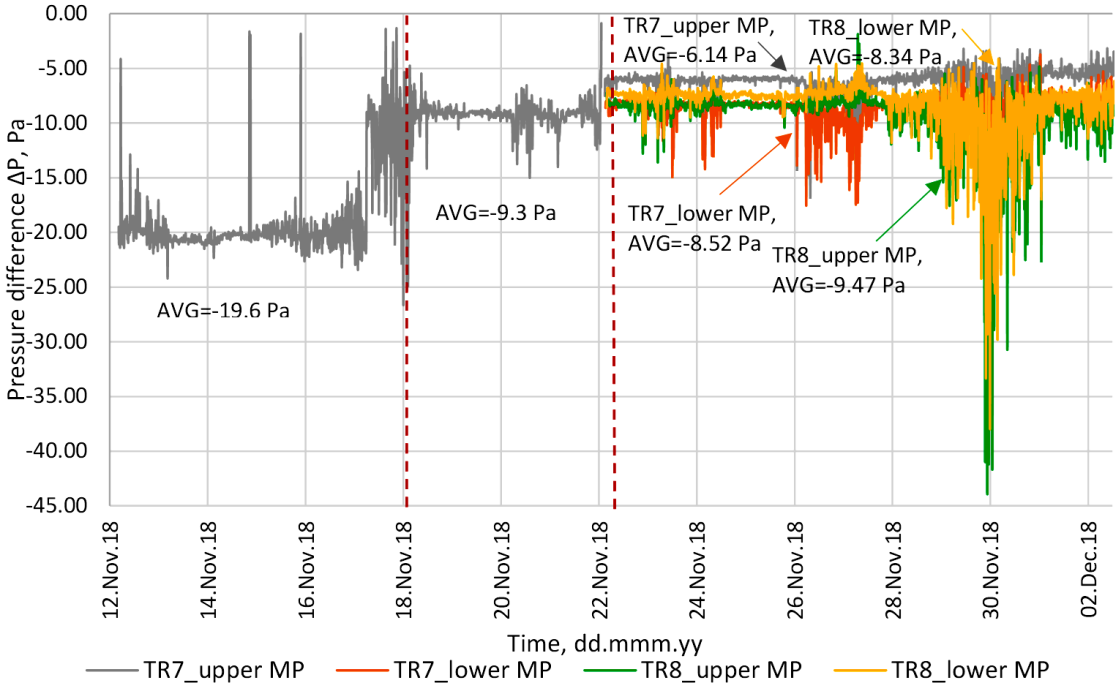

Figure 29. Graph of pressure difference between indoor and outdoor conditions (Author's illustration)

2.2.3 Evaluation criteria

To reach conditions beneficial for mould growth, there are 2 parameters to consider, temperature has to be in a range 0 °C-50 °C and critical relative humidity is estimated as a function of temperature (Viitanen, 2007) (Equation 4.1):

$$RH_{crit} = \{-0.00267\,T^3 + 0.160\,T^2 - 3.13\,T + 100.0\},\ when\ T \leq 20;\quad 80\%\ when\ T > 20 \tag{4.1}$$

To visually show how close to mould growth risk are the RH and T results, there can be created graphical illustrations using the described function (4.1), showing a critical line *(green line in Figure 30)*, above which a risk of mould growth starts. All wall types are analysed this way in *paragraph 4.1*. In this analysis, however, there is not considered the exposure time and material sensitivity.

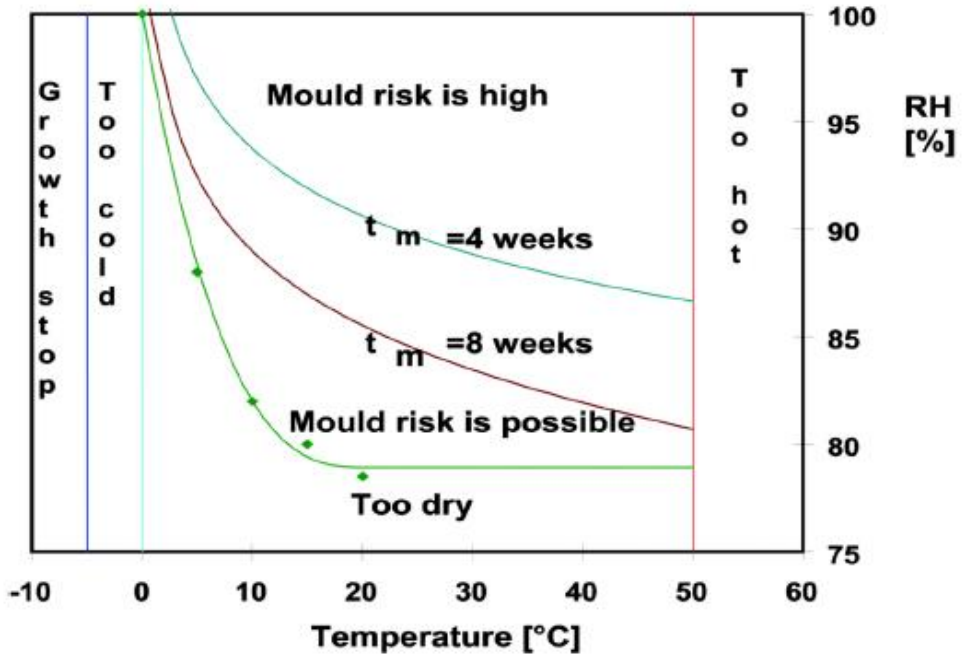

Figure 30. Overall conditions favourable for mould growth on wooden material as a mathematical model (Hukka and Viitanen 1997)

3 RESULTS

The results gained from simulation model (CALC) were exported in graphs, where the values were compared to actual measured data (LAB) for temperature (T), partial pressure (P), relative humidity (RH) and heat flux parameters (q). Graphs of T, P_v and RH show data of gained either from sensors or simulation, placed in certain locations (L1; L2; L3; L4), where L1 is most inner and L4 is most outer location. The q was only measured on inner surface of each test wall. All average differences between calculated and measured results are given in *Appendix 2*.

3.1 Test walls insulated with mineral wool (EW-1)

3.1.1 Field measurements and simulation of Northern side walls with initial MC of 13% (EW 1.1_N)

Temperature graph of EW 1.1_N *(Figure 31)* shows a comparison of measured and calculated data, where all locations follow up through all period of time with no major differences, however, the least of differences are in location 1, having average difference of 0.68 °C over the entire measuring period with a standard deviation of ±0.37 °C, and in location 2, ave. diff. of 0.84 °C with std. dev. of ±0.36 °C. Greater differences were observed in location 3, ave. diff. of 1.41 °C with std. dev. of ±0.53 °C, and in location 4, ave. diff. of 1.56 °C with std. dev. of ±0.68 °C.
When looking at the close ups, the average differences in warm period tend to align better, the ave. diff. of temperature varies from 0.76 °C (std.d.±0.31) to 0.91 °C (std.d. ±0.55). Nevertheless, in the cold period deviation in location 4 reaches 2.03 °C (std.d.±0.44) and 1.92 °C (std.d.±0.17) in location 3. In L1 and L2 the values are still similar as through the whole period of time, location 1 having ave. diff. of 0.62 °C (std.d. ±0.15) and location 2, ave. diff. of 0.92 °C (std.d. ±0.17).
As the location 4 is the most outer position of the wall, the temperature fluctuates from -15 °C to +30 °C, where the lowest temperatures are during January to March and the highest during July and August, which can also be observed in the close ups.
Temperature in locations 1-3 fluctuates from +15 °C to +30 °C following the same pattern, where the highest temperatures are observed in location 1, as the most inner one.

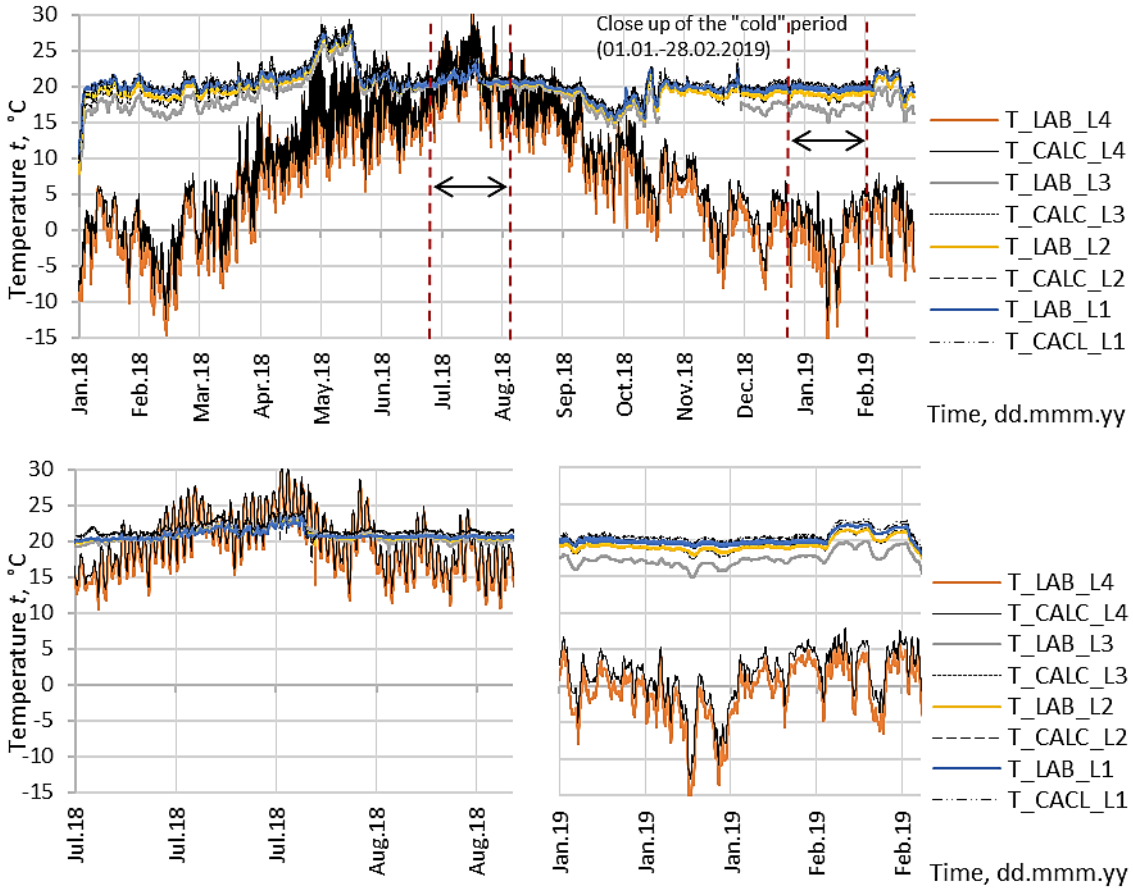

Figure 31. Temperature at locations 1-4, EW 1.1_N (Author's illustration)

Figure 32 shows data of partial pressure where calculated and measured data tend to align more only from the second half of the experiment period. However, the locations 3 and 4 act similar all through the period of time, especially the location 4 where the average difference is the smallest, 104.06 Pa with std. dev. of ±114 Pa and at location 3 – 114.71 Pa (std.d.±83). For locations 1 and 2, the differences are even higher and almost the same, location 1 having ave. diff. of 215.74 Pa with std. dev. of ±204 Pa and location 2 ave. diff. of 215.96 Pa (std. d.±267), which is also caused by high differences from the beginning until May.

The highest partial pressure can be observed in July, around 2500-3000 Pa and the lowest during the winter months when it decreases to around 250-1200 Pa if the second period of measurements is considered.

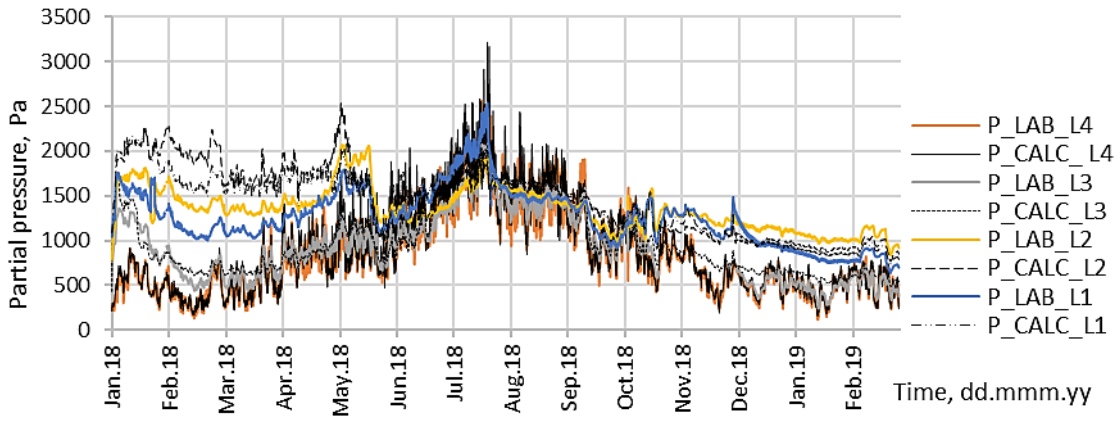

Figure 32. Partial pressure at locations 1-4, EW 1.1_N (Author's illustration)

The results of relative humidity are shown in *Figure 33*, where almost all the locations show quite different data from measured to calculated. The most aligning data considering the fluctuations is in location 4, however the average differences are the highest – 8.73 %RH with std. d. of ±6.23 %RH. Location 3 also shows quite similar data all through the period of time and has the least of the differences between calculated and measured data – 3.91 %RH (std.d.±3.05), although the measured data fluctuate much more than the calculated. Locations 1 and 2 show quite different data from measurements, especially in the period until July. The overall average differences are almost as high as in L4, ave. diff. in L2 is 8.57 %RH (std. d. ±10.32), and for L1 is 7.98 %RH (std.d ±7.43).

When looking at the close ups, the differences are quite different, except for location 4, where average difference for both warm and cold period still stays in the range of 8.69 %RH (std.d. ±5.56) to 9.25 %RH (std.d ±5.56).

During the warm period, the most similar data is at L2, where the ave. diff. is 1.76 %RH with std. d. of ±1.11 %RH, then location 3, 4.17 %RH (std.d ±2.81) and finally L1 which is almost the same through all the period – 7.18 %RH (std.d. ±4.59).

During the cold period, differences in locations 2 and 4 are the highest, where in location 2 the ave. diff. now is 7.31 %RH (std.d.±1.11). Difference in L3 is almost the same as through the all period, having ave. diff. of 3.57 %RH (std.d. ±2.81) and the location 1 having the smallest difference, ave. diff. 1.34 %RH (std.d. ±4.58).

Lowest values of RH are reached during February to June, where the lowest RH is in location 3, around 30 % and around 40-70 % in location 4. The same tendency seems to repeat starting from October, when the outdoor temperature is also decreasing. Highest values are reached during July to October, when the values generally vary from 40-90 %. Highest RH is in location

4, where it constantly exceeds 80 % of RH, which is critical for mould growth. The rest of the locations mostly do not exceed 70 % of RH.

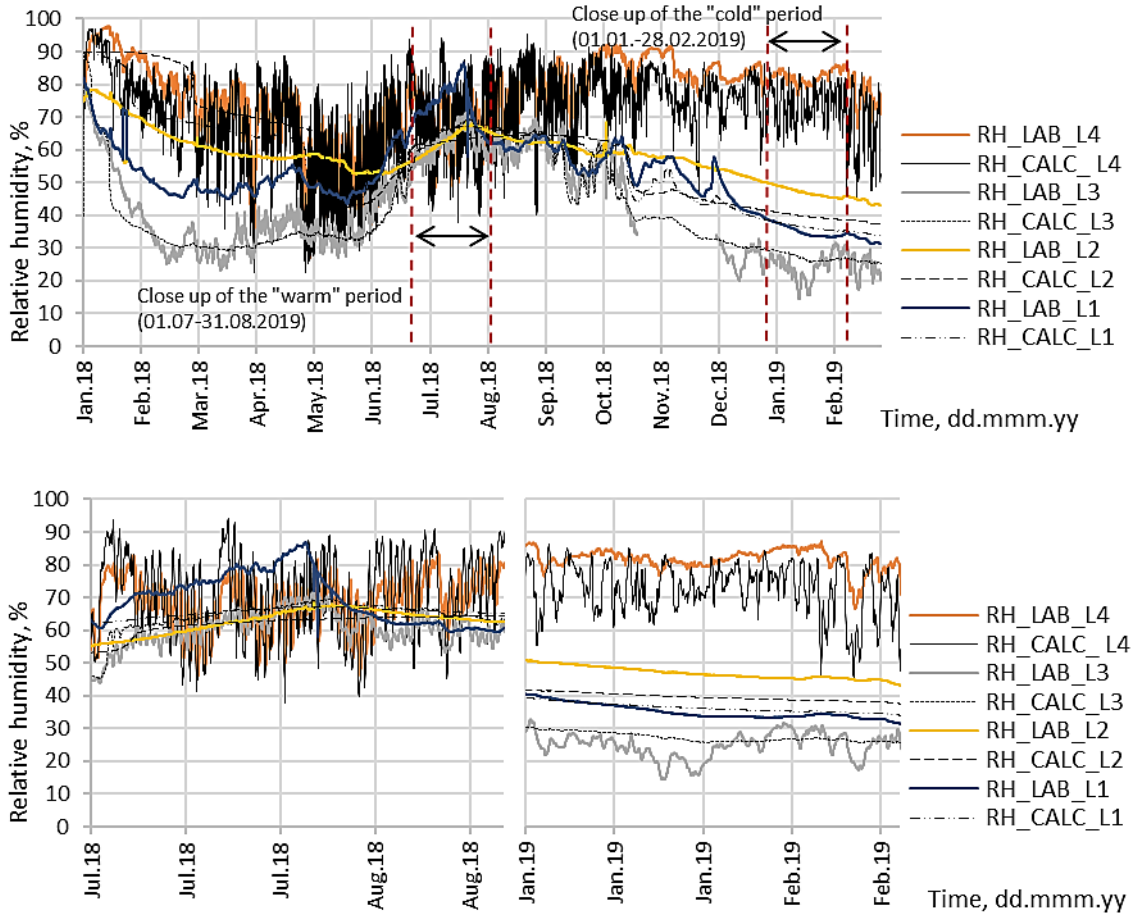

Figure 33.Relative humidity at locations 1-4, EW 1.1_N (Author's illustration)

When talking about the graph of Heat flux of wall EW 1.1_N *(Figure 34),* the calculated results vary much more than the measured ones, where the LAB values tend to increase in time, but the calculated values slightly decrease at the same time. Average calculated q is 3.28 W/m^2 (std.d.±3.05), while average measured value is almost 2 times smaller – 1.92 W/m^2 (std.d.±1.27) and the average difference measured and calculated data is 1.88 W/m^2(std.d.±1.27). Calculated q reaches values up to 25 and even 30 W/m^2, while measured values reach only maximum 7 W/m^2.

When considering thermal transmittance from q values, average thermal transmittance of calculated data is 0.44 W/m²K (std.d. ±0.90) and of measured data – 0.23 W/m²K (std.d. 0.44), where LAB value is closer to initially calculated thermal transmittance (0.10 W/m²K) considering materials and wall thickness.

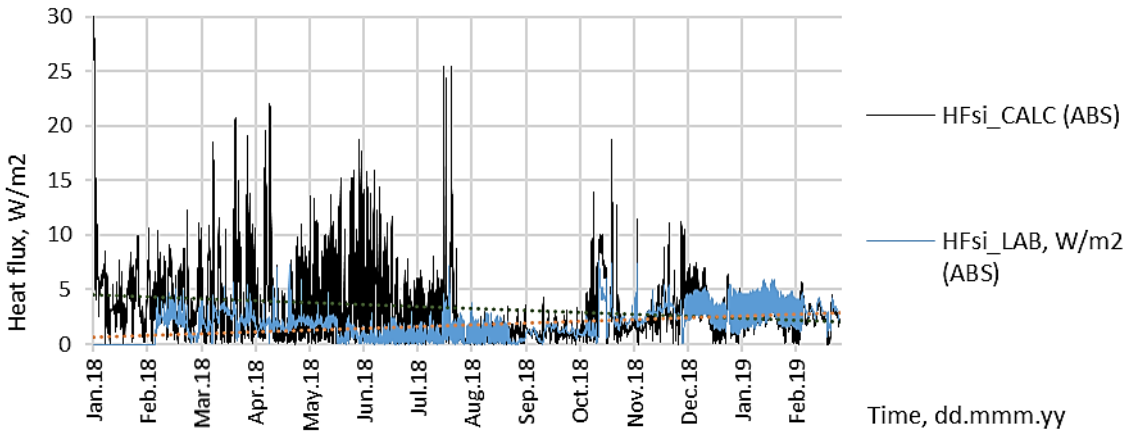

Figure 34. Heat flux of EW 1.1_N (Author's illustration)

3.1.2 Field measurements and simulation of Northern side walls with initial MC of 25% (EW 1.2_N)

Results of temperature values of EW 1.2_N *(Figure 35)* show quite precise alignment with no major differences of calculated and measured data. Generally, the highest variations trough all period are in location 4 with an ave. diff. of 1.06 °C with std. d. of 0.47 °C, followed by already minor differences of 0.5 °C (std.d.±0.34) in location 3, 0.49 °C with std. dev. of 0.27 °C in location 1 and an ave. diff. of 0.28 °C (std.d ±0.29) at location 2.

When looking at the close ups, average differences vary only in a range from 0.29 °C with std. dev. of 0.29 °C to 0.62 °C (std.d. ±0.32) in all locations. During the cold period, highest ave. diff. of 1.35 °C with std. dev. of 0.28 is in location 4, then, half as little in location 3, ave. diff. of 0.67 °C (std.d ±0.14) and 0.5 °C (std.d. ±0.15) in location 1. Almost no difference, 0.09 °C (std.d. ±0.05) in location 2.

Similarly, as for EW 1.1_N, the results of location 4 fluctuate the most and vary from -15 °C to +30 °C, where the lowest temperatures are reached during January to March and the highest during June to September. Meanwhile the locations 1-3 follow the same pattern and vary around +15 °C to +30 °C degrees as they are located more towards indoors.

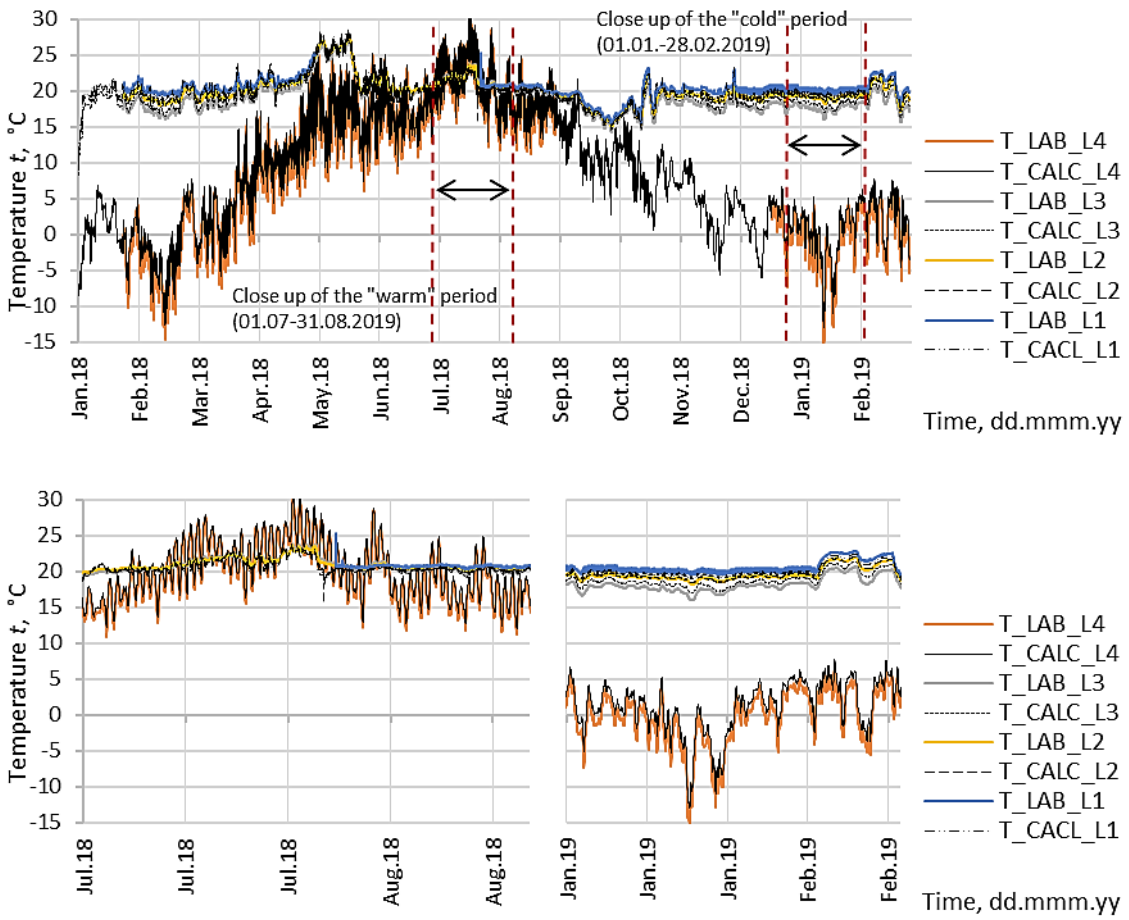

Figure 35. Temperature at locations 1-4, EW 1.2_N (Author's illustration)

Figure 36 shows the results of measured and calculated values of partial pressure, where the measured and calculated results align better than in EW 1.1_N, having no major difference in the starting period. However, the average differences are the same and even bigger. Location 3 and 1 align the most, having ave. diff. of 110.35 Pa (std.d ±79) in L3 and ave. diff. of 89.96 Pa (std.d. ± 81) in location 1 and following more or less the same patterns. Partial pressure in L4 also follow the same fluctuations, however, the difference is still high, ave.diff of 118.33 Pa (std.d. ±125).Results in location 2 also follow the same fluctuations, but the difference is quite constant all through the period, ave diff. of 217.88 Pa (std.d. ±115).

In general, the partial pressure values vary from 250-3000 Pa, having the most fluctuations in location 4 and the highest values for all locations are reached during the period of June to September, when it reaches around 1000-3000 Pa. Lowest values are registered during winter periods, when partial pressure does not exceed 1200 Pa.

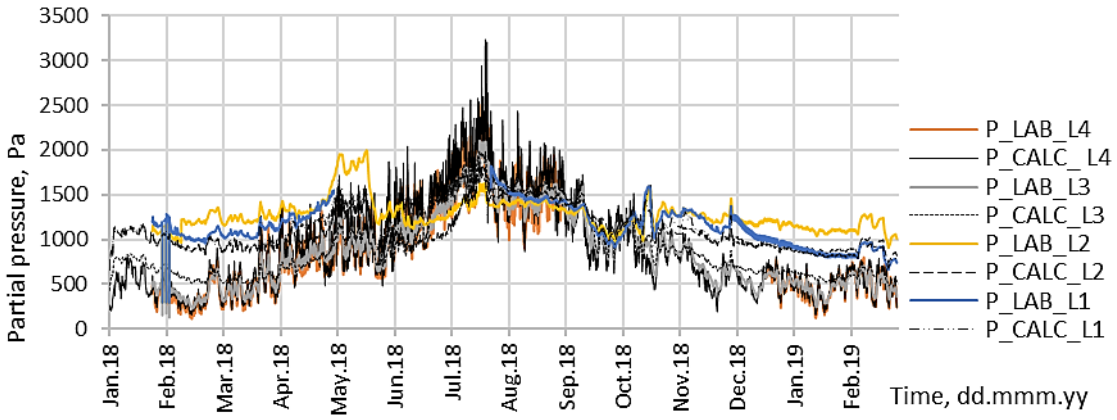

Figure 36. Partial pressure at locations 1-4, EW 1.2_N (Author's illustration)

To analyse RH of EW 1.2_N (Figure 37), in all the locations measured and calculated results more or less align, although the fluctuations are different, generally measured data is less stable. Greatest average difference all through the period is in location 2, 9.42 %RH with std.d of 3.94%RH. Then, already smaller difference is in location 4, ave. diff. 6.77 %RH (std.d. 6.47) and similar differences in locations 3 and 1, having ave diff. of 4.77 %RH (std.d ±3.63) in L3 and ave. diff. of 3.41 %RH (std.d. ±2.84) in L1.

To look at the close ups, average differences change more only in location 2. During the warm period highest difference is in L4, ave. diff. 7.32 %RH (std.d. ±4.96), then almost the same differences in L2, ave. diff. of 5.49 %RH (std.d. ±1.72) and L3, ave. diff. 5.13 %RH (std.d. ±3.29) and finally L1 with ave diff. of 3.47 %RH (std.d. ±1.64). It has to be noted that during the warm period location1 lacks more than half of data, which might also change average differences. During the cold period, differences stay the same for locations 3 and 4, but are much higher in L2, ave diff. of 10.03 %RH (std.d ±0.36) and much smaller in L1, ave. diff. of 0.82 %RH (std.d. ±0.45).

In general, locations 1-3 do not exceed 75 % of RH, while results in location 4 constantly goes above 80 % and reach up to 95 % of RH.

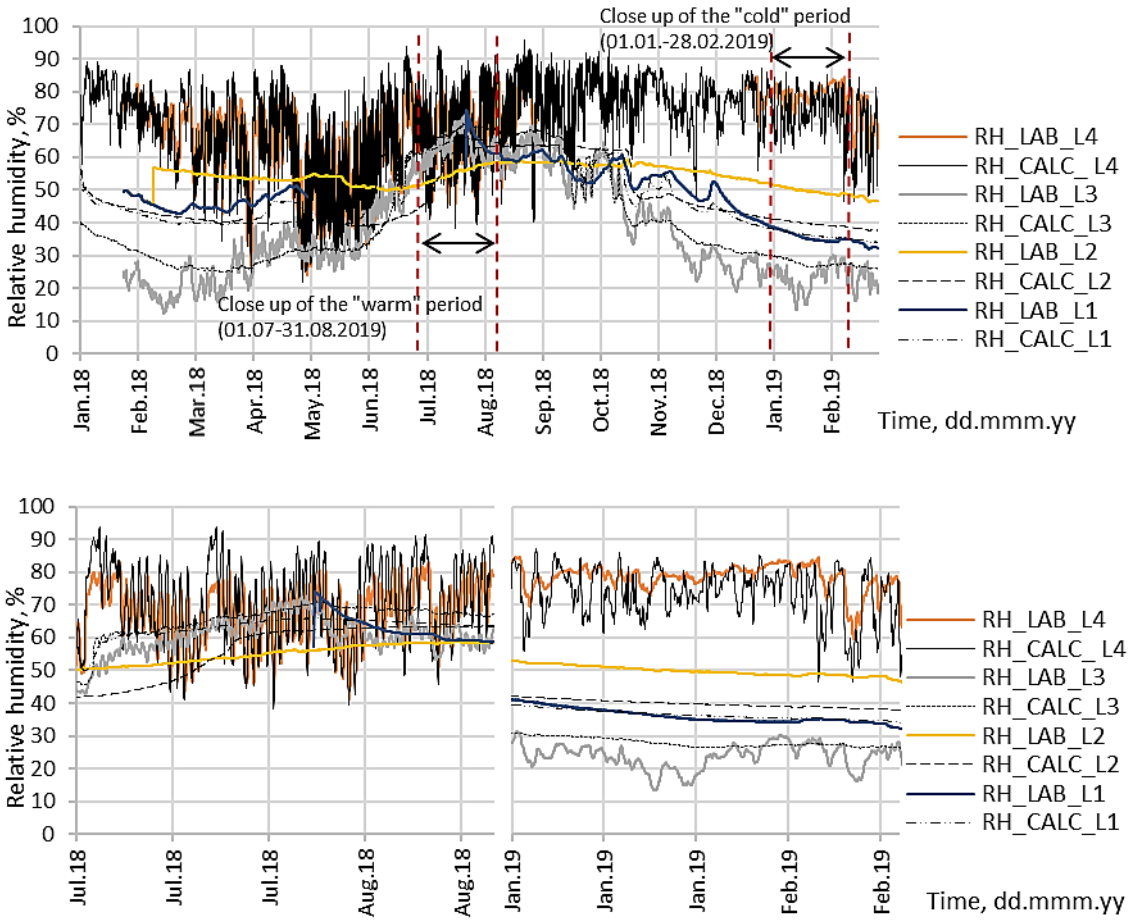

Figure 37. Relative humidity at locations 1-4, EW 1.2_N (Author's illustration)

To analyse graph of Heat flux *(Figure 38),* the calculated results again vary much more than measured ones, where calculate results slightly decrease in time, while measured results tend to increase. The maximum value reaches 23 W/m^2 for calculated data and does not reach more than 7 W/m^2 for measurements. Average value of calculated q is 3.04 W/m^2 (std.d. ±2.77) and 1.81 W/m^2 (std.d ±1.35) for measured values. Average difference between calculated and measured values is slightly higher than for EW 1.1_N, ave. diff. of 1.95 W/m^2 (std.d. ±2.41).

When considering thermal transmittance, measured value is closer to estimated value before (0.10 W/m^{2}K), it is 0.24 W/m^{2}K (std.d ±0.57), however the calculated value is still much higher, 0.47 W/m^{2}K (std.d 1.00).

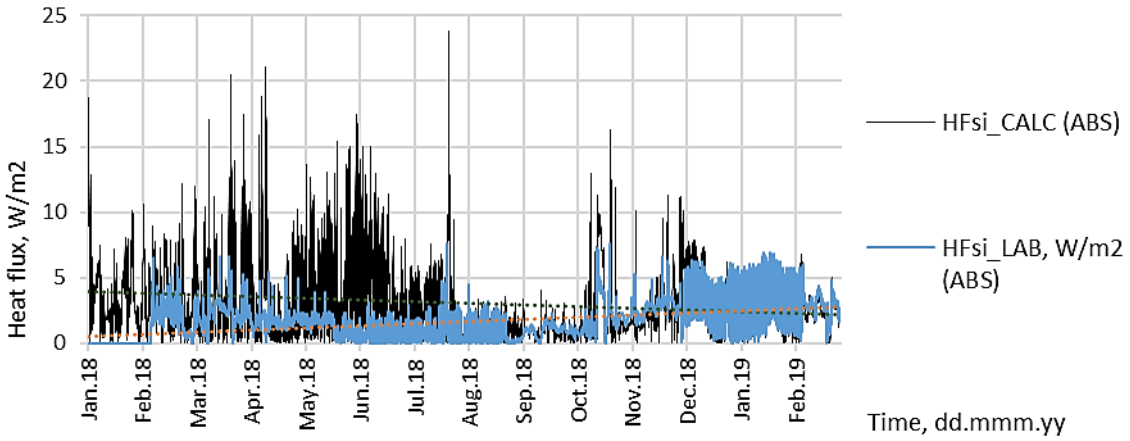

Figure 38. Heat flux of EW 1.2_N (Author's illustration)

3.1.3 Field measurements and simulation of Southern side walls with initial MC of 13% (EW 1.1_S)

Results of temperature values of EW 1.1_S *(Figure 39)* show an alignment of calculated and measured values, where the maximal deviations can be observed in location 4, where the average difference is 1.30 °C with std.d of 0.65 °C. However, the pattern of fluctuations in all locations follows very good through all period of time. Much smaller differences can be observed in location 3, 0.55 °C (std.d. ±0.36), in location 2, ave.diff. 0.35 °C (std.d. ±0.29) and in location 1, 0.27 °C (std.d. ±0.28).

To analyze the results from close ups, in the warm period, average difference varies in a range of 0.23 °C (std.d.±0.26) to 0.7 °C (std.d. ±0.66). In the cold period, difference in L4 is higher, 1.83 °C (std.d. ±0.33), then also higher in L3, ave. diff. 0.9 °C (std.d. ±0.14), and even smaller in L2, 0.48 °C (std.d. ±0.12) and in L1, 0.13 °C (std.d. ±0.07).

Similarly as for the other test walls, the results of location 4 vary the most, where the lowest temperature drops down to -15 °C in February and highest - reaches +35 °C in July. Locations 1-3 follow the same pattern and vary from +12 °C to +27 °C, as they are placed more towards the indoor environment.

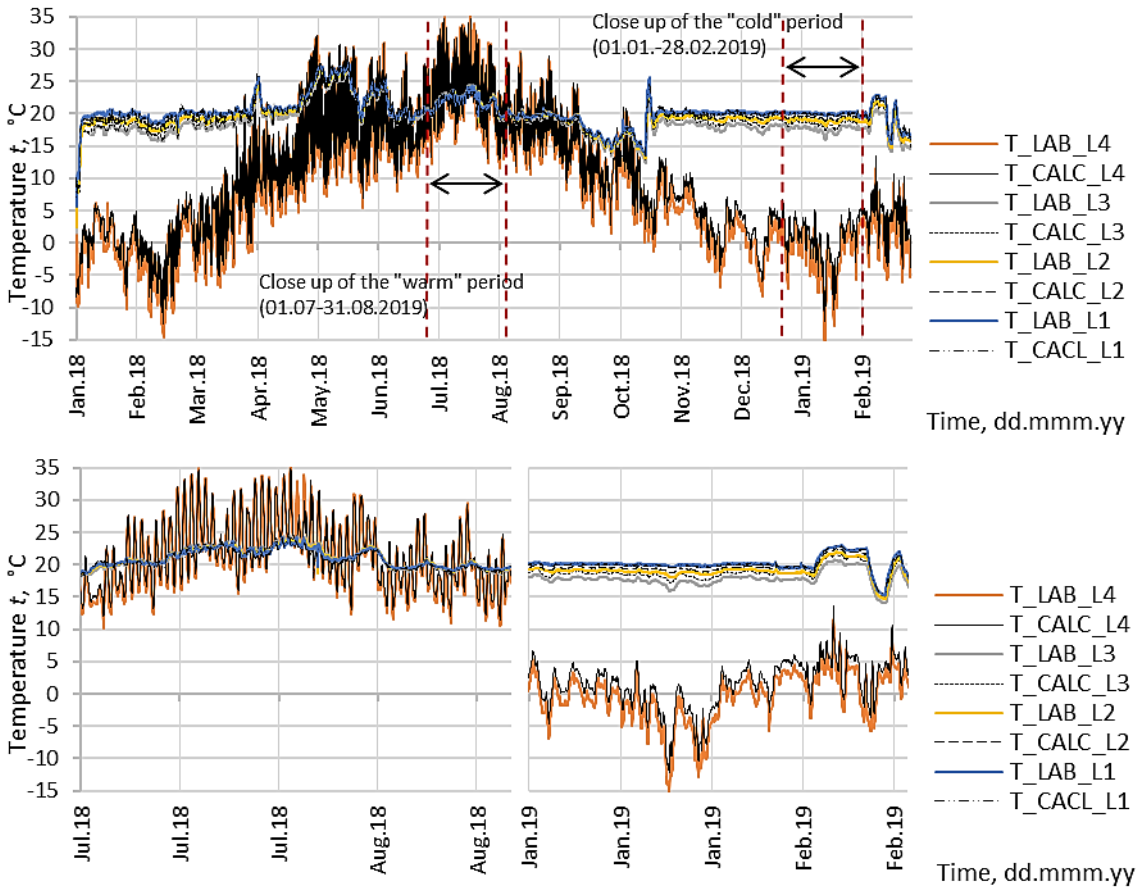

Figure 39. Temperature at locations 1-4, EW 1.1_S (Author's illustration)

Figure 40 shows calculated results and measurements of partial pressure, where it can be noted that most of the lines align with no major differences or errors. Average differences between calculated and measured data are almost the same in all locations, varying in a range of 131.85 Pa (std.d. ±118) to 162.85 Pa (std.d. 140).

Generally, partial pressure values vary from 200-3500 Pa, where the most fluctuating is location 4, followed by location 3, having the lowest values in winter periods and the highest - in period of June to September. The results in locations 1-2 do not vary that much, being in the range of 800-2400 Pa with a tendency to decrease in the last months of experiment – November to January.

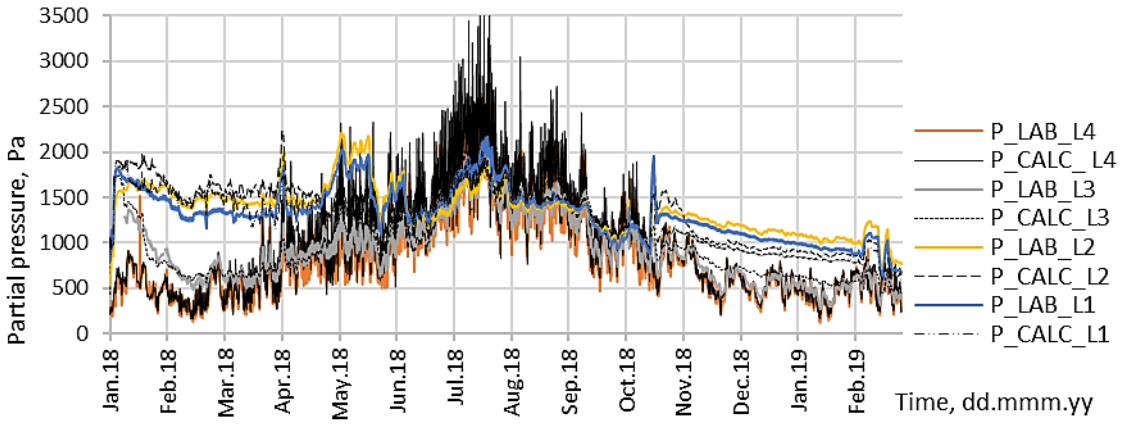

Figure 40. Partial pressure at locations 1-4, EW 1.1_S (Author's illustration)

To analyse RH results of EW 1.1_S *(Figure 41)*, it can be noted that all of the locations align with no major differences, however, the measured relative humidity in locations 3 and 4 tend to fluctuate more than the calculated data. Highest average difference can be observed in L4, 8.54 %RH with a standard deviation of 5.98 %RH, followed by similar differences in L3 to L1, varying in a range of 6.06 %RH (std.d. ±4.69) to 5.25 %RH (std.d. ±2.84).

When looking at the close up for warm period, average difference in location 4 is the highest, 11.71 %RH (std.d. ±6.47), followed by location 3, ave diff. of 10.79 %RH (std.dev. ±3.89), then much smaller differences in L2, 3.10 %RH (std.d. ±1.47) and in L1, 2.24 %RH (std.d. ±1.41). However, in the cold period, highest average difference is in location 2, 8.72 %RH (std.d. ±0.63), followed by ave. diff. of 7.81 %RH (std.d. ±5.58) in location 4, then location 1 with ave. diff. of 5.17 %RH (std.d. ±0.71) and the smallest difference in L3, 3.74 %RH (std.d ±2.71).

Generally, RH values vary from 15 to 95 %RH, having the lowest values during April to June, and the highest during July to October in locations 1 to 3, as the location 4 has constantly quite high RH, exceeding 80 %RH most of the experiment time.

Heat flux results of EW 1.1_S are showed in *Figure 42*, where calculated data vary much more and reach higher values than those of measured. As the calculated data tend to slightly decrease in the period of time, measured results slightly increase. Maximum value of CALC data reaches up to 30 W/m^2 with average value of 2.82 W/m^2 (std.d. ±2.68), which is already smaller than for the same wall types on North side, while the measurements reaches only up to 7 W/m^2 with average value of 1.63 W/m^2 (std.d. ±1.27).

Considering thermal transmittance, average value of measured data is closer to estimated (0.10 W/m²K), 0.22 W/m²K (std.d. ±0.52) and but still much higher for calculated data, having average value of 0.42 W/m²K, (std.d. ±0.92) which is slightly less when compared to walls on North side.

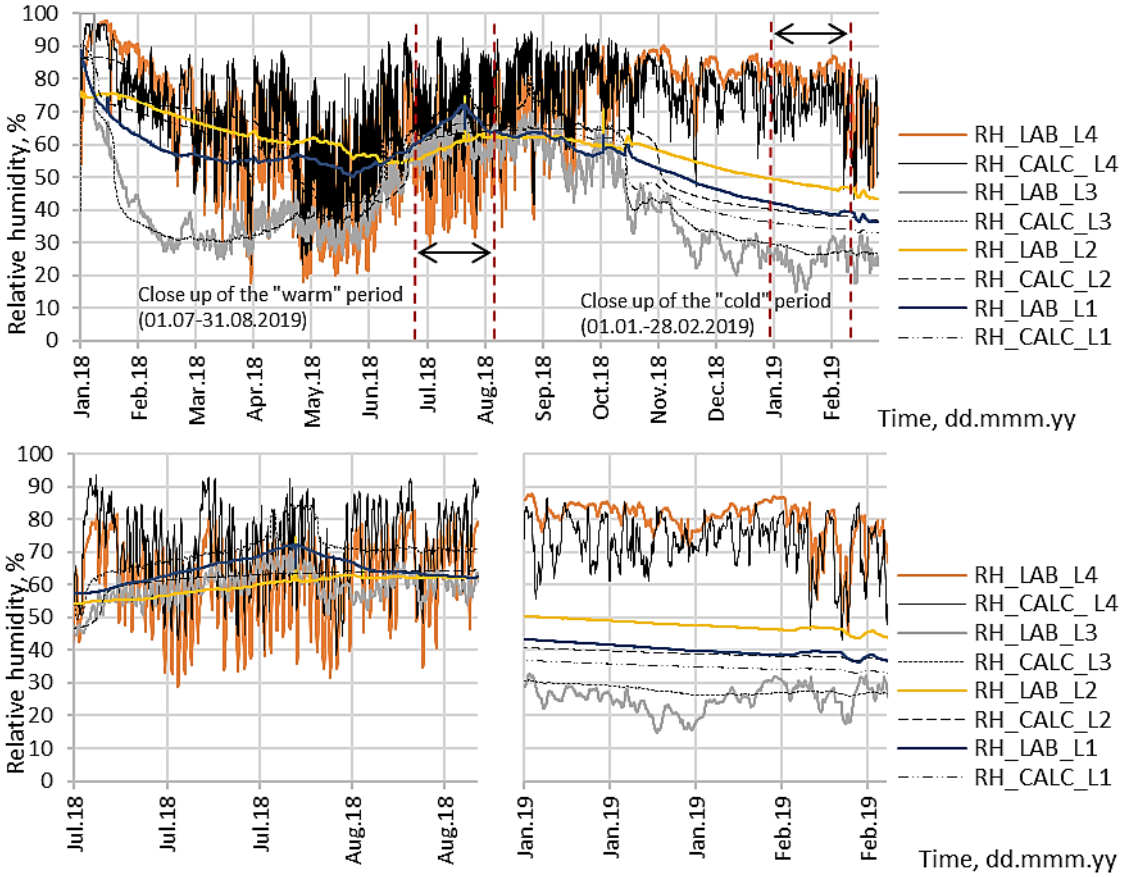

Figure 41. Relative humidity at locations 1-4, EW 1.1_S (Author's illustration)

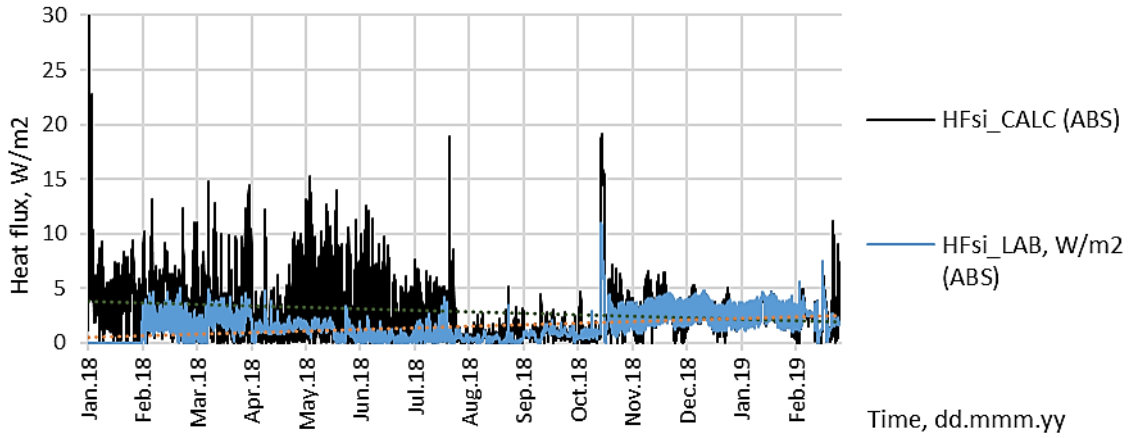

Figure 42. Heat flux of EW 1.1_S (Author's illustration)

3.1.4 Field measurements and simulation of Southern side walls with initial MC of 25% (EW 1.2_S)

Temperature graph of EW 1.2_S *(Figure 43)* shows that all of the locations align with the same fluctuations all through the period, except a lack of data in location 4 in the end period. The biggest difference can be observed in location 4, where the ave. diff. is 1.19 °C with std. d. of

1.01 °C, then smaller in location 3, 1.06 °C (std.d. ±0.48), location 2, 0.94 °C (std.d. ±0.43) and the smallest in location 1, 0.81 °C (std.d. ±0.37).

Average differences in close ups are not much difference from overall period. In the warm period, average difference values vary from 0.54 °C (std.d. ±0.3) to 0.76 °C (std.d. ±0.63). In the cold period, there is no data of location 4, but the difference in L3 is higher, 1.46 °C (std.d ±0.27), then almost the same high in location 2, 1.27 °C (std.d. ±0.27) and smallest in location 1, 1.01 °C (std.d. ±0.30).

Temperature varies mostly in location 4 from -14 °C in the winter months and up to +35 °C in the warm period, July and August. The locations 1-3 vary only a little, from +13 °C to +27 °C, as they are all located on the warm side of insulation.

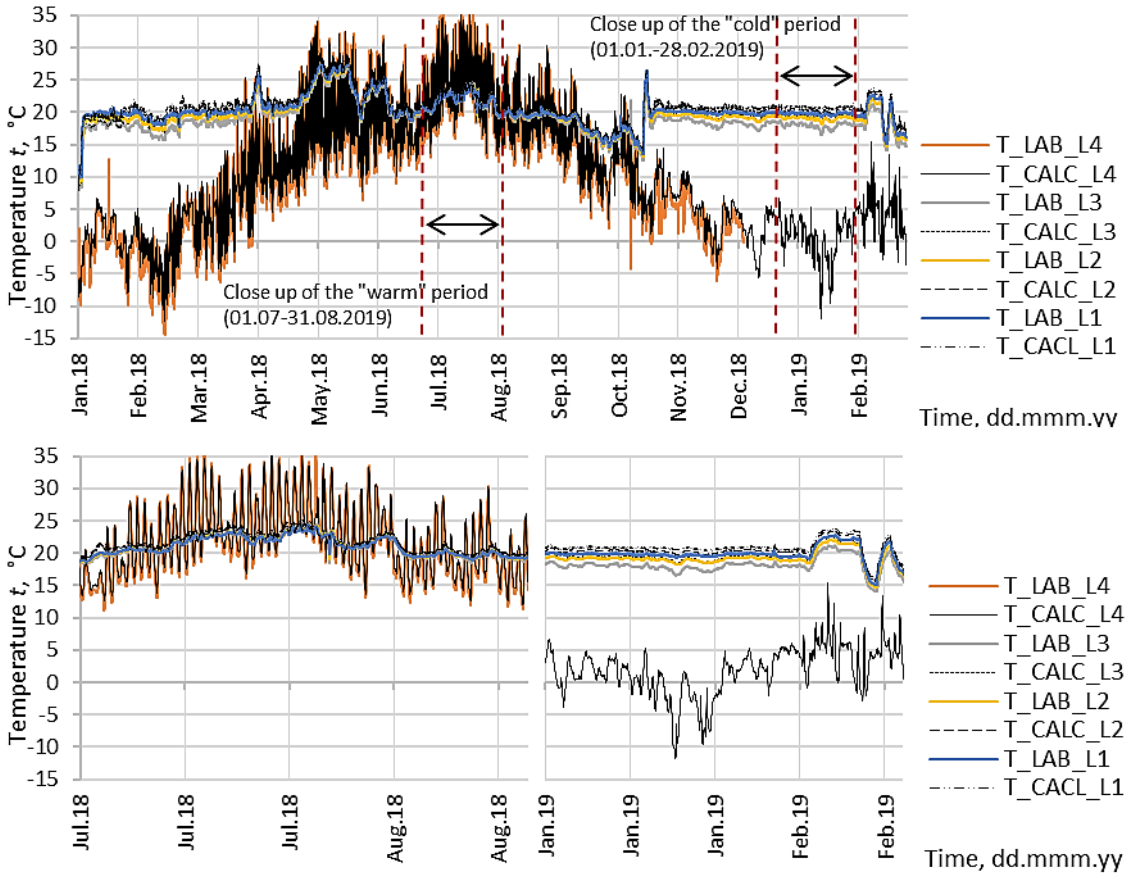

Figure 43. Temperature at locations 1-4, EW 1.2_S (Author's illustration)

Figure 44 shows measured and calculated data of partial pressure where all locations align with the same fluctuations, however the average differences are high, especially in location 3 and 4 where, ave. diff. of L4 is 201.64 Pa (std.d. ±217) and 199.16 Pa (std.d. ±145) in location 3. Lower differences are in location 2, ave diff. 158.41 Pa (std.d. ±102) and 160.69Pa (std.d. ±76) in location 1.

Generally partial pressure varies from 250 to 3500 Pa, where the highest values are reached in location 4 at the warm period, June to September, and the lowest values are in cold periods, January to April.

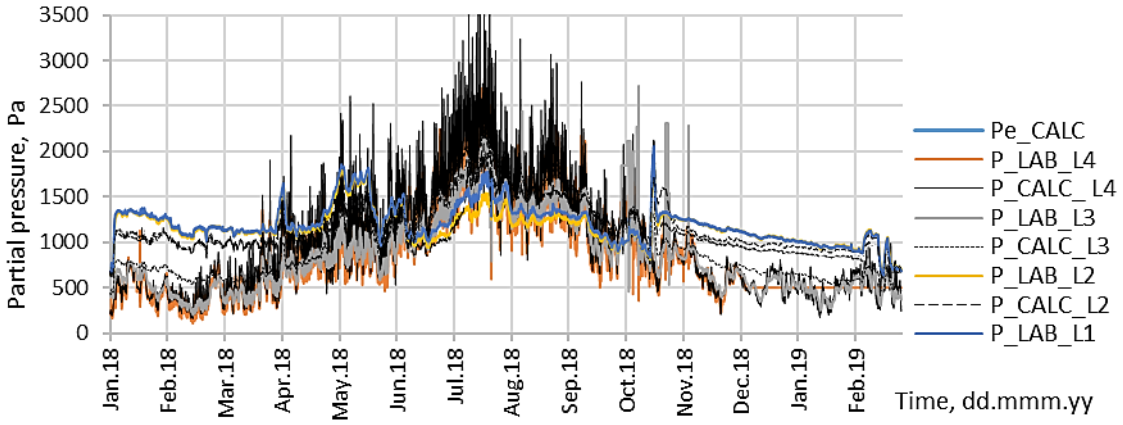

Figure 44. Partial pressure at locations 1-4, EW 1.2_S (Author's illustration)

The results of relative humidity of EW 1.2_S are shown in *Figure 45*, where it can be clearly seen that the line patterns do not align well, however, the average differences are only a little higher than for other walls. Highest differences are in location 4, where average difference is 9.73 %RH (std.d ±6.94), while the general average difference in the locations 1-3 vary in a range of 6.45 %RH (std.d ±4.44) to 7.99 %RH (std.d ±2.44).

When looking at the close ups, differences in L4 during the warm period are even higher, 12.9 %RH (std.d. ±7.15), followed by location 3, 9.15 %RH (std.d. ±3.85), then location 2, 8.36 %RH (std.d. ±3.67) and smallest difference in L1, 6.89 %RH (std.d ±1.53).

During the cold period differences are quite similar in all locations, except L4, where is no data in this period, with average difference in a range of 4.03 %RH (std.d ±2.91) to 6.85 %RH (std.d. ±0.8).

Overall RH ranges from 10 to even 100 % according to measurements, however the calculated values vary only from 22 to 94 %RH. Biggest fluctuations can be noticed in location 4, as it is the most affected by outdoor environment. Also, the location 3 measured values do fluctuate, but the calculated values there are more stable. Lowest relative humidity is during the winter and spring months, February to May, but the highest values are reached during period of July to October. Relative humidity in location 4 constantly exceeds 80 % and measured values even reach 100 %.

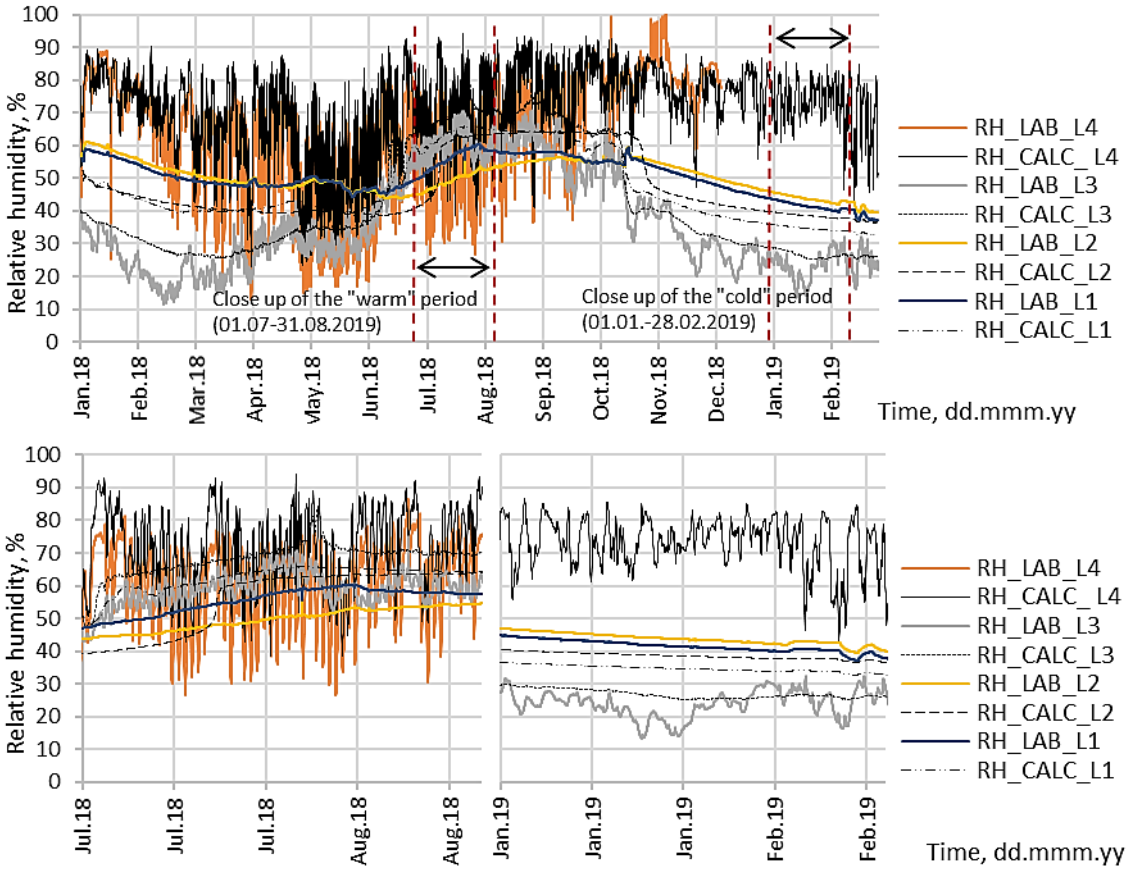

Figure 45. Relative humidity at locations 1-4, EW 1.2_S (Author's illustration)

In *Figure 46* there are shown calculated and measured values of heat flux, where the calculated values are higher than measured, but the maximum value, is lower than for other same type walls. Average value of calculated q is 2.72 W/m^2 (std.d ±2.51), while average measured q is 2 times smaller, 1.32 W/m^2 (std.d. ±1.09). Average difference between calculated and measured data is 1.84 W/m^2 (std.d ±2.01). When considering thermal transmittance, the measured average value is closer to estimated (0.10 W/m²K), 0.29 W/m²K (std.d. ±0.75) and the calculated average value is much higher, 0.40 W/m²K (std.d. ±0.91).

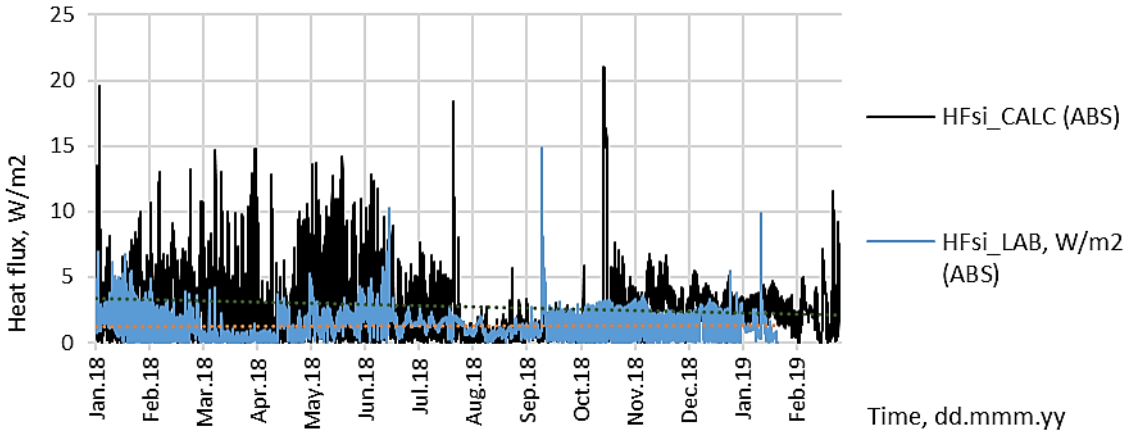

Figure 46. Heat flux of EW 1.2_S (Author's illustration)

3.2 Test walls insulated with cellulose (EW-2)

3.2.1 Field measurements and simulation of Northern side walls with initial MC of 13% (EW 2.1_N)

Temperature values of calculated and measured values of wall EW 2.1_N are showed in *Figure 47*, where the lines align with the same pattern, but some deviations can be noticed. The highest average difference is in location 4, 1.28 °C with standard deviation of 0.59 °C, then a smaller difference is in location 3, 0.96 °C (std.d. ±1.03) and minor differences in location 2, 0.51 °C (std.d. ±0.36) and in location 1, 0.39 °C (std.d. ±0.31).

When looking at the close up of warm period, as the location 2 lacks data, the highest difference is in location 4, 1.01 °C (std.d. ±0.6), then minor differences in L3, 0.35°C (std.d. ±0.37) and in L1, 0.38 °C (std.d ±0.31). During the cold period, highest average difference of 1.50 °C (std.d. ±0.28) is in location 4, then in location 3, 1.42 °C (std.d. ±0.29) and small differences in L2, 0.58 °C (std.d. ±0.19) and in L1, 0.28 °C (std.d. ±0.13).

Generally, temperature fluctuates from -10 °C to +30 °C, where the lowest and highest are reached in location 4, having low temperatures during January to March and the high ones during July and August. Temperature in locations 1-3 only from +14 °C to +27 °C, as it is closer to indoor environment.

To analyse partial pressure values of EW 2.1_N, *Figure 48* shows that in general partial pressure in locations 1 and 2 are higher in the first period until summer and then tend to align more with partial pressure in other locations. Highest average differences between calculated and measured data can be noticed in location 1, having ave. diff. of 130.36 Pa with std.d. of 138.95 Pa, then already smaller in location 2, 108.24 Pa (std.d. ±127), and almost the same in location 3, 94.20 Pa (std.d. ±70.41) and in location 4, 89.90 Pa (std.d. ±102).

Overall values of partial pressure vary from 250 to 3000 Pa, where the highest value is around 200-500 Pa lower than for other walls from type 1. Lowest values are reached during January to April and the highest, during July and August.

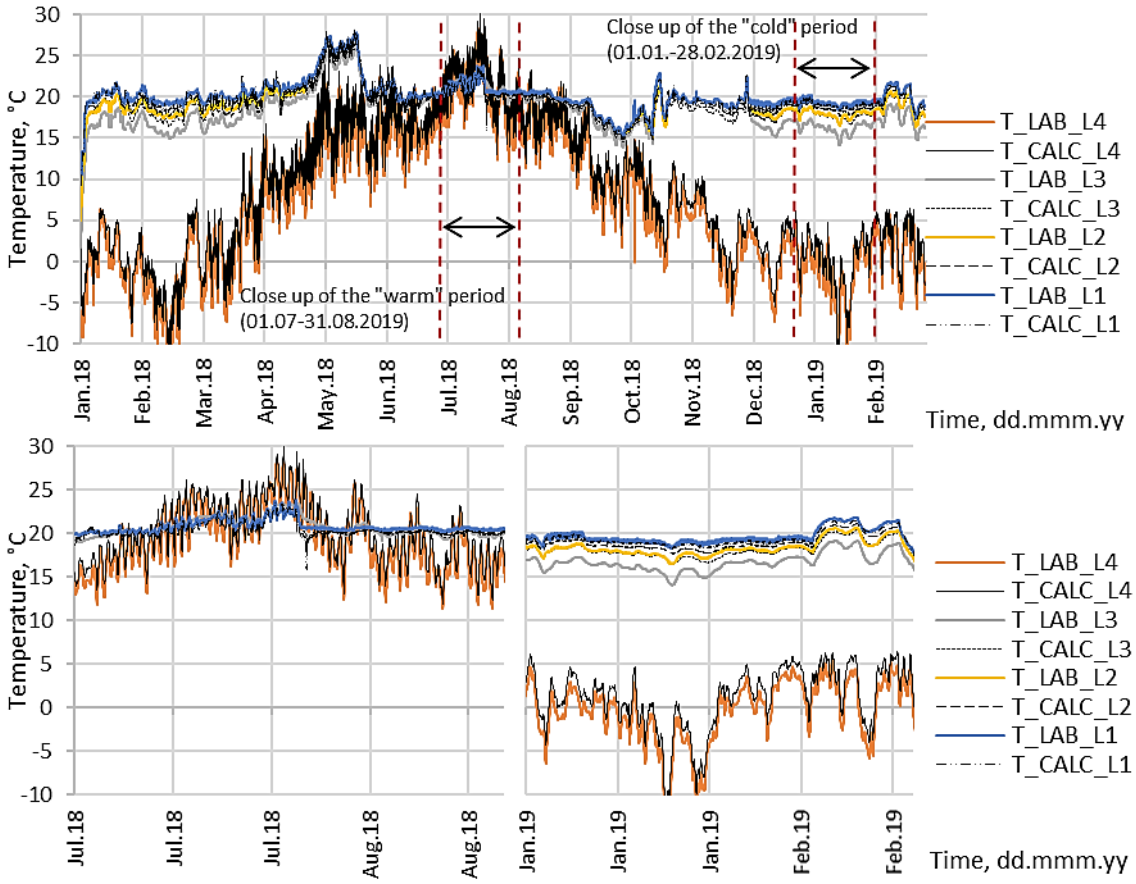

Figure 47. Temperature at locations 1-4, EW 2.1_N (Author's illustration)

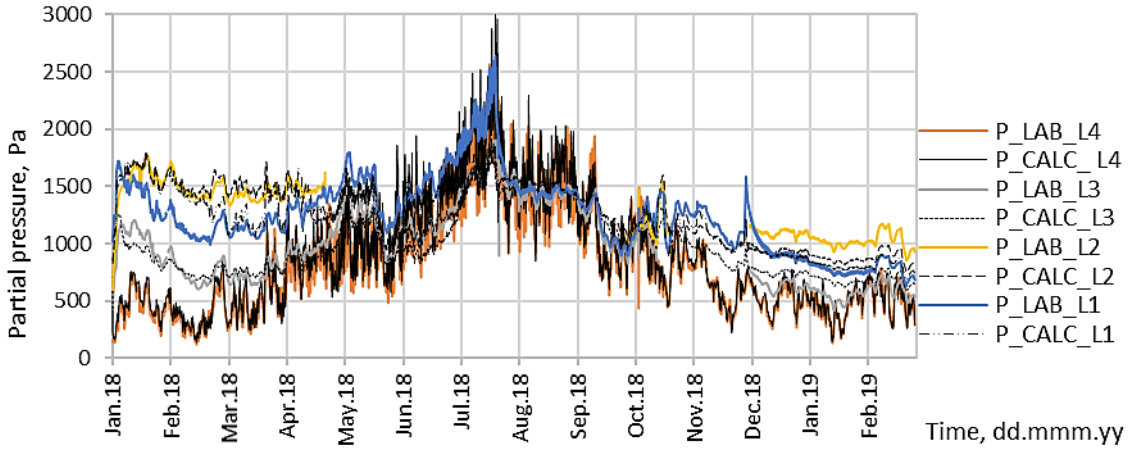

Figure 48. Partial pressure at locations 1-4, EW 2.1_N (Author's illustration)

Results of relative humidity are showed in *Figure 49*, where the calculated and measured values align more in the second half of experiment time. However, the average differences are generally lower than for walls of type 1. The average difference between calculated and measured data varies from 3.86 %RH (std.d. ±3.11) to 5.44 %RH (std.d. 4.39). During the warm period, there is a lack of data for location 2, but the only change of difference is in location 1,

reaching difference of 8.68 %RH (std.d. ±5.34). During the cold period, situation is again a bit different, where the highest average difference is in L2, 8.71 %RH (std.d. ±0.39), then 6.64 %RH (std.d. ±3.37) in L4, then already smaller differences in L3, 2.92 %RH (std.d. ±1.78) and in L1, 1.82 %RH (std.d. ±0.82).

Overall relative humidity is the lowest, around 25 to 35 %RH during cold months (January to April) and the highest during the summer period, up to 90 %RH. However, the highest measured values are in location 4, constantly exceeding 80 % starting from August.

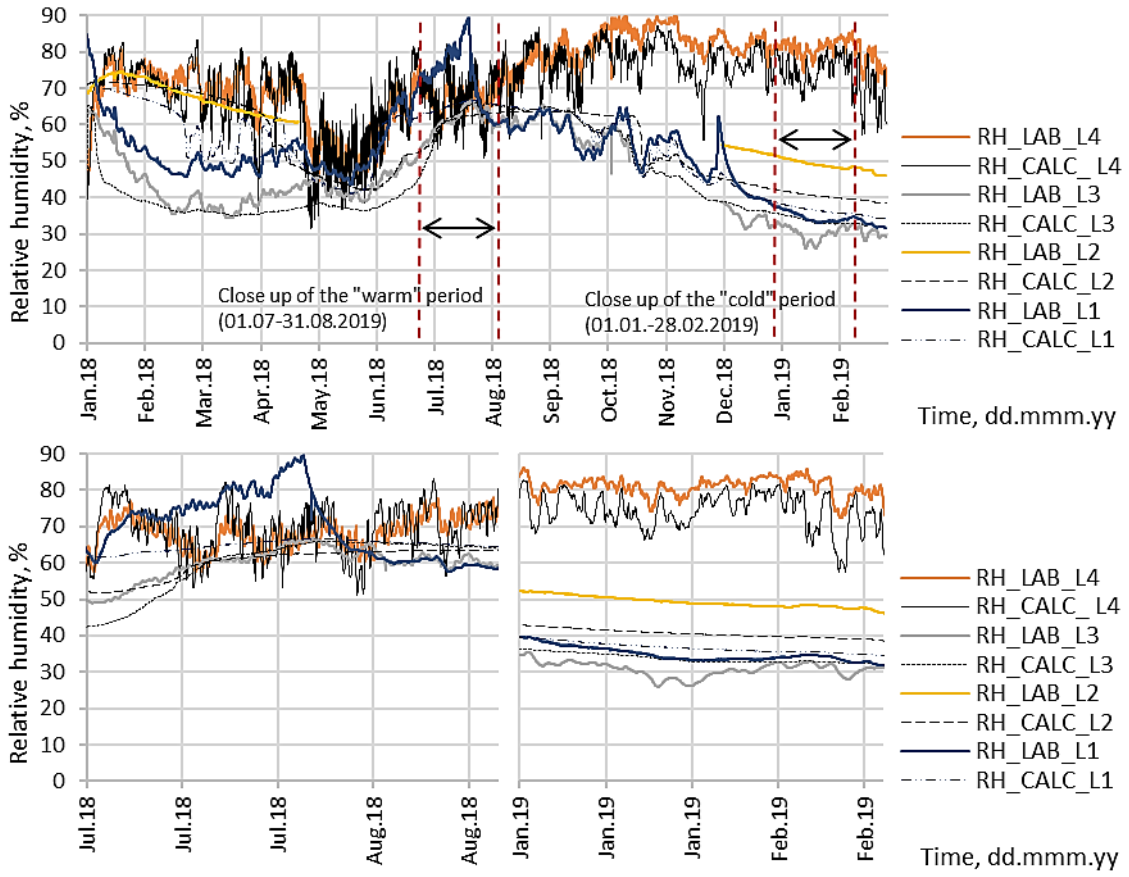

Figure 49. Relative humidity at locations 1-4, EW 2.1_N (Author's illustration)

Graph of heat flux of EW 2.1_N *(Figure 50)*, shows that the calculated values vary much more and reach higher values than the measured data, similarly as in the rest of the wall types. Maximum heat flux value of calculated data is 25 W/m^2, having average value of 3.09 W/m^2 (std.d. ±3.02) and the one of measured reaches only up to 9 W/m^2, with average value of 2.44 W/m^2, which is still quite similar to calculated value. Average difference between CALC and LAB heat flux is 1.89 W/m^2 (std.d. ±2.22). When considering thermal transmittance, the closet value

to estimated thermal transmittance (0.10 W/m^{2}K) is from measured data, 0.30 W/m^{2}K (std.d. ±0.58), while the calculated thermal transmittance is 0.44 W/m^{2}K (std.d. ±0.94).

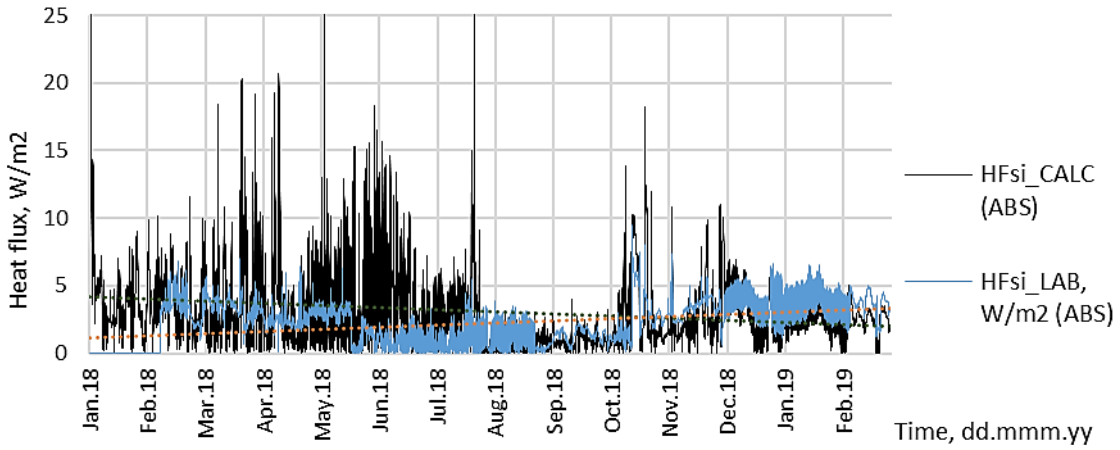

Figure 50. Heat flux at EW 2.1_N (Author's illustration)

3.2.2 Field measurements and simulation of Northern side walls with initial MC of 25% (EW 2.2_N)

Temperature results of calculated and measured data are shown in *Figure 51*, where both of results align with similar deviations as for other wall types. The average difference in all locations are quite similar and vary from 0.56 °C (std.d. ±0.31) to 1.00 °C (std.d. ±0.55). Similar also during the warm period, where the differences vary in a range of 0.51 °C (std.d. ±0.24) to 0.87 °C (std.d. ±0.71). During the cold period, difference range is a bit wider and the highest average difference is in location 3, 1.26 °C (std.d. ±0.12), then location 4, 1.08 °C (std.d. ±0.26), then, smaller in location 2, 0.90 °C (std.d. ±0.10), finally a minor difference in location 1, 0.43 °C (std.d. ±0.16).

Overall values of temperature vary from -10 °C to +35 °C, where the highest value is slightly higher than the walls of type 1 also located on North side. The lowest temperature values are during January to March and the highest during July and August, however these are achieved only because of location 4, where results vary the most. Temperature in locations 1-3 vary only between +13 °C to +27 °C.

Results of partial pressure of EW 2.2_N are shown in *Figure 52*, where result lines align better than for EW 2.1_N, however the average differences are higher here. The highest difference is in location 3 with ave. diff. of 191.87 Pa with std.d. of 90 Pa, then almost the same in location 4, 188.30Pa (std.d. ±204), smaller in location 2, 146.88 Pa (std.d. ±81) and the smallest in location 1, 119.14 Pa (std.d. ±80).

Overall values vary from 250 to 3500 Pa, which is the same as in the most of other walls. Lowest and highest values are reached in location 4, from 250 Pa during January to March to 3500 Pa

during July and August, where all through the period of experiment, calculated data shows slightly higher values than measured.

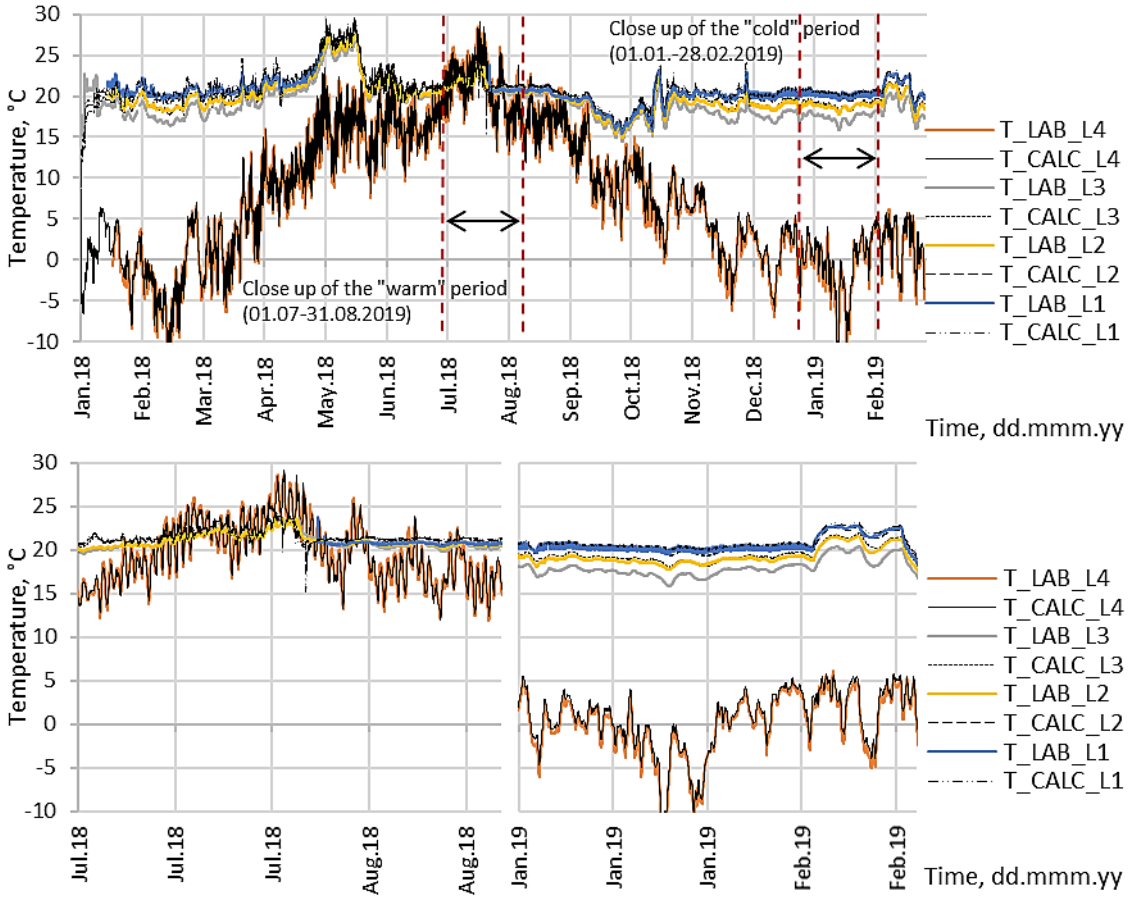

Figure 51. Temperature at locations 1-4, EW 2.2_N (Author's illustration)

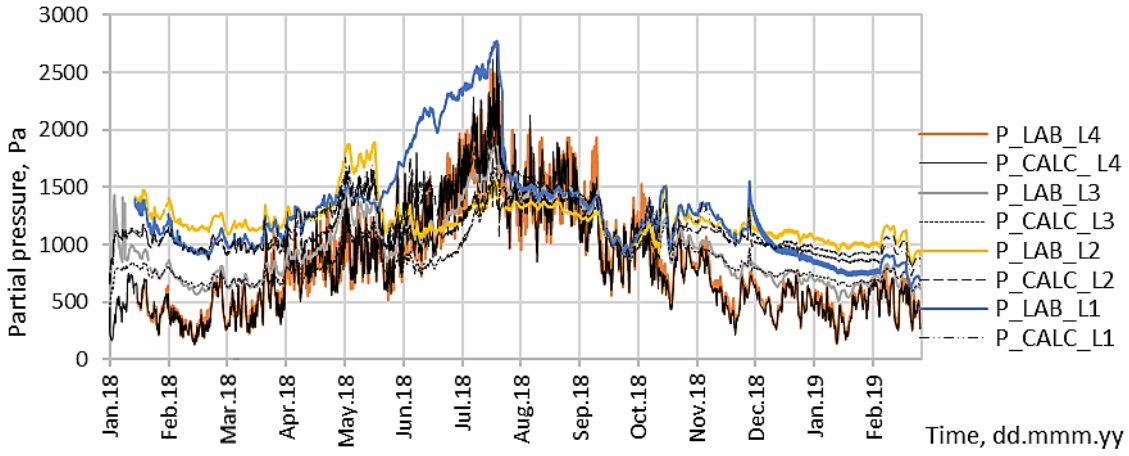

Figure 52. Partial pressure at locations 1-4, EW 2.2_N (Author's illustration)

Results of relative humidity are shown in *Figure 53*, where lines seem to align better than EW 2.1_N, but the average differences are actually higher. The highest difference is in location 4,

8.75 %RH (std.d. ±6.11), then 7.11 %RH (std.d. ±2.19) in location 2, smaller in location 3, 6.50 %RH (std.d. ±3.79) and the smallest in location 1, 4.49 %RH (std.d. ±3.52).

Looking at the close up during the warm period, highest difference is in location 4, having ave. diff. of 13.74 %RH with std.d of 5.24 %RH, while in locations 1-3 average difference varies in a range from 6.92 %RH (std.d. ±4.05) to 7.4 7%RH (std.d. ±4.88). During the cold period differences are very similar, in a range from 4.68 %RH (std.d. ±2.88) to 5.78 %RH (std.d. ±1.11).

In general RH varies from 20 to 90 %RH, which is lower than EW 2.1_N and the RH of 80 % is exceed only during August to November, actually only in calculated data, while measured RH reaches maximum 82 %RH. Lowest values are during January to April in location 3 and the highest RH is reached in location 4, starting from August.

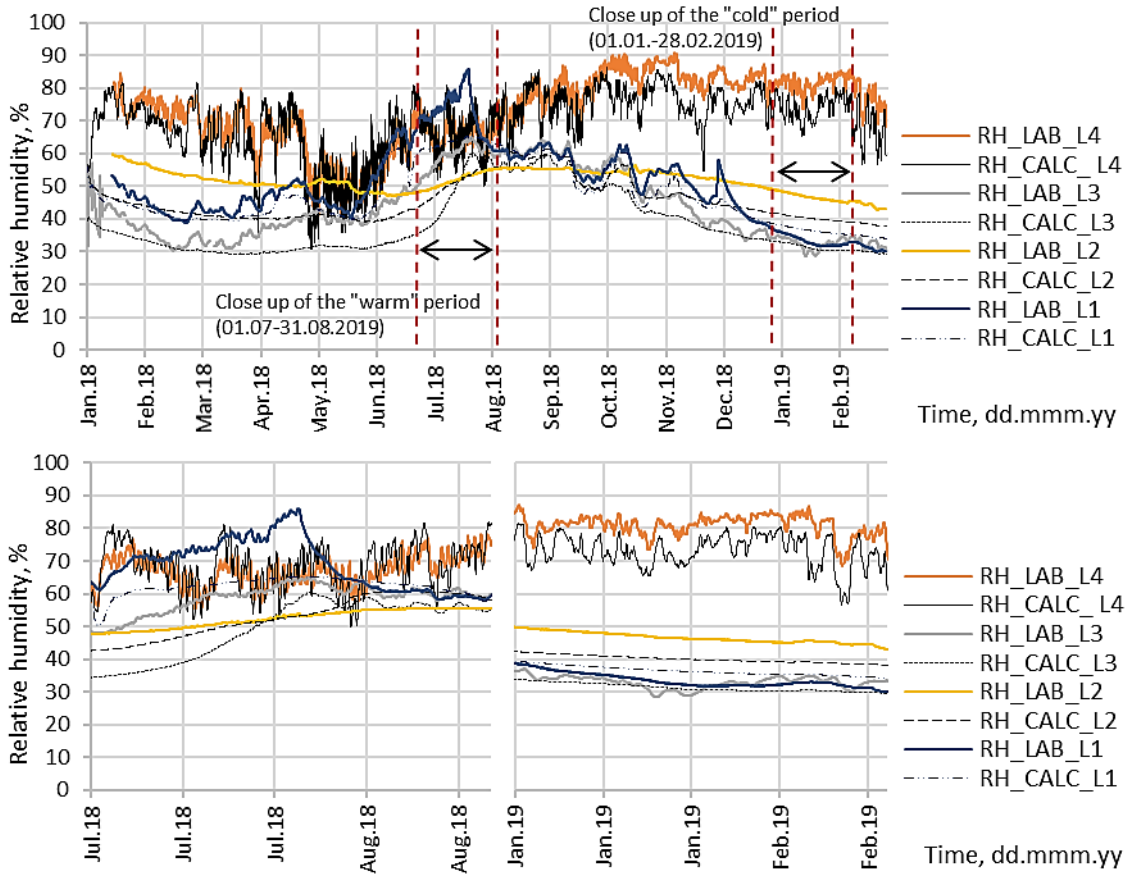

Figure 53. Relative humidity at locations 1-4, EW 2.2_N (Author's illustration)

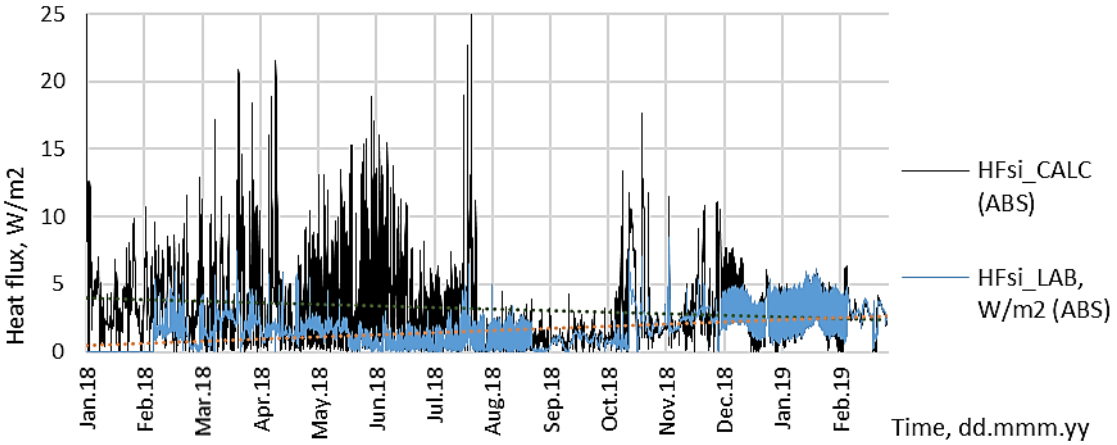

Graph of heat flux *(Figure 54)* shows that calculated values vary much more than measured, just as in the rest of walls. The maximal calculated value is 25 W/m^2 having average value of 2.70 W/m^2 (std.d. ±2.48), while average measured value is almost 2 times smaller, 1.44 W/m^2(std.d. ±1.23) having maximal value up to 8 W/m^2 only. Average difference between calculated and measured values is 1.71 W/m^2(std.d. ±1.71) similar as for other wall types. When considering thermal transmittance, the average measured value 0.18 W/m^{2}K (std.d. ±0.41) is more similar to estimated (0.10 W/m^{2}K), while the calculated thermal transmittance is higher, but still more similar to the estimated than for the other wall types, 0.39 W/m^{2}K (std.d. ±0.83)

Figure 54. Heat flux at EW 2.2_N (Author's illustration)

3.2.3 Field measurements and simulation of Southern side walls with initial MC of 13% (EW 2.1_S)

Results of temperature data of EW 2.1_S are shown in *Figure 55*, where the calculated values align with measurements with some differences, still following the same fluctuations. The differences are minor and for whole experiment time vary in a range from 0.22 °C (std.d. ±0.28 to 1.10 °C (std.d. ±0.44), where the highest difference is in location 3, followed by location 4. During the warm period there is a lack of data for location 3, but the highest difference is in L4, 1.11 °C (std.d. ±1.35) and only minor differences in L2, 0.20 °C (std.d. ±0.25) and in L1, 0.15 °C (std.d. 0.24). During the cold period highest difference is in the location 3, having ave. diff. of 1.43 °C (std.d. ±0.20) and in location 4, 1.12 °C (std.d. ±0.27), then smaller in location 2, 0.80 °C (std.d. ±0.14) and smallest in location 1, 0.14 °C (std.d. ±0.12).

Overall temperature varies from -10 °C to +35 °C, caused by location 4, which varies the most. Temperature in locations 1-3 vary from +13 °C to +27 °C, being closer to indoor environment. Lowest values are during January and February, while highest peaks are in July and August.

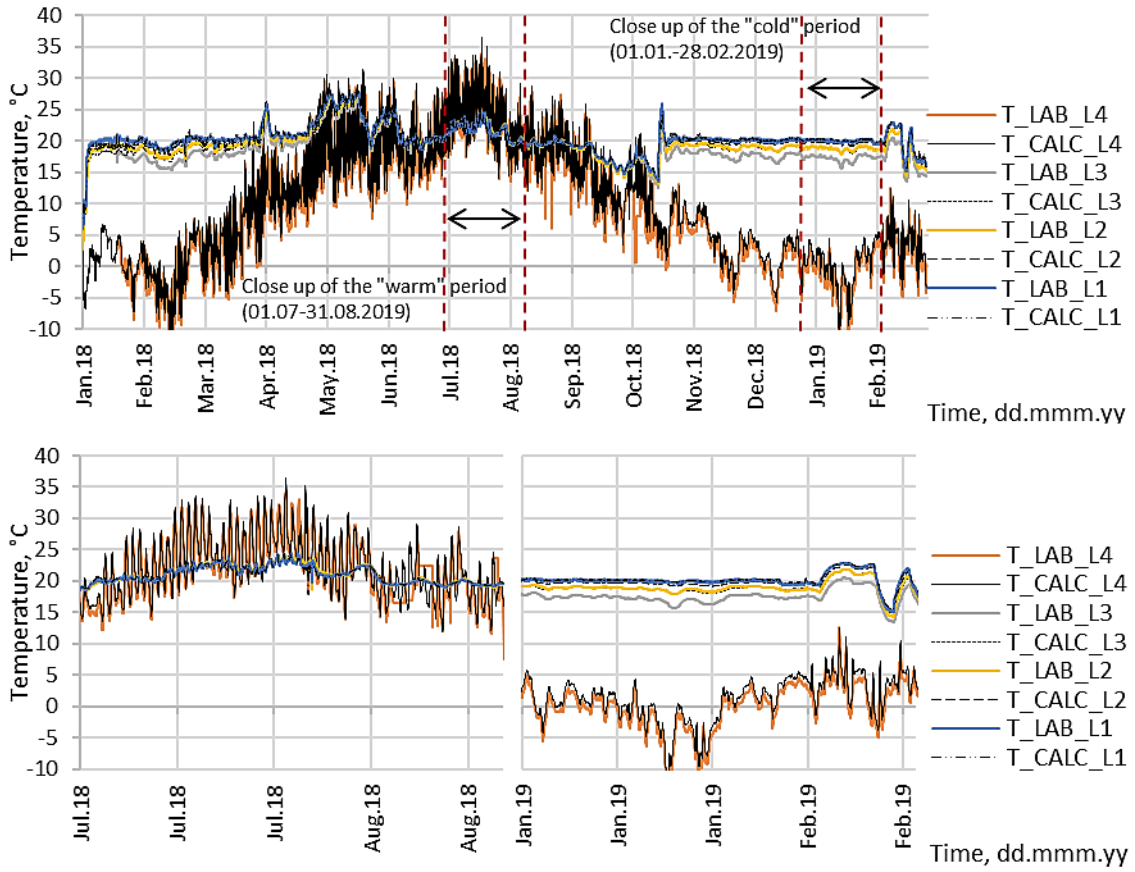

Figure 55. Temperature at locations 1-4, EW 2.1_S (Author's illustration)

Partial pressure values of EW 2.1_S are showed in *Figure 56*, where similarly as for EW 2.1_N, values at locations 1 and 2 tend to align with other lines only after May. However, the average differences are extremely high in location 3, having ave. diff. of 573.52 Pa (std.d. ±216), then much smaller in location 4, 200.07 Pa (std.d. ±224) and already comparatively small in location 2, 148.63 Pa (std.d. ±130) and in location 1, 104.13 Pa (std.d. ±129).

Generally, the lowest values are in location 3, LAB, which is different from other wall types, where lowest values are gained from location 4. The range of general partial pressure is from 100 to 3500 Pa, where lowest values are during January to March and highest are gained by calculated values of location 4 during July and August.

Results of calculated and measured relative humidity are showed in *Figure 57,* where the data align good when looking at the fluctuations. Average RH differences are similar as for wall 2.2_N, where highest difference now is in location 4, 8.81 %RH (std.d. ±6.40), then already smaller in location 3, 5.62 %RH (std.d. ±4.32), almost the same in location 2, 5.63 %RH (std.d. ±2.64) and smallest in location 1, 3.80 %RH (std.d. ±2.96).

During the warm time, there is a lack of data for location 3, but the highest average difference is reached in location 4, 14.19 %RH (std.d. ±4.82), then much smaller in location 3, 4.64 %RH (std.d. ±1.37) and in location 1 3.14 %RH (std.d. ±2.25). In the cold period, the differences in locations 2-4 are very similar, in a range from 5.04 %RH (std.d. ±2.89) to 5.45 %RH (std.d. ±1.75) and a very small difference of 1.80 %RH (std.d. ±0.71) in location 1.

Overall range of RH is from 29 to 90 %RH, which is comparatively lower result when compared to wall type 1. The lowest RH is gained by location 3, measured results and the highest values are in location 4, where the calculated and measured values stay constantly just above 80 %RH starting from September.

Graph of heat flux *(Figure 58)* shows similar results as for other walls, where calculated data varies much more and reaches 25 W/m^2, having average value of 2.78 W/m^2 (std.d. ±2.67) while measured data reaches up to 10 W/m^2, having average value almost 2 times smaller, 1.44 W/m^2 (std.d. ±1.15). Average difference between CALC and LAB results is 1.44 W/m^2 (std.d. ±1.15). Thermal resistance values are quite different from estimated (0.10 W/m^{2}K), where average measured value is 0.21 W/m^{2}K (std.d. ±0.60) and calculated value even higher 0.39 W/m^{2}K (std.d. ±0.85).

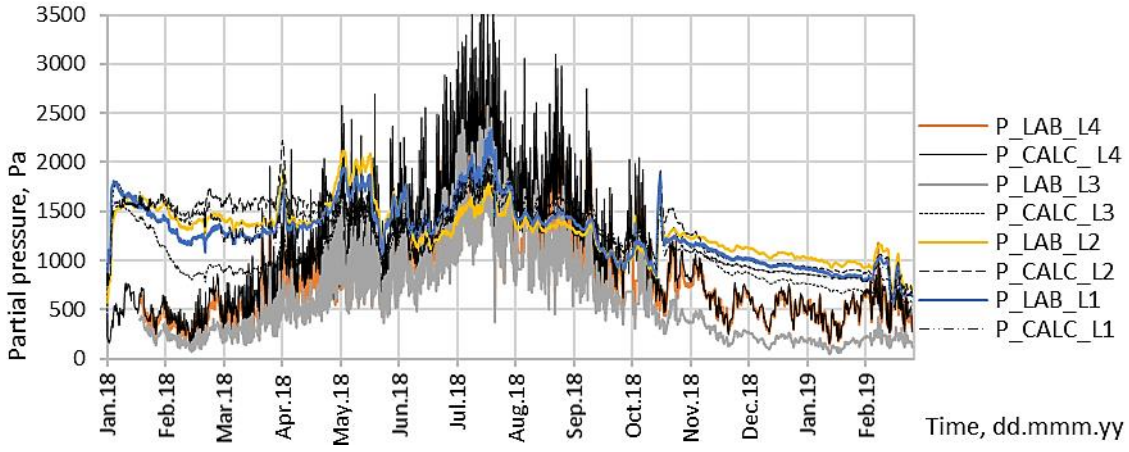

Figure 56. Partial pressure at locations 1-4, EW 2.1_S (Author's illustration)

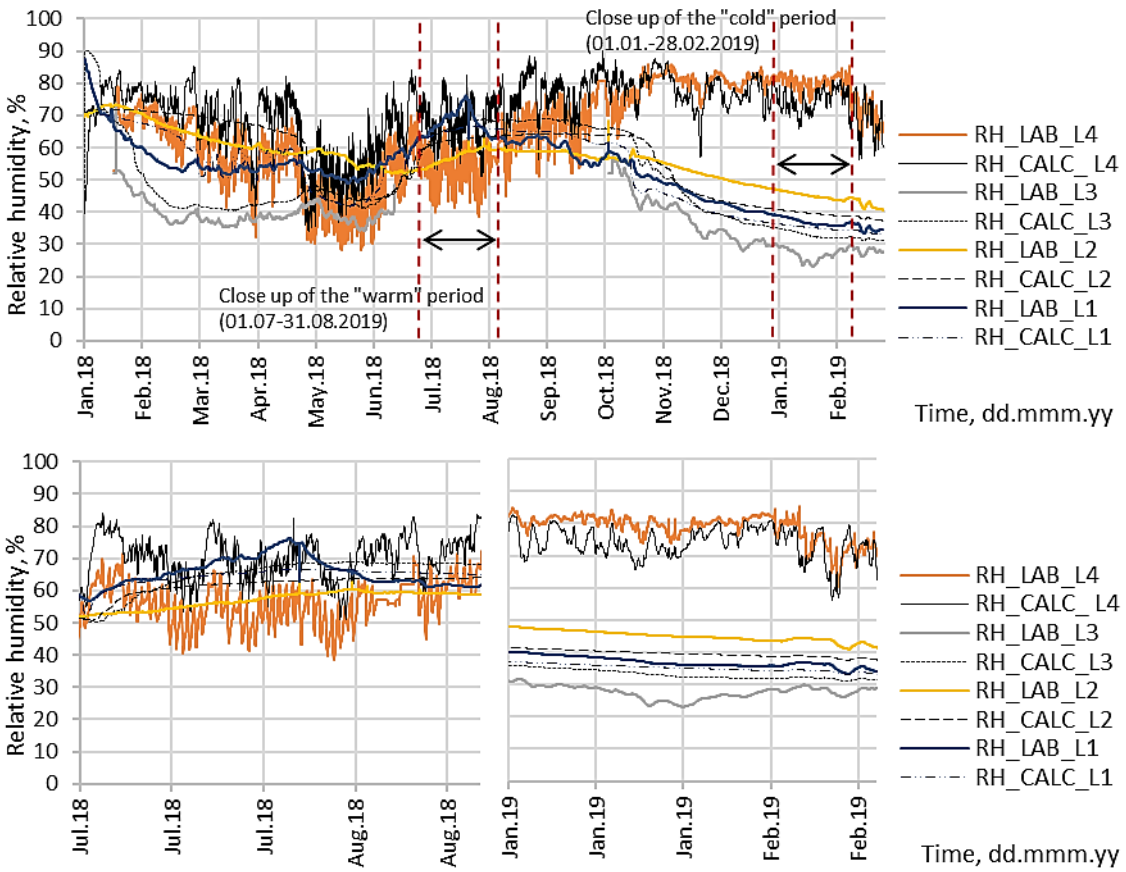

Figure 57. Relative humidity at locations 1-4, EW 2.1_S (Author's illustration)

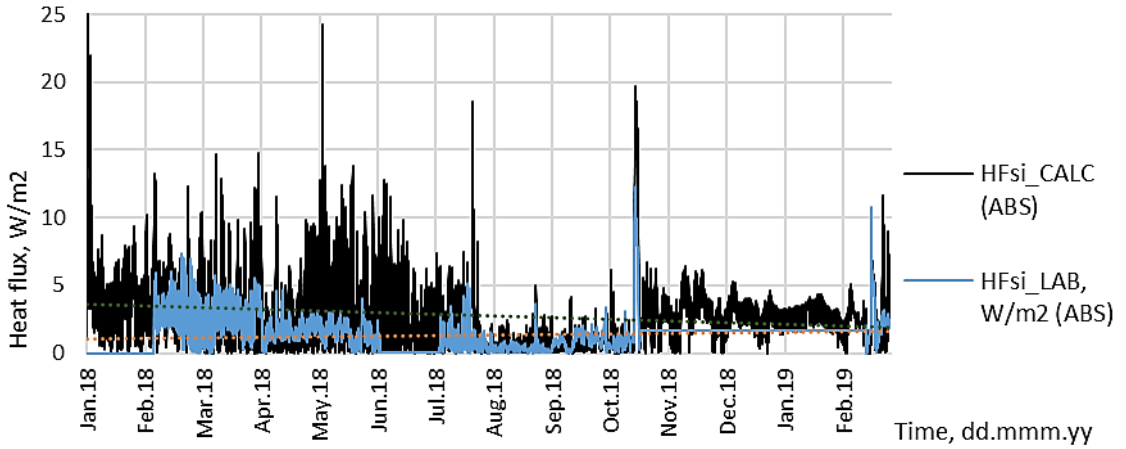

Figure 58. Heat flux at EW 2.1_S (Author's illustration)

3.2.4 Field measurements and simulation of Southern side walls with initial MC of 25% (EW 2.2_S)

Results of calculated and measured temperature data is showed in *Figure 59*, where all lines follow up the same pattern with no major differences, having the average differences in a range from 0.56 °C (std.d. ±0.31) in location 1 to 1.00 °C (std.d. ±0.55) in location 4.

During the warm period differences are even in smaller range, from 0.51 °C (std.d. ±0.24) to 0.87 °C (std.d. ±0.71). In the cold period, differences slightly increase, location 3 having the highest difference, 1.26 °C (std.d. ±0.12), then location 4 with ave.diff. of 1.08 °C (std.d. ±0.26), then location 2, 0.90 °C (std.d. ±0.10) and the smallest difference in location 1, 0.43 °C (std.d. ±0.16). Generally, the temperature varies from -10 °C to 35 °C as in most of the other walls. The most fluctuating data is in location 4, which provides the lowest temperatures in January and February and the highest values during July and August. Temperature in locations 1-3 varies only around +13 °C to +28 °C, being closer to indoor environment.

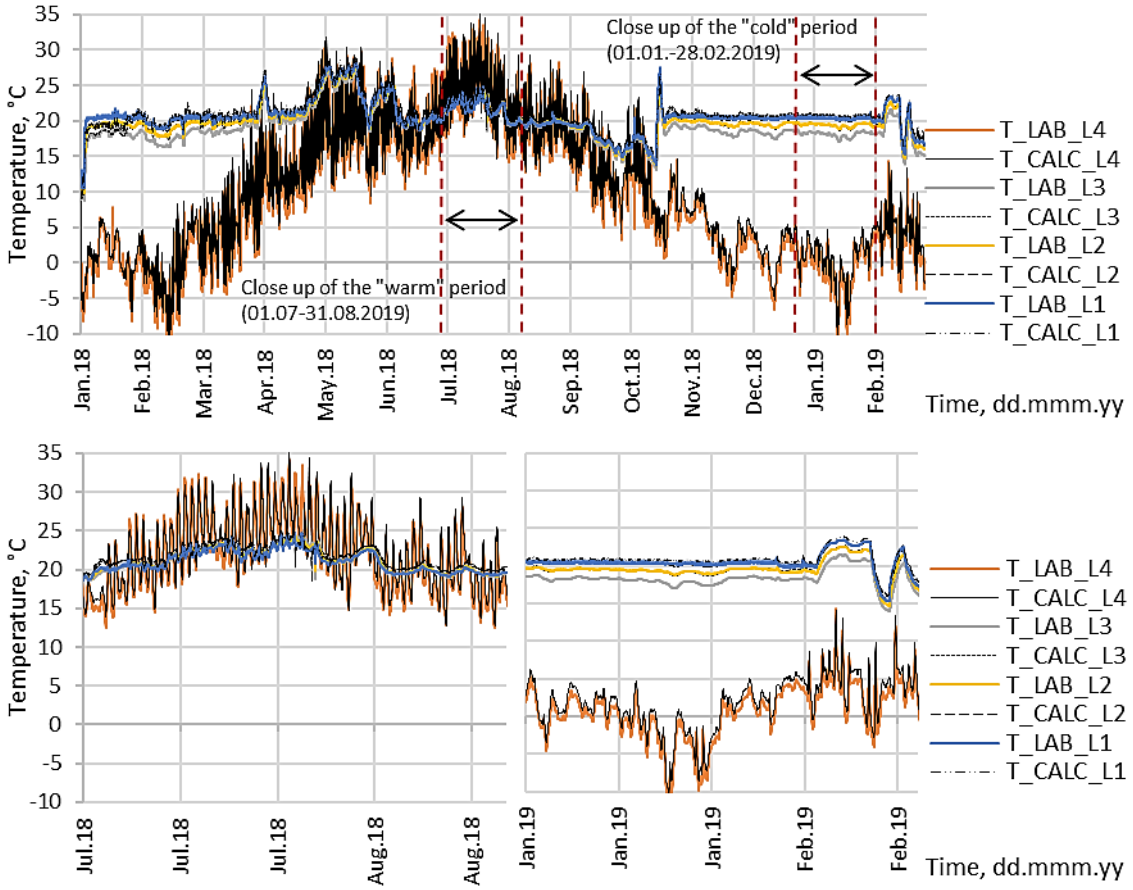

Figure 59. Temperature at locations 1-4, EW 2.2_S (Author's illustration)

Figure 60 shows results of partial pressure in EW 2.2_S, where the lines align well and the differences are not too high, compared to other walls. Average differences vary from 119.14 Pa (std.d. ±80) in location 1 to 191.14 Pa (std.d.±90) in location 3.

Overall partial pressure is the lowest and highest in location 4, which is the same as for most of other walls, having a range of 200 to 3500 Pa, where the lowest values are gained during January to March and the highest during July and August.

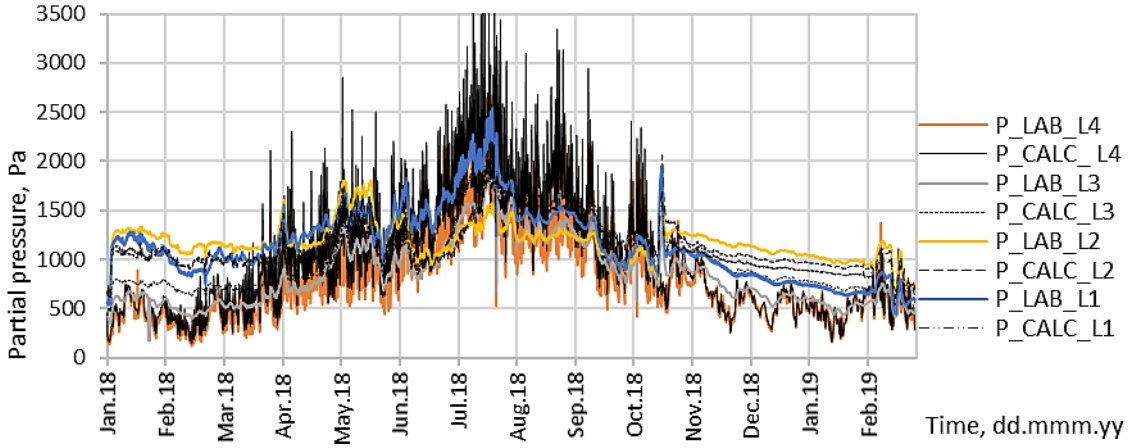

Figure 60. Partial pressure at locations 1-4, EW 2.2_S (Author's illustration)

To analyse results of relative humidity of EW 2.2_S *(Figure 61),* the measured and calculated values follow up, having more or less the same fluctuations and the average differences are quite low compared to other walls of type 2. Average difference in all period of experiment varies in a range from 4.49 %RH (std.d. ±3.52) to 8.75 %RH (std.d. ±3.52).

During the warm period, the highest difference increase in location 4, having ave. diff. of 13.74 %RH (std.d. ±5.24), while the difference in locations 1-3 varies in a range from 6.92 %RH (std.d. ±4.05) to 7.47 %RH (4.88). During the cold period differences are very similar ranging from 4.68 %RH (std.d ±2.88) to 5.78 %RH (std.d. ±1.11).

Overall RH values vary from 21 %RH, which is lower than for other walls to 90 %. Lowest RH is in location 3 during January to March, while the highest relative humidity is in location 4, where the values vary around 80-90 %RH starting from August.

Graph of heat flux of EW 2.2_S *(Figure 62)* shows that the calculated values vary much more and reach higher heat flux, up to 20 W/m^2, which is slightly lower than for other walls, but the measured values are more stable and reach only up to 13 W/m^2. Average value of calculated q is 2.70 W/m^2 (std.d. ±2.48), while average measured q is half as little, 1.44 W/m^2 (std.d. ±1.23). Average difference is 1.71 W/m^2 (std.d. 1.92).

To consider thermal transmittance, average measured thermal transmittance, 0.29 W/m^{2}K (std.d. ± 0.75) is higher than estimated (0.10 W/m^{2}K), and the measured average value is even higher than that, 0.39 W/m^{2}K (std.d. ±0.89).

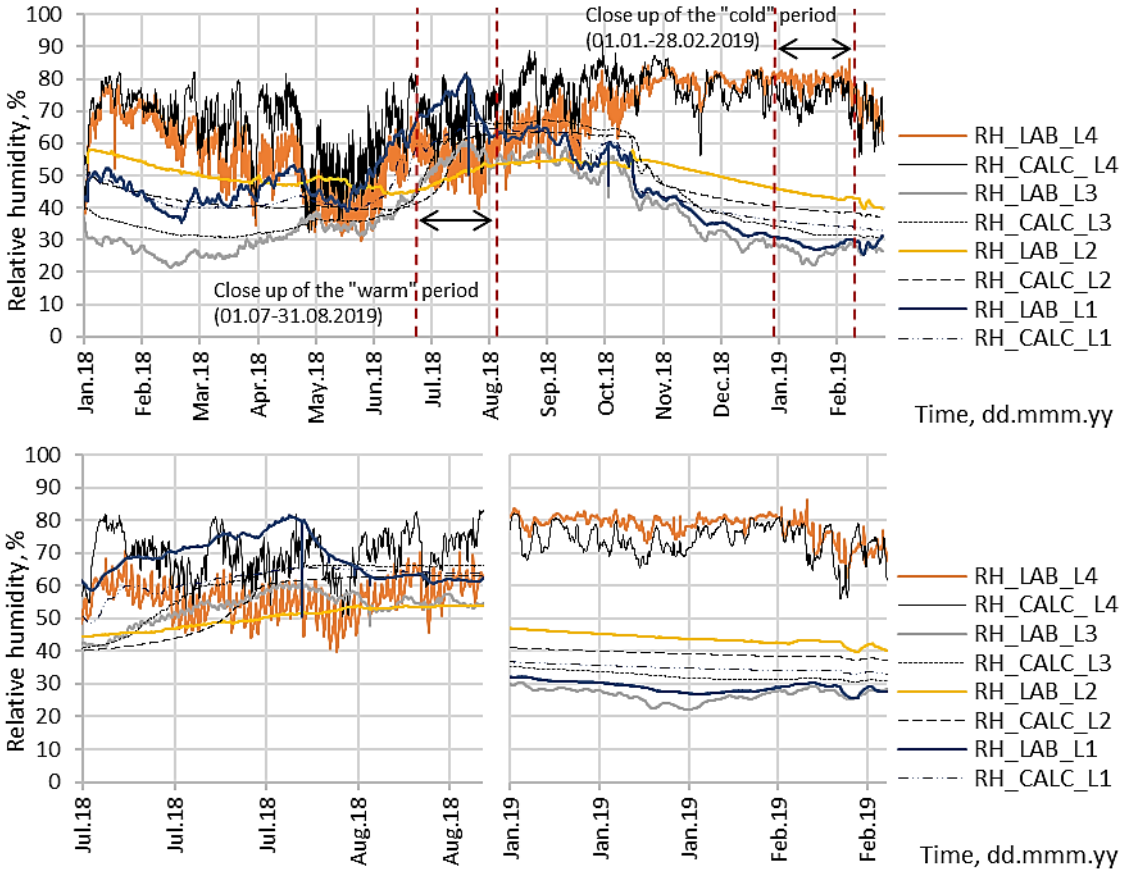

Figure 61. Relative humidity at locations 1-4, EW 2.2_S (Author's illustration)

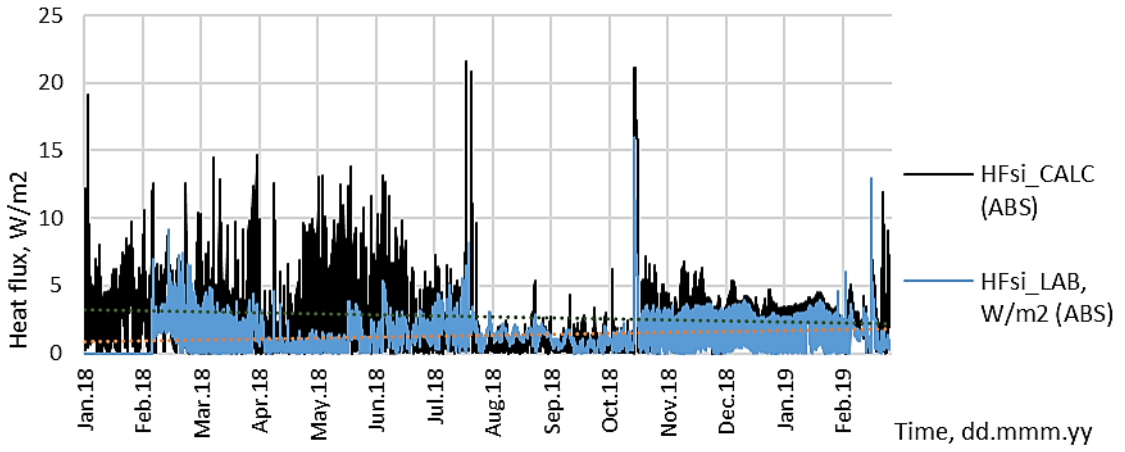

Figure 62. Heat flux at EW 2.2_S (Author's illustration)

3.3 Test walls insulated with PIR (EW-3)

3.3.1 Field measurements and simulation of Northern side walls with initial MC of 13% (EW 3.1_N)

Calculated and measured temperature results are shown in *Figure 63*, where both results align with no major differences, although the average differences are slightly higher than for walls of type 1 and 2. As the smallest difference is in location 1, 0.68 °C (std.d. ±0.35), in locations 2-4, average difference vary in a range from 1.13 °C (std.d. ±0.37) to 1.63 °C (std.d. ±0.64).

Looking at the close up of warm period, differences are very similar, having average difference in a range from 0.69 °C (std.d. ±0.29) to 0.86 °C (std.d. ±0.34). In the cold period, differences mostly increase, where the highest ave. diff. is in location 3, 2.22 °C (std.d. ±0.28), then location 2, 1.89 °C (std.d. ±0.23), location 4, 1.24 °C (std.d. ±0.12) and finally the smallest difference in location 1 0.69 °C (std.d. ±0.11).

Overall temperature values range from -14 °C to +30 °C, which are gained by data of location 4, which is the closest to outdoors. Lowest temperature values are during January to March, and highest – during July and August. However, values up to +28 °C are gained by locations 1-3 during May also. Overall range of temperature in locations 1-3 varies around +14 °C to +27 °C, as they are more related to indoor environment.

Figure 64 shows data of partial pressure of EW 3.1_N, where most obvious difference can be noted in locations 2 and 3, where the calculated data is constantly higher through all the period of experiment. Accordingly, the highest average difference of 682 Pa (std.d. ±279) is in location 3, then in location 2, 438 Pa (std.d. ±210) and already much smaller in location 1, 194.80 Pa (std.d. ±161) and in location 4, 125.90 Pa (std.d. ±147).

In general, the values vary from 200 to 3500 Pa, which is similar to most of other walls. Highest and lowest values are gained by location 4, where the lowest partial pressure is during January to March and the highest, during July and August.

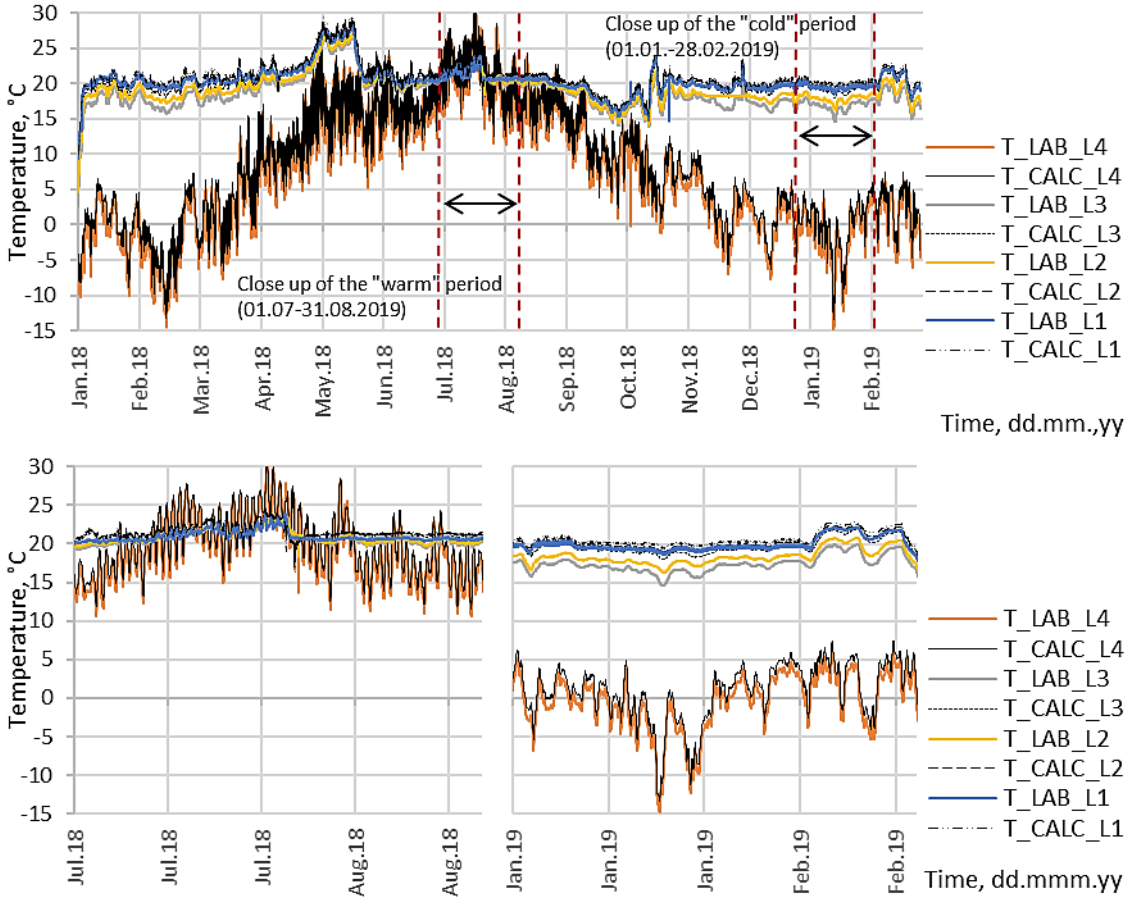

Figure 63. Temperature at locations 1-4, EW 3.1_N (Author's illustration)

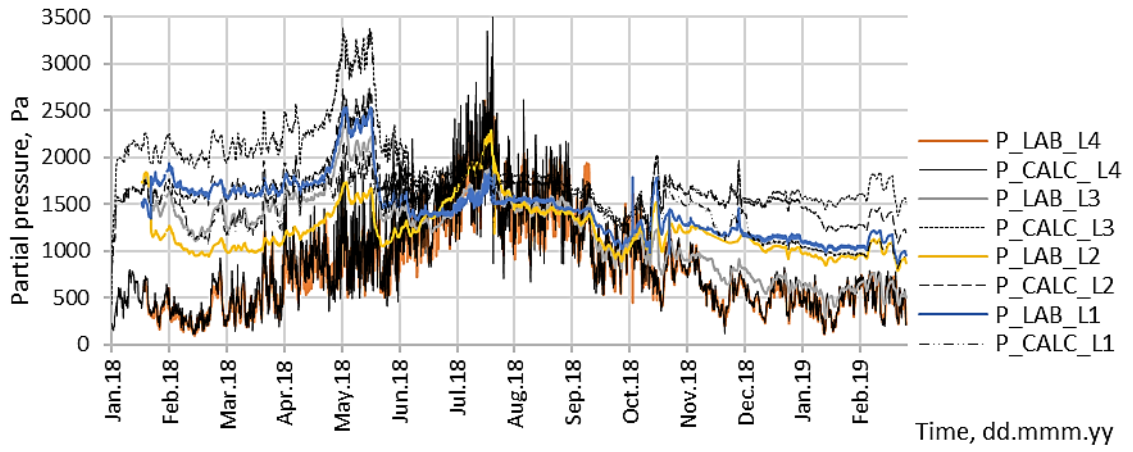

Figure 64. Partial pressure at locations 1-4, EW 3.1_N (Author's illustration)

Results of relative humidity of EW 3.1_N are showed in *Figure 65*, where overall RH is higher than for other walls. Calculated and measured data aligns with similar differences as for other walls, however, especially high average difference is in location 3, 22.64 %RH (std.d. ±10.96), where calculated data is much higher. Next biggest difference is in location 2, 12.93 %RH (std.d. ±5.68), then already smaller in location 4, 7.83 %RH (std.d. ±6.71) and in location 1, 7.23 %RH (std.d. ±4.91).

During the warm period differences are generally smaller, but still high in location 3, 10.78 %RH (std.d. ±3.85) and in location 4, 10.10 %RH (std.d. ±6.90), then smaller in location 1, 6.64 %RH (std.d. ±1.52) and in location 2, 5.66 %RH (std.d. ±3.06). During the cold period, a very high difference is in location 3, having ave. diff. of 40.27 %RH with std. d. of 3.32 %RH, then already much smaller in location 2, 11.06 %RH (std.d. ±3.23), smaller and in location 4, 6.29 %RH (std.d. ±5.77) and finally 4.78 %RH (std.d. ±0.41) in location 1.

In general, the relative humidity varies from 18 to 95 %RH, where the lowest values are gained by location 3 during January and February and the highest, mostly by location 4, quite constantly varying around 90 %RH during June to November. Critical value of 80 %RH is reached by calculated and measured data of location 4 and also by the calculated values of location 3.

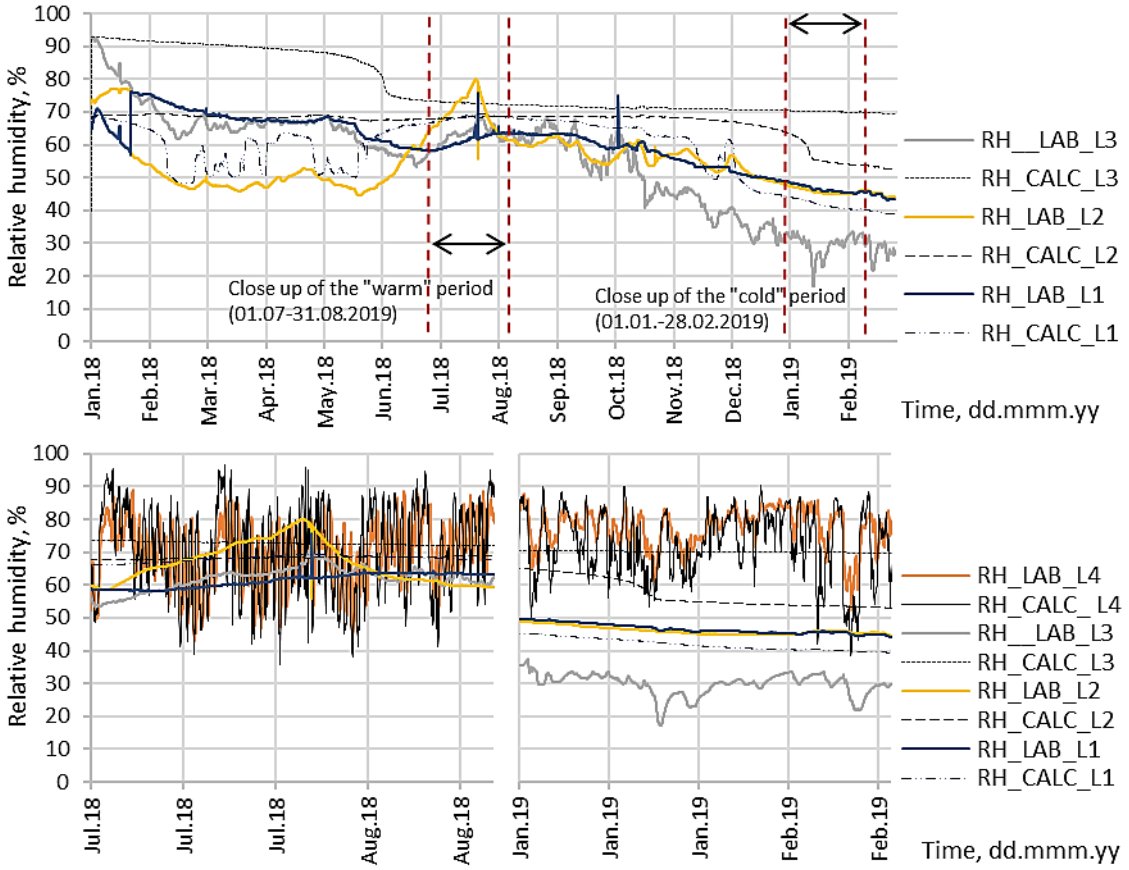

Figure 65. Relative humidity at locations 1-4, EW 3.1_N (Author's illustration)

Results of heat flux of wall EW 3.1_N are showed in *Figure 66*, where as in all the other walls, calculated data varies much more and reaches values up to 25 W/m^2 with an average value of 3.00 W/m^2 (std.d. ±2.97), while measured q reaches up to 12 W/m^2 with an average value of 2.27 W/m^2 (std.d. ±1.50). Average difference between CALC and LAB results is 1.92 W/m^2 (std.d. 2.37). When considering thermal transmittance, values are much higher than estimated (0.09

W/m^{2}K), having measured value of 0.24 W/m^{2}K (std.d. ±0.48) and much higher calculated value of 0.40 W/m^{2}K (std.d. ±0.89).

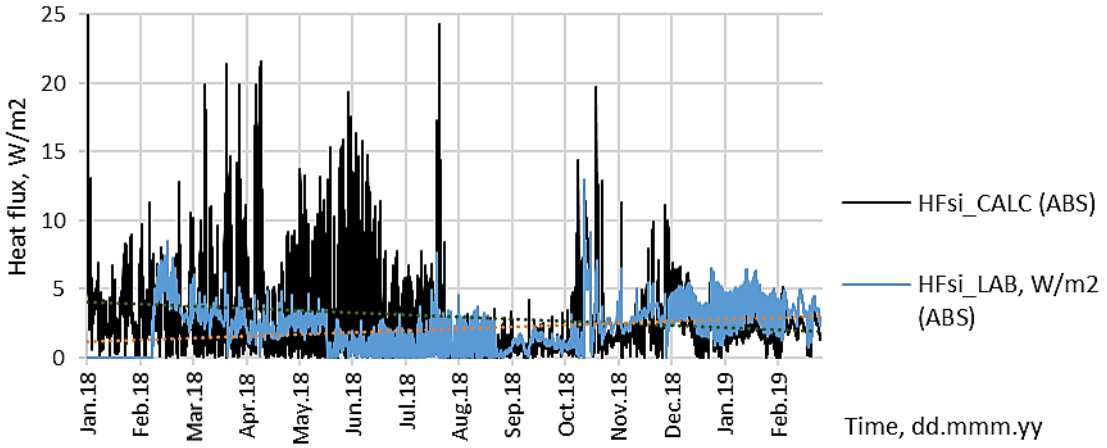

Figure 66. Heat flux at EW 3.1_N (Author's illustration)

3.3.2 Field measurements and simulation of Northern side walls with initial MC of 25% (EW 3.2_N)

Temperature results of EW 3.2_N are showed in *Figure 67*, where the values align better than in EW 3.1_N. Highest difference is in location 3 with ave.diff. of 1.05 °C (std.d. ±0.49), while the differences in locations 1, 2 and 4 vary in a range of 0.33 °C (std.d. 0.30) to 0.60 °C (std.d. ±0.32). During the warm period, differences are very similar, varying in a range from 0.30 °C (std.d. ±0.24) to 0.51 °C (std.d. ±0.28). During the cold period highest differences are in location 3, 1.46 °C (std.d. ±0.17), then already smaller in location 4, 0.80 °C (0.19) and much smaller in location 2, 0.43 °C (std. d. ±0.10) and in location 1, 0.16 °C (std.d. ±0.12).

Overall temperature values vary from -14 °C to +30 °C, where both of these are reached by location 4. Lowest temperature is during January to March and the highest – during July and August. Temperature in locations 1-3 varies from +15 °C to +30 °C, as they are located more towards indoor environment.

Figure 68 shows results of partial pressure, where most of data aligns with no major differences. As the differences are lower than for EW 3.1_N, in location 3, the ave.diff. is still high, 249.24 Pa (std.d. ±147), then the average difference in locations 1, 2 and 4 is smaller and varies in a range from 115.24 Pa (std.d. ±135) to 158.47 Pa (std.d. ±147).

In general, partial pressure varies from 200 to 3000 Pa, where the lowest values are reached during January to April by location 4 and the highest values are during July and August, reached by locations 3 and 4.

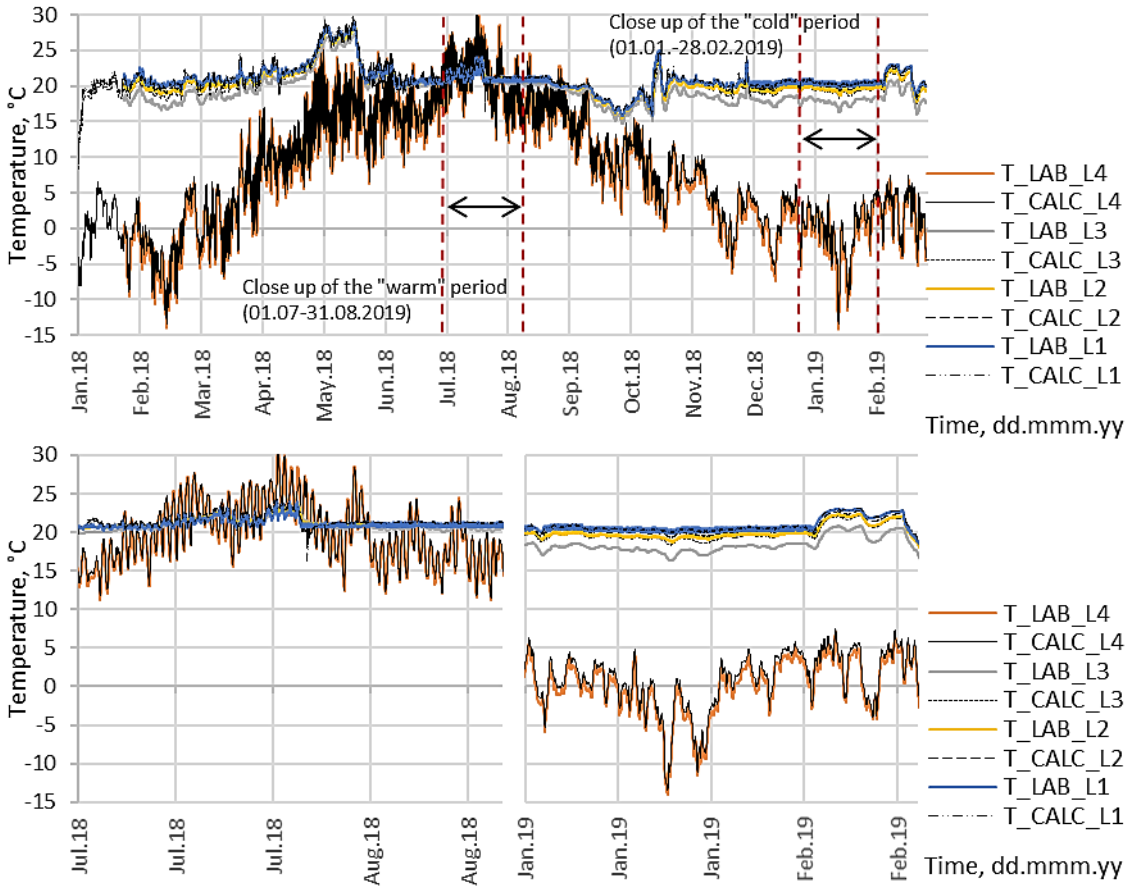

Figure 67. Temperature at locations 1-4, EW 3.2_N (Author's illustration)

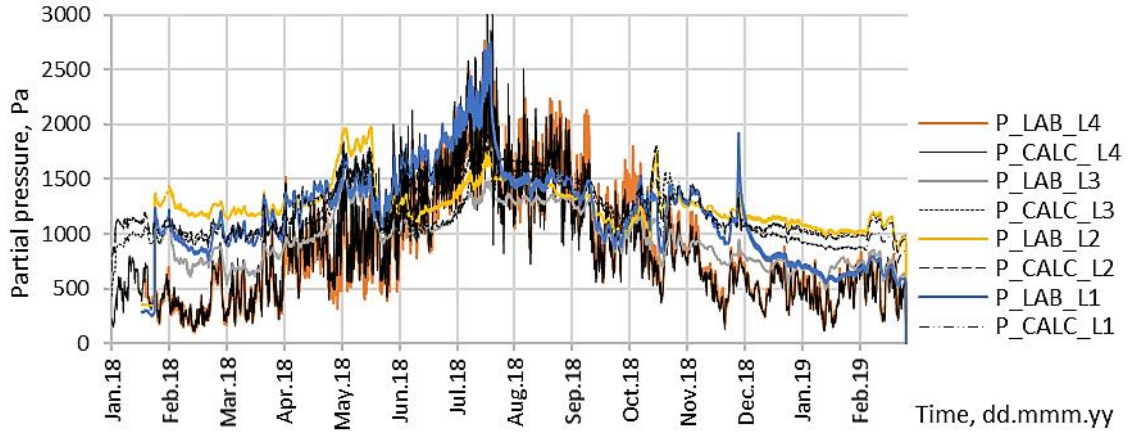

Figure 68. Partial pressure at locations 1-4, EW 3.2_N (Author's illustration)

Results of relative humidity are shown in *Figure 69*, where calculated and measured data aligns with no major differences. However, the highest average difference of 15.60 %RH (std.d. ±43.71) is in location 3, then already smaller in location 4, 9.62 %RH (std.d. ±8.02) and then already small and quite similar in location 1, 5.95 %RH (std.d. ±5.25) and in location 2, 5.38 %RH (std.d. ±3.72). When looking at the close up of warm period, highest difference is in location 1, 10.32 %RH (std.d. ±5.96), then in location 4, 8.04 %RH (std.d. ±6.93), smaller in location 3, 5.01 %RH (std.d. ±2.72) and the smallest in location 2, 3.47 %RH (std.d. ±0.96). During the cold period only small difference is in location 2, having ave.diff. of 3.32 %RH (std.d. ±0.51), but then much higher differences in locations 1, 3 and 4, varying in a range of 9.68 %RH (std.d. ±1.57) to 12.15 %RH (std.d. ±2.69), where the highest difference is in location 3.

In general, relative humidity varies from 13 to 100 %RH, where the highest and lowest values are gained by location 4. As the lowest values are during April to June, constantly high values, above 90 %RH start from July, in location 4. As only the location 3 reaches to a higher RH of 90 % during July, the rest of the time, together with locations 1 and 2, RH varies only from 25 to 65 %RH.

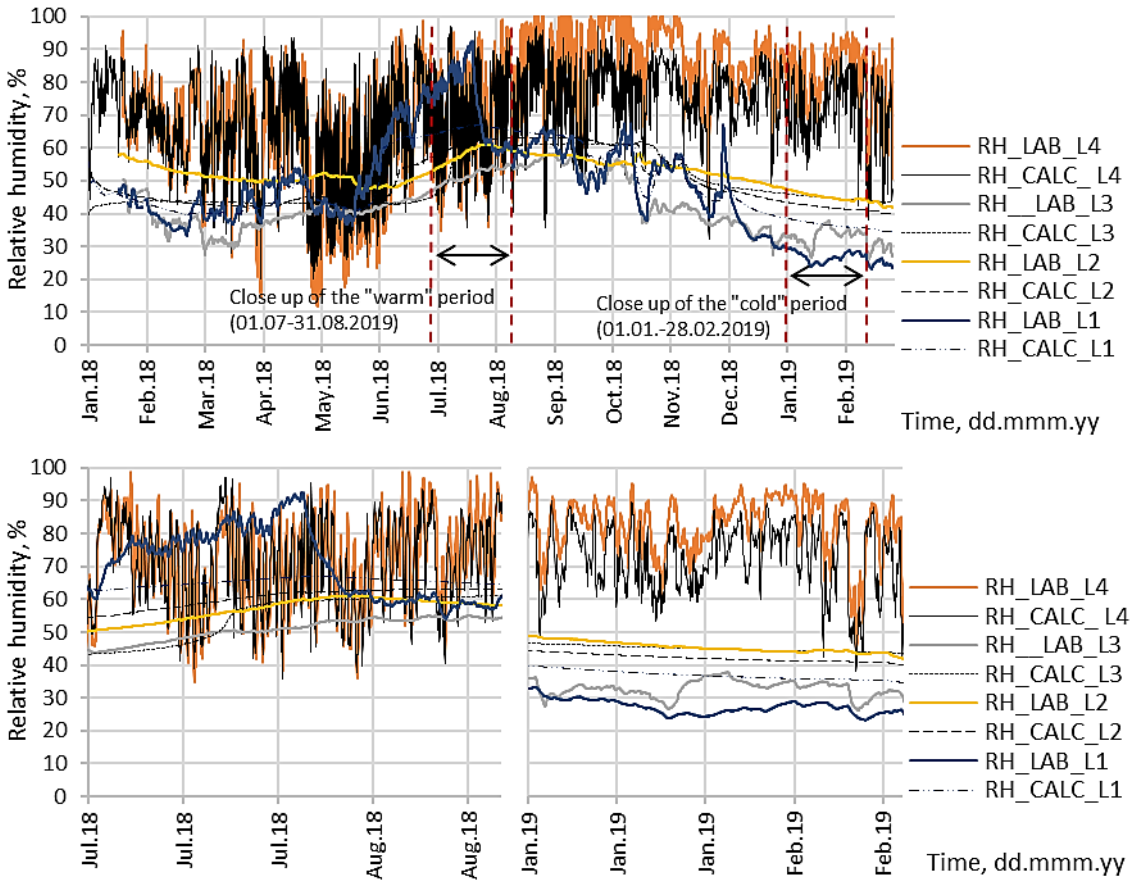

Figure 69. Relative humidity at locations 1-4, EW 3.2_N (Author's illustration)

Figure 70 show results of q at EW 3.2_N, where calculated data varies much more and reaches up to 20 W/m^2, having average value of 2.96 W/m^2 (std.d. ±2.81) and measured data reaches up to 12W/m^2 with an average value of 1.91 W/m^2 (std.d. ±1.32). Average difference between CALC and LAB data is 1.93 W/m^2. Considering thermal resistance, it is similar as for EW 3.1_N, where here the measured value of 0.22 W/m^{2}K (std.d. ±0.44) is closer to estimated value (0.09 W/m^{2}K), and the calculated one is again much higher, 0.41 W/m^{2}K (std.d. ±0.91).

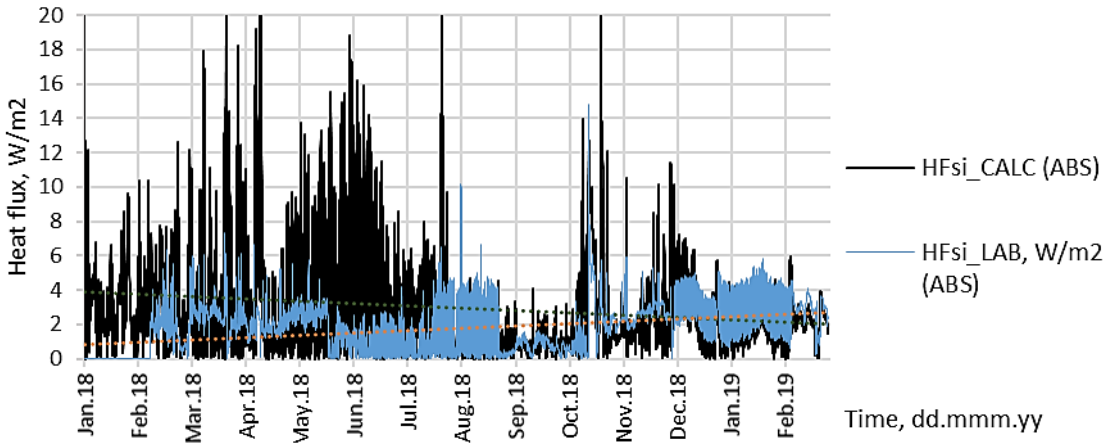

Figure 70. Heat flux at EW 3.2_N (Author's illustration)

3.3.3 Field measurements and simulation of Southern side walls with initial MC of 13% (EW 3.1_S)

Results of calculated and measured temperature values are showed in *Figure 71*, where data aligns with the same pattern. However, there are some differences between calculated and measured data, especially in location 3, where the ave. diff. is 1.67 °C (std.d. ±0.78), then in the rest of locations already smaller, in a range of 0.92 °C (std.d. ±0.35) to 1.18 °C (std.d. ±0.49).

During the warm period, average differences are very similar, ranging from 0.67 °C (std.d. ±0.35) to 0.77 °C (std.d. ±0.56). During the cold period, differences are already higher, where the highest difference is in location 3, having ave. diff. of 2.47 °C (std.d. ±0.36), then in location 2, 1.61 °C (std.d. ±0.17), then almost the same in location 4, 1.15 °C (std.d. ±0.11) and in location 1, 1.13 °C (std.d. ±0.13).

In general, temperature varies from -15 °C to +35 °C, gained by location 4, because the rest of the locations (1-3) are placed more towards indoors, having a temperature in a range from +13

°C to +30 °C. Lowest temperatures of location 4 are gained during January to March and highest ones are reached in July and August.

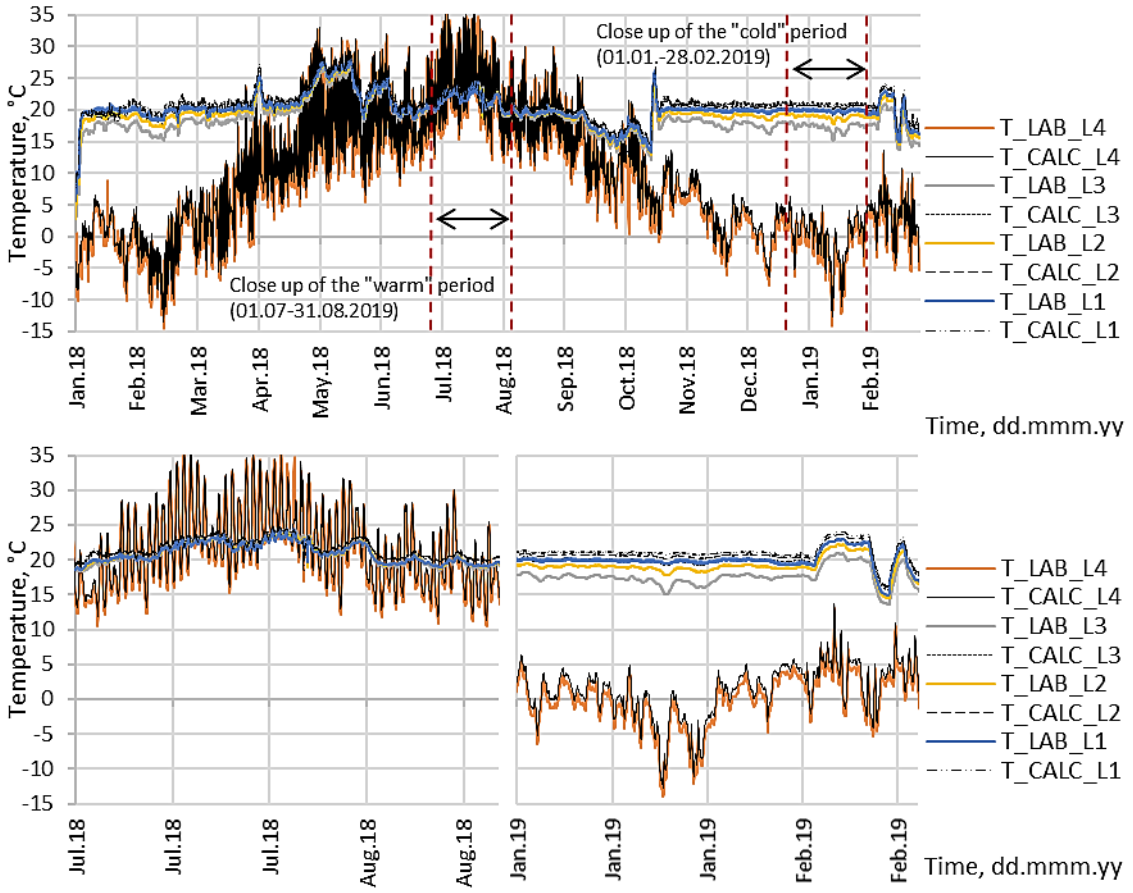

Figure 71. Temperature at locations 1-4, EW 3.1_S (Author's illustration)

Figure 72 shows results of partial pressure, where measured and calculated data again, similarly as for EW 3.1_N, do not align well, especially in the first and last 5 months, where the calculated results in locations 2 and 3 are much higher. The highest difference can be observed in location 3, where the ave. diff. is 790.97 Pa (std.d. ±337), which is extremely high. Then, already smaller difference is in in location 2, 225.40 Pa (std.d. ±123.52), smaller in L4, 178.96 Pa (std.d. ±224) and finally the smallest in location 1, 121.34 Pa (std.d. ±118).

Overall values of partial pressure vary from 200 to 3500 Pa, where the minimal and maximal values are gained by location 4. Lowest values are during the cold months, January to March and the highest ones are during July and August.

Results of RH in different locations of EW 3.1_S are showed in *Figure 73*. Differences between calculated and measured data are the highest on location 3, 27.94 %RH (std.d. ±12.53) and in location 4, 9.88 %RH (std.d. ±7.32), while the differences are quite small in location 2, 4.92 %RH (std.d. ±2.32) and in location 1, 3.26 %RH (std.d. ±2.76).

When looking at the close ups, differences in the warm period are still quite high in location 4, 12.77 %RH (std.d. ±7.51) and in location 3, 11.89 %RH (std.d. ±3.86), while are much smaller in location 2, 4.61 %RH (std.d. ±1.94) and in location 1, 2.43 %RH (std.d. ±1.43). During the cold period, difference is extremely high in location 3, where the average difference reaches 40.87 %RH (std.d. ±4.10), then in the rest of locations, difference ranges from 2.29 %RH (std.d. ±1.03) to 7.61 %RH (std.d. ±5.79).

In general, RH varies from 10 to 95 %RH, where the lowest values are gained from location 4 during April to June and from location 3 in January, and the highest values reached by location 4 during June to October. Relative humidity in location 4 constantly exceeds critical 80 %RH.

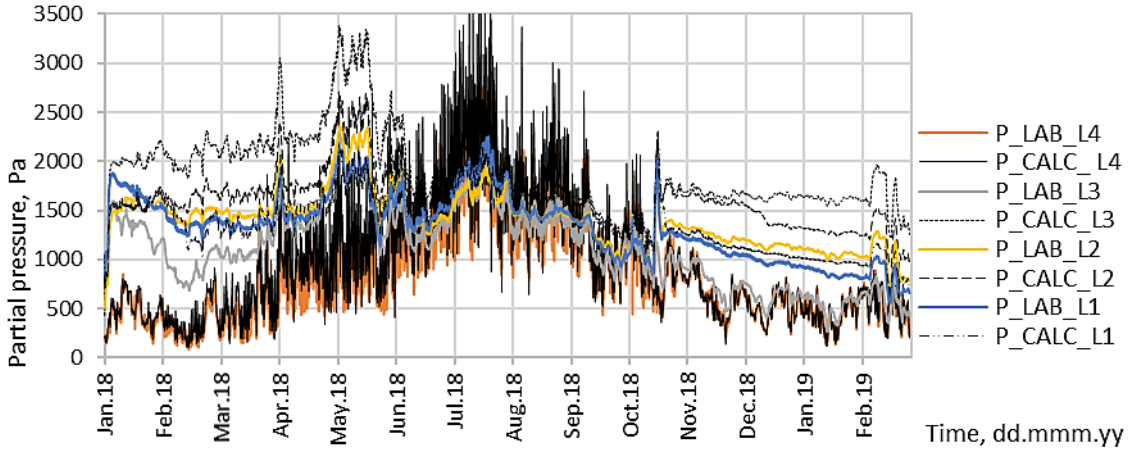

Figure 72. Partial pressure at locations 1-4, EW 3.1_S (Author's illustration)

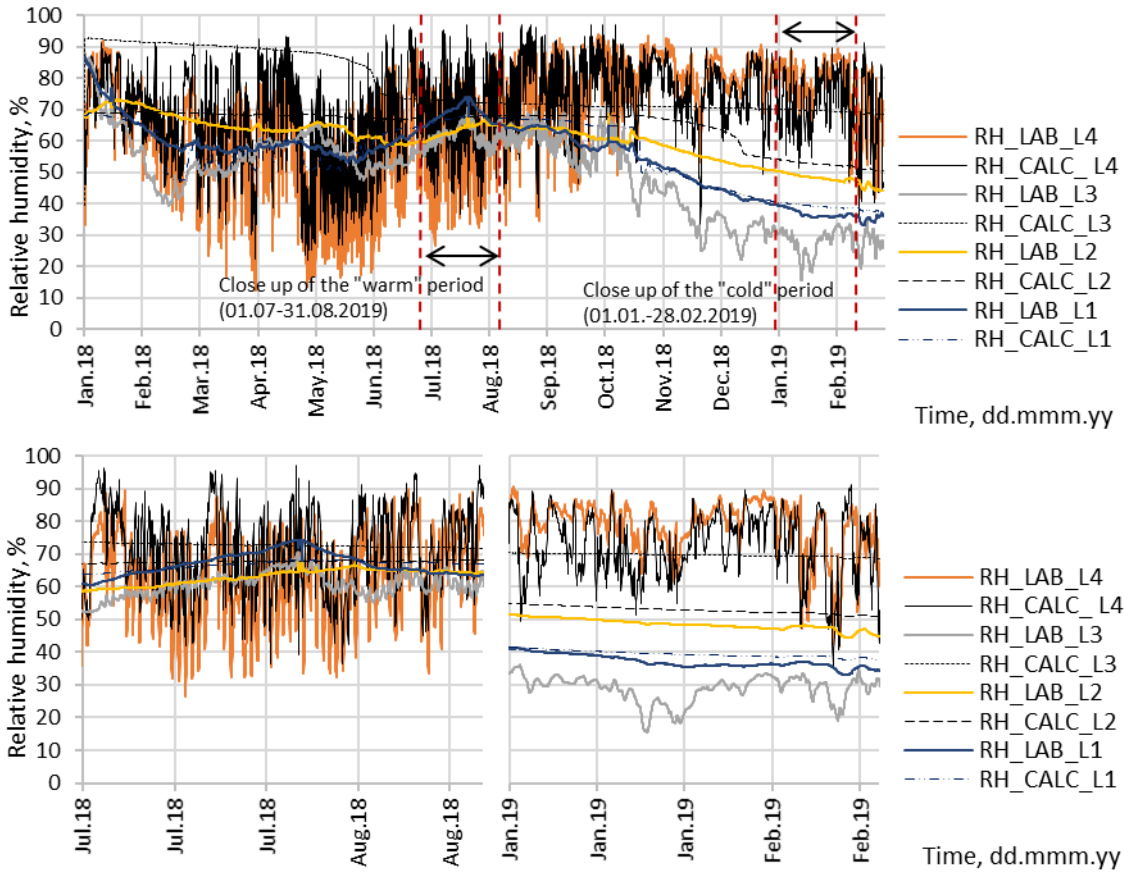

Figure 73. Relative humidity at locations 1-4, EW 3.1_S (Author's illustration)

Figure 74 shows results of heat flux of EW 3.1_S, where as in all other walls, calculated data varies much more and reaches 20 W/m^2 with an average value of 2.62 W/m^2 (std.d. ±2.61), which is smaller than for other walls of type 3. Measured values reach up to 14 W/m^2 having the average value of 1.82 W/m^2 (std.d. ±1.47). Average difference between CALC and LAB data is 1.57 W/m^2 (std.d. ±1.90), which is slightly smaller than for other walls. Considering the thermal transmittance, the measured value of 0.22 W/m^{2}K (std.d. ±0.52) is closer to estimated (0.09 W/m^{2}K), while the calculated value is higher, 0.39 W/m^{2}K (std.d. ±0.89).

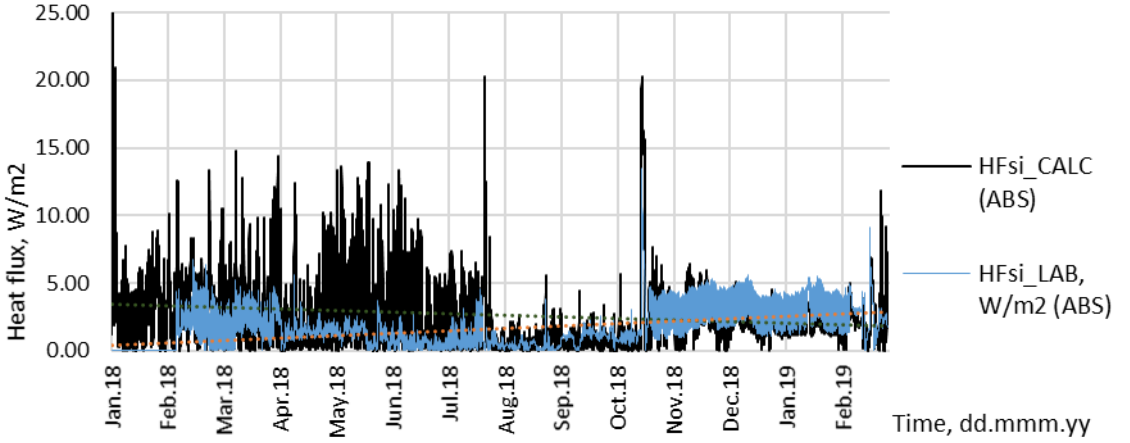

Figure 74. Heat flux at EW 3.1_S (Author's illustration)

3.3.4 Field measurements and simulation of Southern side walls with initial MC of 25% (EW 3.2_S)

Results of temperature at EW 3.2_S *(Figure 75)* show that data aligns slightly better than for wall EW 3.1_S, where now the average difference varies only in a range of 0.73 °C (std.d. ±0.29) to 1.02 °C (std.d. ±0.48), having the highest differences in location 3.

When looking at the close ups, results align well, with an average difference in a range of 0.49 °C (std.d. ±0.28) to 0.64 °C (std.d. ±0.28). However, in the cold period differences are higher, having the highest ave. diff. of 1.43 °C (std.d. ±0.12) in location 3, then the same difference in location 2, 1.42 °C (std.d. ±0.11). Already smaller, the same differences in locations 1 and 4, 0.76 °C (std.d. ±0.11).

In general, temperature varies from -10 °C to +35 °C, reached by data of location 4. Lowest temperatures are during January to March and the highest during July and August. As the values in location 4 varies the most, much smaller temperature range is for location 1-3, from +13 °C to +28 °C.

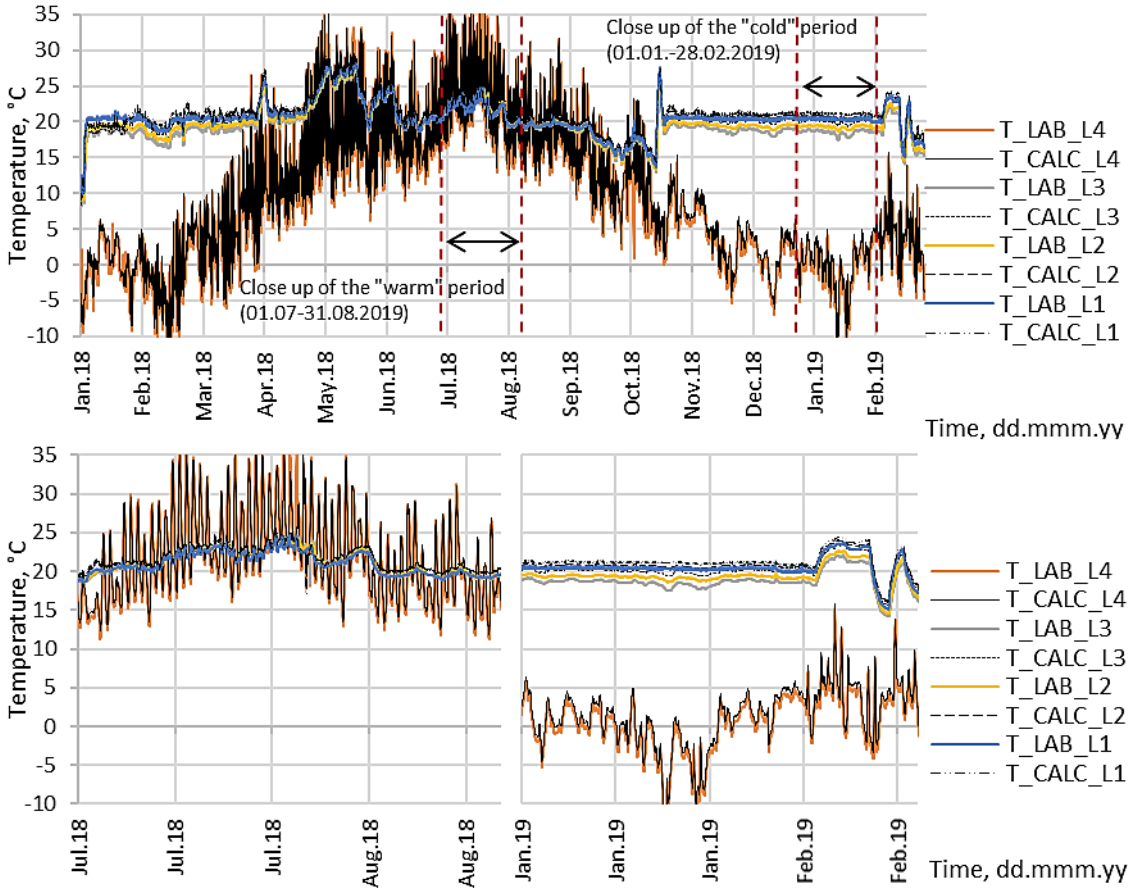

Figure 75. Temperature at locations 1-4, EW 3.2_S (Author's illustration)

Figure 76 shows calculated and measured results of partial pressure, where data aligns better than in 3.1_S. The highest difference is in location 3, having average difference of 265.47 Pa (std.d. ±155), then in L4, 197.36 Pa (std.d. ±249), then smaller in L2, 100.21 Pa (std.d. ±101) and the smallest in L1, 73.12 Pa (std.d. ±75.38).

Overall partial pressure varies from 200 to 3500 Pa, where the highest and lowest values are gained by location 4. Lowest partial pressure is during January to March and the highest values in July and August.

Results of relative humidity of EW 3.2_S are showed in *Figure 77*, where data aligns quite well, except locations 3 and 4, where the highest average difference of 10.15 %RH (std.d. ±8.08) is in location 4 and a bit smaller in location 3, 8.73 %RH (std.d. ±6.11). Smaller differences are in location 2, 3.91 %RH (std.d. ±2.75) and in location 1, 3.29 %RH (std.d. ±2.11).

During the warm period, highest difference is in L4, 13.40 %RH (std.d. ±8.11), then in locations 1 – 3 differences are quite similar, in a range of 3.92 %RH (std.d. ±2.81) to 7.95 %RH (std.d. ±1.44). During cold period highest difference is in L3, 15.18 %RH (std.d. 3.87) and in L4, 6.32 %RH (std.d. 8.09). Only minor differences in location 2, 0.92 %RH (std.d. ±1.42) and in location 1, 0.78 %RH (std.d. ±2.81).

In general, relative humidity varies from 15 to 95 %RH, where the highest and lowest RH is reached by location 4. Lowest RH is gained during April to June and highest, during June to October. Relative humidity in location 4, exceeds 80 %RH almost all the experiment time, except during month of May.

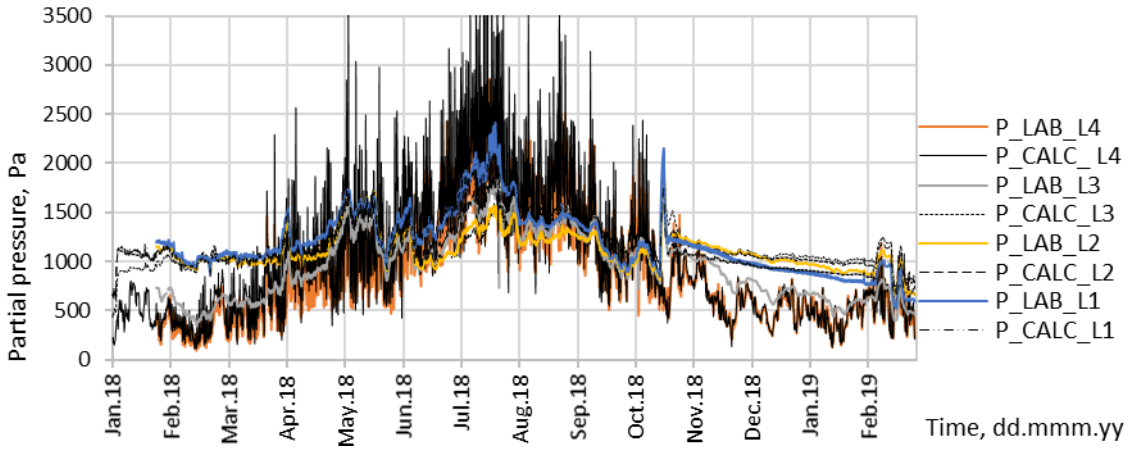

Figure 76. Partial pressure at locations 1-4, EW 3.2_S (Author's illustration)

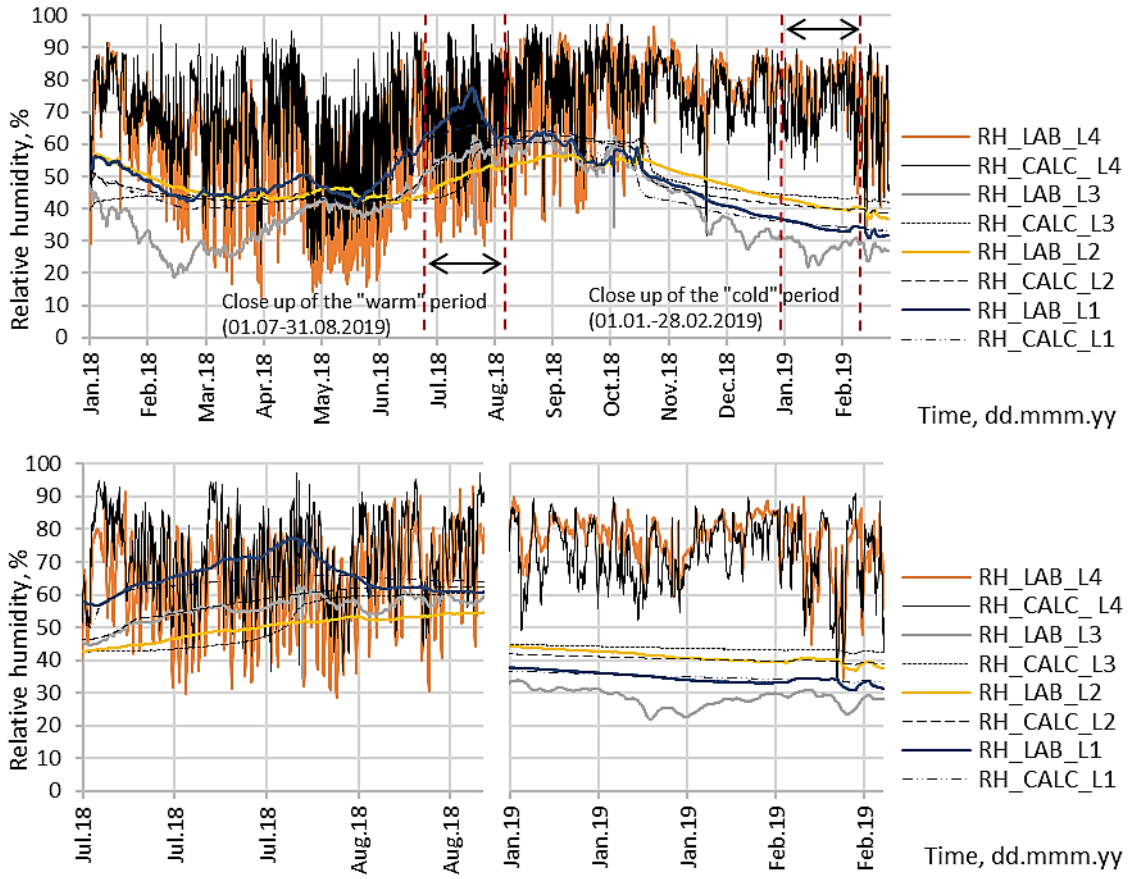

Figure 77. Relative humidity at locations 1-4, EW 3.2_S (Author's illustration)

Figure 78 shows results of heat flux, where the calculated values vary more than measured, but the average calculated q value of 2.55 W/m^2 (std.d. ±2.46) is slightly lower than for other wall types. Average value of measured q is almost 2 times smaller, 1.38 W/m^2(std.d. ±1.28) Average difference between calculated and measured data is 1.61 W/m^2 (std.d. ±1.98). When considering thermal transmittance values, measured value of 0.26 W/m^{2}K (std.d. ±0.66) is closer to estimated value (0.09 W/m^{2}K), while the calculated value is even higher, 0.37 W/m^{2}K (std.d. ±0.85).

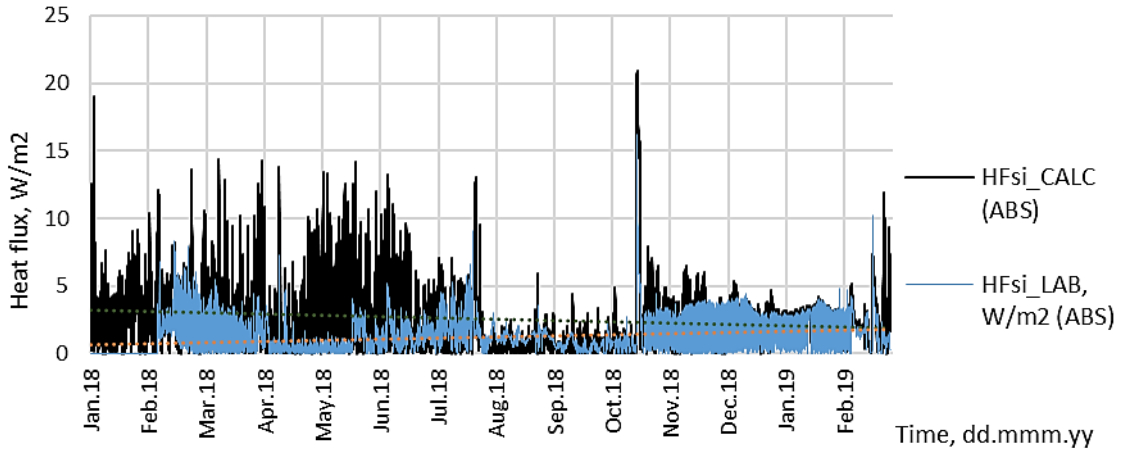

Figure 78. Heat flux at EW 3.2_S (Author's illustration)

4 DISCUSSION

4.1 Field measurements

When looking at the measured results, in all of the tested wall types, the critical location for mould growth risk was in location 4, which is located between the insulation and wind barrier, from all locations, placed the most towards outdoor environment.

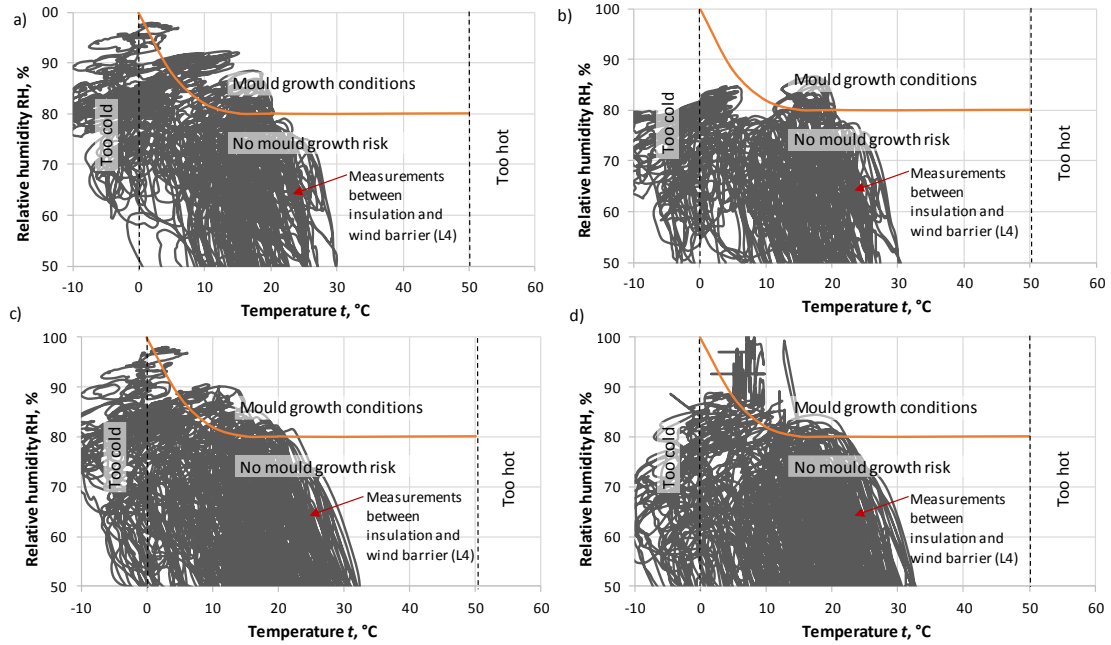

Figure 79. RH and T results for mould growth conditions of test walls with mineral wool insulation and with initially higher MC on North side EW 1.1_N (a), initially lower MC on North side EW 1.2_N (b), with initially higher MC on South side EW 1.1_S (c), initially lower MC on South side EW 1.2_S (d). (Author's illustration)

Starting with the walls of type 1, insulated with mineral wool, the critical location 4 results of RH and T are showed in *Figure 79*. There is a possible risk of mould growth as it exceeds the critical RH in all 4 kinds of walls of this type. The smallest risk is in wall EW 1.2_N (b), which has a lower initial MC. On South side the risk is not smaller for EW 1.2_S (d), which means that the initial MC effect on lower mould growth risk is only for Northern walls. When compared from North to South side, mould growth risk possibilities are basically the same, only slightly smaller for Southern walls. However, mineral wool as a material is considered medium resistant to mould growth, which can still decrease the risk.

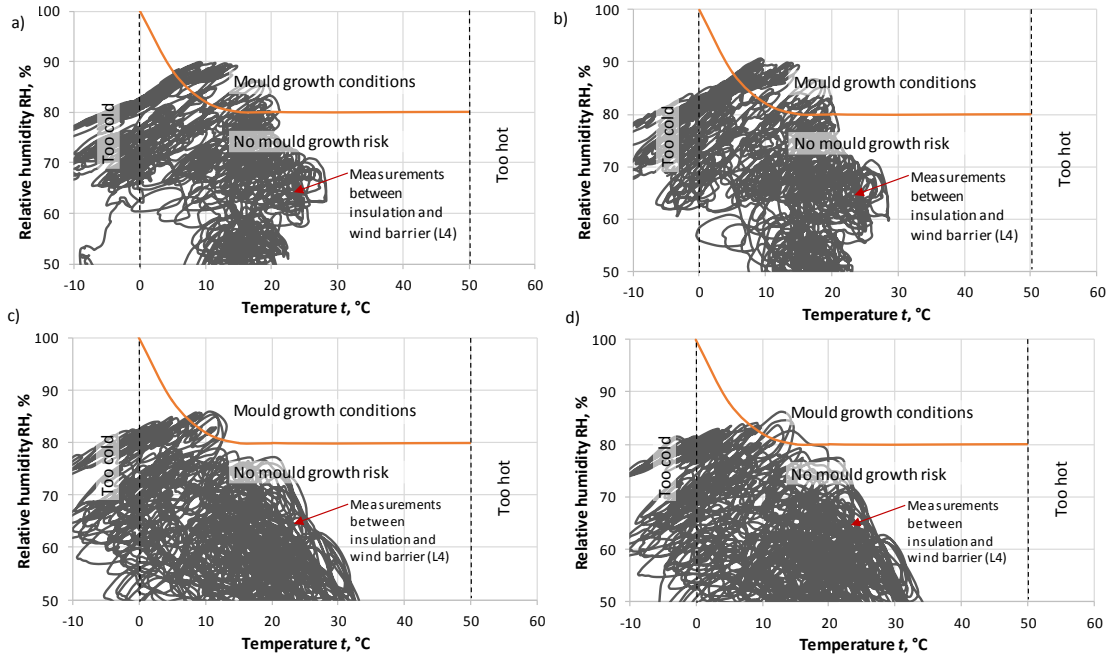

Figure 80. RH and T results for mould growth conditions of test walls with cellulose insulation and with initially higher MC on North side EW 2.1_N (a), initially lower MC on North side EW 2.2_N (b), with initially higher MC on South side EW 2.1_S (c), initially lower MC on South side EW 2.2_S (d). (Author's illustration)

When analysing walls of type 2, insulated with cellulose insulation, results are given in *Figure 80*. Generally, the results are already better than for wall type 1. In this type of walls, relation of placement on either North or South side is obvious, where the mould growth risk on EW 2.1_S (c) and EW 2.2_S (d) is much smaller than for Northern side walls. However, effect of higher or lower initial MC cannot be observed as in-between both Southern or both Northern walls risk of mould growth is the same.

Results of wall type 3, insulated with PIR insulation are showed in *Figure 81*, where the risk of mould growth is the highest, as the points above critical line are concentrated and exceed even 90 %RH. When RH reaches up to 100 %, water vapour condensates.

In general, the risk of mould growth is very similar in all 4 kinds of the walls, the only difference, with an extremely high RH is in EW 3.2_N (b). This can only show a relation that walls on South side has less of mould growth risk than walls on North, however, for EW 3.1_N (a), EW 3.1_S (c) and EW 3.2_S the risk is the same. Factor of initial MC does not give any effect, what is more, for Northern walls it is even the opposite, where wall with lower initial MC (EW 3.2_N) has a higher risk.

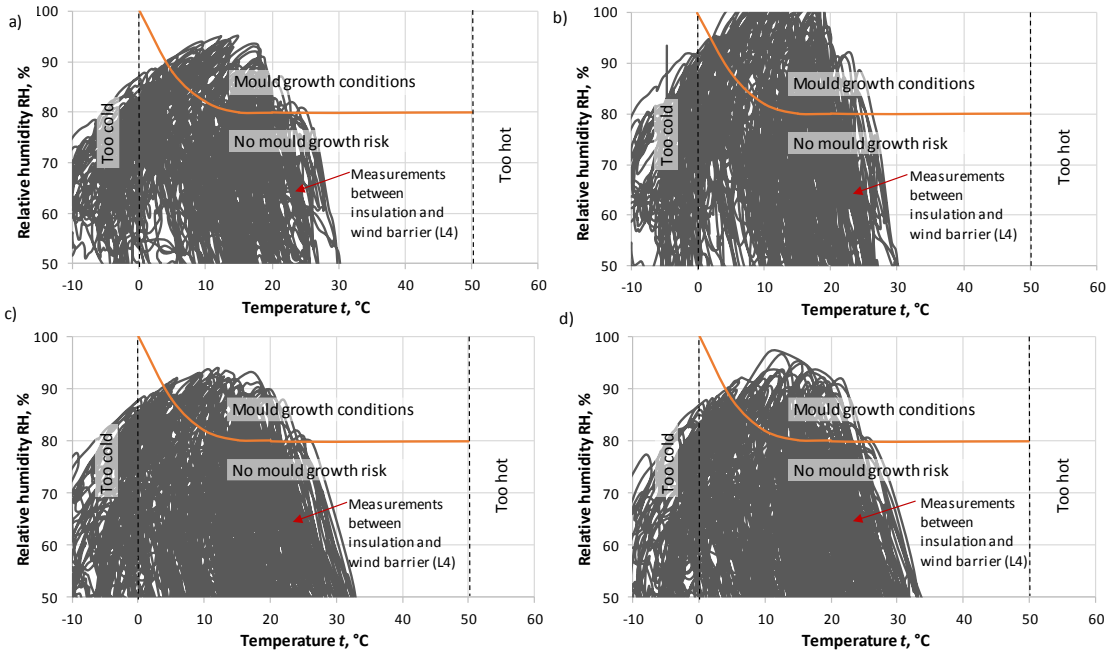

Figure 81. RH and T results for mould growth conditions of test walls with PIR insulation and with initially higher MC on North side EW 3.1_N (a), initially lower MC on North side EW 3.2_N (b), with initially higher MC on South side EW 3.1_S (c), initially lower MC on South side EW 3.2_S (d). (Author's illustration)

To sum up the results of critical conditions for mould growth risk in all 3 types of walls, least of the risk is in wall type 2, insulated with cellulose insulation, where there were least of measurement points above the critical line. Besides that, walls of this type, placed on Southern side, act better and shows lower RH. In this wall type the placement on South side was most visible.

Nevertheless, cellulose insulation is considered as most sensitive for mould growth, where the mineral wool (type 1) is medium resistant and PIR (type 3) is resistant (Viitanen, Ojanen and Peuhkuri, 2011).

Another important aspect to consider is moisture storage capacity of insulation materials, which shows how much moisture can be bound in pore structure of material. In this case one of the reasons why the walls of type 2 showed least favourable conditions of mould growth is the high moisture storage capacity of cellulose insulation, $6.33 \cdot 10^{-3}$ m^3/m^3, which is higher than the values for mineral wool or PIR *(see Table 3)*. This accordingly means that during the dry out of CLT panel, cellulose insulation can store more moisture in short time period and slows down the dry-out process, which leads to lower RH between insulation and wind barrier (L4) and thereby decreases risk of high humidity which also can be observed in results.

Same, but slightly higher mould growth risk than for type 2, is in wall type 1, insulated with mineral wool. Here could be observed the logic of the higher initial MC, although only on

Northern walls where the walls with smaller initial MC gave better results, but placement either on Northern or Southern side did not give any effect.

The highest risk of mould growth was in wall type 3, insulated with PIR, showing the most measurement points above critical line in all 4 kinds of walls compared to type 1 and 2. Besides that, even the higher MC did not seem to affect the results anyhow, as the wall 3.2_N (lower MC) had higher risk than for wall 3.1_N (higher MC). There is a possibility of some errors of sensors, where there was some lack of data. What is more, in practise the PIR insulation in wall assemblies usually does not require a wind barrier and is directly facing external conditions (air gap), which would decrease the risk in location 4 (between PIR and wind barrier).

Reason for initial MC not giving a considerable effect on results is that the CLT was kept open to internal side (indoor environment), which provided a sufficient dry out also towards indoors.

Although this data gives insight on how the moisture behaves in a wall structure and when the mould growth risk could start, the results and assumptions still have to be further investigated to evaluate a certain risk of mould growth, considering material sensitivity and exposure time using VTT mould growth model.

When compared to findings of similar researches, there can be drawn some parallels with their results. First passive house in Estonia was made using wall construction of CLT block elements, cellulose insulation, wind barrier and internal and external plastering. Results showed that similarly as in our research, critical location was between insulation and wind barrier, where RH exceeded 80 % and the dry out of CLT panel was prevented by wood fiber sheeting board as a wind barrier. This caused condensation and favourable conditions for mould growth, which, based on VTT mould growth model, reached index value near 3, meaning that some mould growth could be detected visually, possibly forming new spores. (Kalamees *et al.*, 2014)

Another experiment was done using CLT wall panels (13 % or 20 % initial MC), mineral wool insulation and wind barrier on outer side and either glass wool or PIR insulation used on interior side of CLT panel. For both construction types, the critical point in the wall structure was between interior insulation and CLT panel, especially for walls using CLT with higher initial MC. Moisture movement by CLT dry out was towards indoors, where the moisture accumulated before the interior insulation. Similar as in our research, higher risk was caused in walls using PIR as insulation, as it has higher vapour diffusion resistance and it prevents moisture movements. (Kukk *et al.*, 2019)

Experiment done with MHM nailed wood panels, having a wall construction of gypsum board, MHM panel, air and vapour tight membrane, mineral wool insulation and ETICS silicone resin plaster placed in external wall for a period of 1 year, showed no risk of mould growth. As the most critical locations were considered the ones between membrane and MHM panel and

between the plaster and mineral wool, no critical RH was reached as the walls dried out on the interior side and the membrane helped to keep the insulation dry from interior side. (Kukk, Kers and Kalamees, 2019)

When compared with other researches, it can be concluded that often the critical location in wall structure is between outer insulation and wind barrier, where the moisture accumulates and can cause a mould growth. When using an insulation layer on interior side, critical location moves to point between CLT panel and internal insulation, especially for PIR insulation, which, the same as in our experiment, gave the highest risk for mould growth. (Kukk *et al.*, 2019) What is more, influence of initial MC of CLT panel can be observed, when using CLT panels that have been in contact with water leakages or rainwater during construction, especially when being covered with additional internal layers, in this way also increasing risk of mould growth.

4.2 Simulations

To compare the calculated data from simulations to actual measurements, the highest differences are in results of partial pressure, relative humidity and heat flux. The most problems were usually caused by locations 2, 3 and 4, where the location 4 followed the fluctuations the best, while the calculated values of locations 2 and 3 usually were more stable than measurements. Least of differences were usually in location 1, which is the most inner location and least affected by outdoor conditions.

When comparing different types of walls, least of differences were in types 1 and 2, insulated with mineral wool or cellulose, accordingly. However, for some walls the differences were higher (EW 1.1_N; EW 1.2_N; EW 2.2_N; EW 2.1_S) and for some, the differences were only minor and they can be used for validation (EW 1.1_S; EW 1.2_S; EW 2.1_N; EW 2.2_S).

The differences were caused by many uncertainties:

1) Different material properties from calculations to real life, where in simulation model there were added properties of a solid wood and separate properties of adhesive, which can be different from actual CLT characteristics.
2) Pressure difference from indoors to outdoors, which was considered as 20 Pa and can cause the air and moisture movements through the wall. However, the measurement of pressure was held only for a short period of time in the second part of experiment and we did not know the pressure difference for the whole experiment time. By adding pressure difference in calculation models, there were gained less differences in results, which also proves that pressure difference existed.

3) Size of gaps between plywood frame around wall and CLT, where the vapour could also go through. Uncertain size of this gap in each wall assembly also explains why the measurements of air permeability showed different results for each wall.

The highest differences were in wall type 3, insulated with PIR, where the average differences between measured and calculated results were much higher than for wall types 1 and 2. This, however, can be also related to some errors of sensors and lack of data. To explain possible reasons for differences, additionally to uncertainties explained before, for this wall assembly the PIR insulation is almost 2 times more water vapour resistant than the surrounding film faced plywood frame around the wall. That is why vapour diffusion tries to find ways how to get out faster, why it is possible that the movement was not only through the insulation, but also by the connections to wall assembly frame of plywood, which water vapour resistance is low. *(Figure 82)* This also provides a faster dry out, so the actual results show lower partial pressure of water vapour than the calculations, which considers only one way of dry out. In order to prevent that, at the time of wall construction there were installed airtight tapes around all perimeter of the frame, but that, as results show, did not work properly and made some air leakages. Also, the properties of materials might have been different from simulations to real life, where the PIR actually had lower vapour diffusion resistance than in calculations and let the vapour move out faster.

If the water vapour movement concerns more the results of location 3, the differences in L2 in all types of walls can be explained also by not knowing an exact position of sensor, where measurement point was supposed to be exactly in the middle of CLT panel, but in real life it could be slightly to one or another side, as there was drilled a hole in the panel.

As the models of wall types 1 and 2 are more acceptable for further use in independent modelling, models of wall type 3 have to be further developed, adjusting some material properties and parameters in order to gain results as close as possible to measurements.

At first the calculated results were gained by 1D simulation, where the difference in L3 was even higher and more influenced by outdoor environment. What is more, there was a pressure difference from outdoors to indoors, which also causes the air movement through the wall.

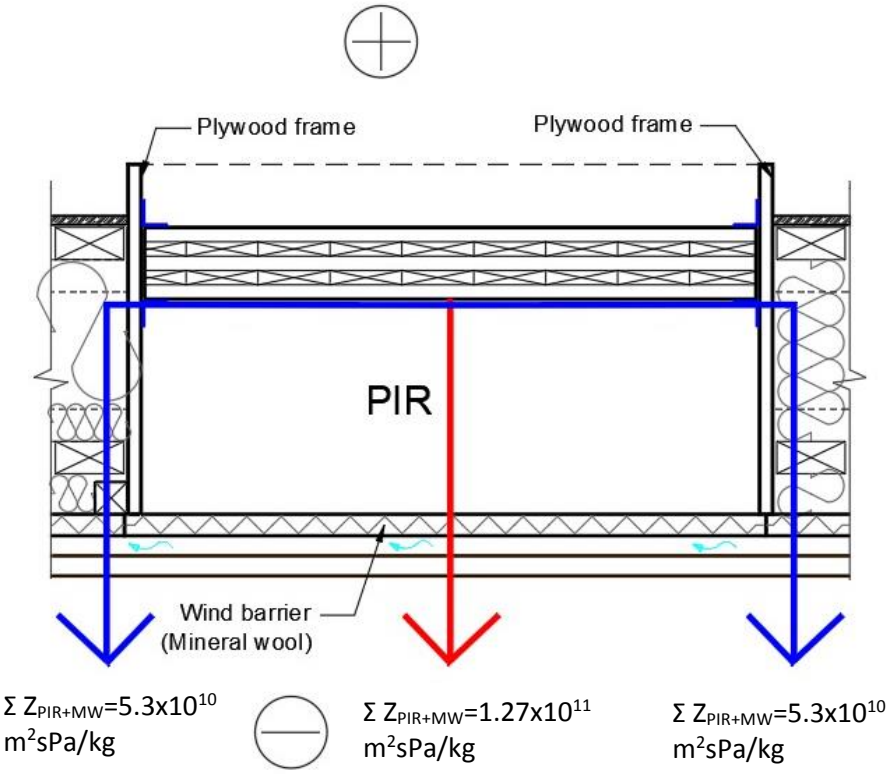

Figure 82. Scheme of water vapour movement through wall assembly and through surrounding plywood frame with a lower resistance in wall type 3. (Adapted illustration from V.Kukk)

4.3 Improvement of flaws

During the experiment there were observed several flaws. For the purposely moisturized CLT panels, the MC was only measured by weighting, not by actual measurements in different layers of CLT, in this way gaining only an overall MC based on weight. The moisture in panel does not distribute equally and the MC can vary from layer to layer, where the outer layers can differ from the core of panel. That is why the measurements should be done by a moisture meter and in different layers.

Another improvement would be having a larger size of test walls, which would give better and more objective results, as there is a larger surface to investigate and errors like air gaps by connection to frame would affect less. There would be also a possibility to insert MC sensors in each layer of CLT which would give more data, and ability to see the moisture distribution in CLT panel. Besides, that would be closer to real life situation, as it is used in external walls.

Another suggestion for further research would be to do a separate experiment to describe moisture distribution in CLT panel during exposure to liquid water. This would be preferred in order not to harm the existing walls by adding additional sensors.

CONCLUSION

Field measurements were analysed by critical RH above 80% and temperature higher than 0°C at the same time, which are the favourable conditions for mould growth. Risk of mould growth was observed in all tested walls, having the critical location at L4, which is between insulation and wind barrier. Presence of a higher initial MC did not give any considerable effect, as the CLT panels were not covered from interior side and provided a dry-out towards indoors. The placement on Southern side gave better results only for walls of type 2 (cellulose insulation), where was also the least of mould growth risk compared to the other wall types. This can be explained by moisture storage capacities of insulation materials, where the cellulose had the highest moisture storage capacity compared to mineral wool or PIR and it provided a slower dry out, which leads to lower RH values in a short period of time and least favourable conditions for mould growth. The highest risk was in wall type 3 (PIR insulation) where all walls showed high risk of mould growth, which can be explained by a dry-out only towards indoor environment as the PIR insulation has a high water vapour resistance. Nevertheless, in practice the PIR usually does not require an additional wind barrier, which would eliminate the critical location between PIR and wind barrier. However, these assumptions still have to be further investigated by mathematical mould growth model, considering material sensitivity classes and exposure time.
When the results of calculated and measured data were compared, the least of differences were observed in graphs of temperature, while differences in graphs of P_v, RH and q, were generally higher, depending on wall type. Majority of differences were noticed in location 2-3, and the least in location 1, which is the closest to indoors. Mostly, the calculated results were higher than measured, which can point out differences in material properties, pressure difference from indoors to outdoors, gaps between CLT and the surrounding plywood frame and that the water vapour finds more ways to equalize and provides a faster dry out of CLT panel than in calculations. Overall the smallest average differences between calculated and measured data was for wall types 1 and 2, but for walls of type 3, the material properties still have to be adjusted, in order to use the model for independent simulations.
This study does show some results regarding possibility of mould growth and gives more knowledge of hygrothermal performance in case of the risk of mould growth in CLT wall assemblies, but the results of certain mould growth risk are still not complete and have to be further investigated.
As this study is only a part of a bigger research, and there are more wall types and parameters to analyse, this project will be continued and more certain results will be gained.

SUMMARY

As CLT is a comparatively new material, its performance in constructions still needs to be investigated, especially considering its hygrothermal performance, as by a certain arrangement of relative humidity, temperature and oxygen supply favourable conditions for mould growth are gained. As the wood gains moisture faster than it loses it, the crucial part to consider is the dry out of the panel in a wall assembly. Presence of adhesive in CLT material affects its properties insignificantly.

CLT panels are a good competitor for other building materials and can be used in various kinds of buildings, providing a good bending and shear strength and a dimensional stability, at the same time being light weight. One of the applications for these panels can be Nearly Zero Energy buildings (NZEB), where by adding insulation, an acceptable thermal transmittance value can be achieved.

There were tested 3 types of wall assemblies with different insulation types, different initial MC (11-14 % or 25-27 %) and a placement in building. Hygrothermal performance was analysed through parameters of temperature, water vapour partial pressure, relative humidity and heat flux. Field measurements were gained by sensors, fixed either in between materials or on internal or external surfaces. Test walls were placed in a NZEB in Tallinn, Estonia and measurements were held for 13 months.

Based on field measurements there were made computer simulation models for each wall and the data was compared to measured results. When realising certain flaws, such as air gaps and pressure difference from indoors to outdoors, there were made 2D models which considered air and moisture movements in vertical and horizontal directions.

Field measurements showed a risk of mould growth in all tested walls in a critical location between insulation and wind barrier. Higher initial MC did not give any considerable effect, while the placement on Southern side gave better results only for wall type 2 (cellulose), where generally was also the least of mould growth risk, explained by a high moisture storage capacity of cellulose. The highest risk was in wall type 3 (PIR) because of a CLT dry-out only towards indoors as the water vapour resistance of PIR is high.

Comparison of calculated and measured data gave highest differences in locations 2 and 3, where the calculated results were mostly higher than measured. Generally, the smallest average differences were observed in wall types 1 and 2, while the simulation models of wall type 3 still need to be developed.

KOKKUVÕTE

Ristkihtliimpuit on suhteliselt uus ehitusmaterjal, mille omadused ehituses vajavad endiselt veel uurimist. Uurmist vajab eriti ristkihtliimpuidu hügrotemriline jõudlus, kuna piisava suhtelise õhuniiskuse ja temperatuuri juures konstruktsioonis tekib soodne keskkond hallituse tekke ohuks. Puit talletab niiskust kiiremini kui see jõuab välja kuivada, seega niiskustehnilise seisukohalt osutub määravaks paneeli välja kuivamise võimekus hoone piirdes. Liimikihi mõju paneeli hügrotermilistele omadustele on väike.

Ristkihtliimpuit pakub võrdväärset konkurentsi sarnastele ehitusmaterjalidele (teras, betoon) ja seda saab kasutada mitmesuguste hoonete ehitamiseks tagades seejuures kandevõime ja mõõtmete stabiilsuse ning samas on tegu kerge materjaliga. Tänu puidu suurele soojustakistusele on ristkihtliimpuitu hea kasutada ka liginullenergiahoonete ehitamisel.

Antud lõputöö raames uuriti kolme erinevat tüüpi ristkihtliimpuidust välisseina, erinevate soojustusmaterjalidega, erineva paneelide algniiksuega (11-14 % ja 25-27 %) ja seinte erineva asukohaga (lõuna ja põhja poolse asetusega). Uuritud välisseinte hügrotermilist jõudlust hinnati mõõdetud temperatuuri, veeauru osarõhu, suhtelise õhuniiksuse ja soojusvoo abil. Välimõõtmised teostati andurite abil, mis paigaldati nii välisseinte materjalide kihtide vahele kui ka seinte pindadele. Välisseinad paigaldati Tallinna Tehnikaülikooli Liginullenergia testhoonesse ja mõõtmisi teostati kogu pikkusega 13 kuud.

Välimõõtmiste tulemuste põhjal koostati arvutusmudel iga uuritud välisseina kohta ja tulemused valideeriti võrreldes mõõte- ja arvutustulemusi. Tulemuste analüüsi käigus leiti mõningaid vigu, mis katse käigus esines, näiteks mitte õhupidavad ühendused ristkihtliimpuitpaneeli ja katseraami vahel ja suur sise- ja väliskeskkonna õhurõhu erinevus, mida katse käigus ei mõõdetud. Antud vigade arvesse võtmiseks koostati kahe dimensioonilased arvutusmudelid, mis võimaldas arvestada võimalike õhuleketega välisseintes.

Välimõõtmised näitasid, et võimalik hallituse oht esines kõigis uuritud välisseintes ja uuritud kriitiliseks asukohaks oli soojustuse ja tuuletõkke vaheline ala. Kõrgem paneelide algne niiskussisaldus ei näidanud märkimisväärset mõju hallituse ohu tekkimisele, küll aga oli mõju seinte asukohtades. Lõuna ilmakaare suuna asetatud seintes oli hallituse oht väiksem, seda eriti tselluvillaga soojustatud välisseintes. Tselluvilla soojustusega välisseintes esines üleüldiselt väikseim hallituse tekkerisk, mida võib seletada tseluvilla kõrge niiskuse salvestusvõimekusega. Suurim risk esines polüisotsüanuraat (PIR) soojustusega välisseintes, kus niiksus sai välja kuivada ainult sisse poole.

Võrreldes mõõtmis- ja arvutustulemusi, suurim erinevus esines asukohtades paneeli keskel ja soojustuse ning paneeli vahel (asukohad 2 ja 3), kus arvutustulemused hindasid olukorda kõrgema niiskuse ja temperatuuriga. Üleüldiselt sarnanesid tulemused hästi esimese ja teise välisseina tüübi korral, kolmanda välisseina tüübi arvutusmudelit tuleb edasi täiendada.

LIST OF REFERENCES

AlSayegh, G. (2012) *Hygrothermal Properties of Cross Laminated Timber and Moisture Response of Wood at High Relative Humidity*.

Ansell, M. P. (2015) *Wood Composites*, *Composites*. Edited by M. P. Ansell. Elsevier Science & Technology. doi: 10.1016/0010-4361(80)90419-X.

Arumägi and Kalamees (2016) 'Design of the first net-zero energy buildings in Estonia', pp. 1039–1049.

Asaee, S. R., Ugursal, V. I. and Beausoleil-Morrison, I. (2019) 'Development and analysis of strategies to facilitate the conversion of Canadian houses into net zero energy buildings', Energy Pol.

Bucur, V. (ed.) (2011) *Delamination in Wood, Wood Products and Wood-Based Composites*. Dordrecht: Springer Netherlands. doi: 10.1007/978-90-481-9550-3.

Byttebier, M. (2018) 'Hygrothermal performance analysis of cross-laminated timber (CLT) in Western Europe'.

D'Agostino, D. and Parker, D. (2019) 'A framework for the cost-optimal design of nearly zero energy buildings (NZEBs) in representative climates across Europe', (Energy 149), pp. 814–829.

Domone, P. L. J. and Illston, J. M. (2010) *Construction materials : their nature and behaviour*. Spon Press.

Espinoza, O. *et al.* (2016) 'Cross-laminated timber: Status and research needs in Europe', *BioResources*, 11(1), pp. 281–295. doi: 10.15376/biores.11.1.281-295.

Estonian Centre for Standardisation (2015) 'EVS-EN 16351_2015_Timber structures-Cross laminated timber- Requirements.pdf'. Estonian centre for Standardisation, p. 108.

Gagnon, S., Pirvu, C. and FPInnovations (Institute) (2011) *CLT handbook : cross-laminated timber*. FPInnovations.

Glass, S. V. and Zelinka, S. L. (2010) 'Chapter 4: Moisture Relations and Physical Properties of Wood', *Wood Handbook - Wood as an Engineering Material. General technical report FPL: GTR-190*, 190, pp. 4.1-4.19. Available at: http://www.fpl.fs.fed.us/products/publications/specific_pub.php?posting_id=17964&header_id=p.

ISO 15148 (2002) *International Organization for Standardization (ISO 15148).*

'Hygrothermal Performance of building materials and products - Determination of water absorption coefficient by partial immersion', International Organization for Standardization, Geneva, Switzer. Available at: https://www.iso.org/standard/26500.html (Accessed: 23 February 2019).

Kalamees, T. *et al.* (2014) 'The first year's results from the first passive house in Estonia', *Proceedings of the 10th Nordic Symposium on Building Physics*, pp. 758–765.

Karacabeyli, E. and Douglas, B. (2013) *Hand book cross laminated timber*, *Book*. doi: 10.1017/CBO9781107415324.004.

Karamanos, A., Hadiarakou, S. and Papadopoulos, A. M. (2008) 'The impact of temperature and moisture on the thermal performance of stone wool', *Energy and Buildings*, 40(8), pp. 1402–1411. doi: 10.1016/j.enbuild.2008.01.004.

Van De Kuilen, J. W. G. *et al.* (2011) 'Very tall wooden buildings with Cross Laminated Timber', *Procedia Engineering*. Elsevier B.V., 14, pp. 1621–1628. doi: 10.1016/j.proeng.2011.07.204.

Kukk, V. *et al.* (2019) 'Influence of interior layer properties to moisture dry-out of CLT walls'.

Kukk, V., Kers, J. and Kalamees, T. (2019) 'Field measurements and simulation of an massive wood panel envelope with ETICS'.

Lebow, S. T. and White, R. H. (2007) 'Durability of wood in construction', *Marks' standard handbook for mechanical engineers. New York : McGraw Hill, c2007: pages 6.129-6.131.*, pp. 6.129-6.131. Available at: https://www.fs.usda.gov/treesearch/pubs/34298 (Accessed: 23 February 2019).

Louwet, D. and Tricht, J. V. (2017) *"Wat zijn de hygrothermische eigenschappen van Cross Laminated Timber in de Belgische context? (Dutch) [What are the hygrothermal properties of Cross Laminated Timber in the Belgian context]"*.

McClung, R. *et al.* (2014) 'Hygrothermal performance of cross-laminated timber wall assemblies with built-in moisture: Field measurements and simulations', *Building and Environment*. doi: 10.1016/j.buildenv.2013.09.008.

Official Journal of the European Union (2010) *DIRECTIVE 2010/31/EU OF THE EUROPEAN PARLIAMENT AND OF THE COUNCIL on the energy performance of buildings*.

Radu, A. *et al.* (2012) 'Heat , Air and Moisture Transfer Terminology Parameters and Concepts', p. 50.

Raji, S. *et al.* (2009) 'Thermophysical characterization of a laminated solid-wood pine wall', *Construction and Building Materials*, 23(10), pp. 3189–3195. doi:

10.1016/j.conbuildmat.2009.06.015.

Reinberg, G. W. *et al.* (2013) 'First Certified Passive House in Estonia.', in *Proceedings of 17th International Passive House Conference*.

Republic of Estonia Ministry of Economic Affairs and Communications (2015) *Energy performance of buildings*. Available at: https://www.mkm.ee/en/objectives-activities/construction-and-housing-sector/energy-performance-buildings (Accessed: 31 March 2019).

Republic of Estonia Ministry of Economic Affairs and Communications (2018) *Minimum energy performance requirements for a building (Hoone energiatõhususe miinimumnõuded – Riigi Teataja)*. Estonia. Available at: https://www.riigiteataja.ee/akt/113122018014 (Accessed: 31 March 2019).

Sandberg, I. (2009) 'Effect of Moisture on the Thermal Performance of Insulation Materials', in *Moisture Control in Buildings: The Key Factor in Mold Prevention—2nd Edition*. 100 Barr Harbor Drive, PO Box C700, West Conshohocken, PA 19428-2959: ASTM International, pp. 38-38–16. doi: 10.1520/MNL11543M.

Sankelo, P. *et al.* (2019) 'Cost-optimal energy performance measures in a new day care building in cold climate', Int. J. Su, pp. 104–122.

Sonderegger, W. *et al.* (2010) 'Quantitative determination of bound water diffusion in multilayer boards by means of neutron imaging', *European Journal of Wood and Wood Products*, 68(3), pp. 341–350. doi: 10.1007/s00107-010-0463-5.

Viitanen, H. (2007) 'Improved Model to Predict Mold Growth in Building Materials', *Buildings X*, pp. 1–8.

Viitanen, H., Ojanen, T. and Peuhkuri, R. (2011) 'Mould growth modelling to evaluate durability of materials', *Proceedings of the 12DBMC - International Conference on Durability of Building Materials and Components*, pp. 1–8. Available at: http://www.irbnet.de/daten/iconda/CIB22377.pdf.

Volkmer, T. *et al.* (2012) 'Untersuchungen zum Einfluss der Klebstoffart auf den Diffusionswiderstand von Holzverklebungen', *Bauphysik*. John Wiley & Sons, Ltd, 34(2), pp. 55–60. doi: 10.1002/bapi.201200006.

Wood and Moisture | The Wood Database (no date). Available at: https://www.wood-database.com/wood-articles/wood-and-moisture/ (Accessed: 24 February 2019).

Wu, Y. (2007) *Experimental Study of Hygrothermal Properties for Building Materials*.

Zillig, W. (2009) *Moisture transport in wood using a multiscale approach*.

APPENDICES

Appendix 1 – Graphs of MC change in walls

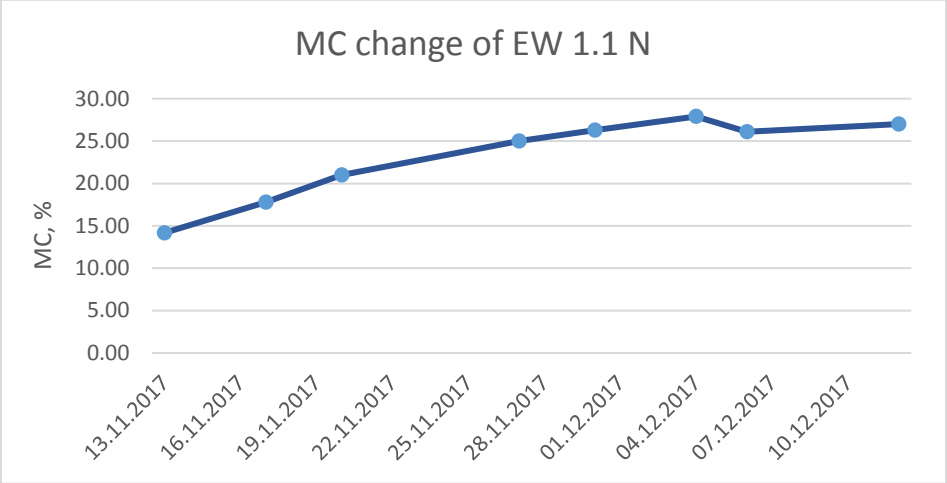

Figure 83. MC change of EW 1.1 N (Author's illustration)

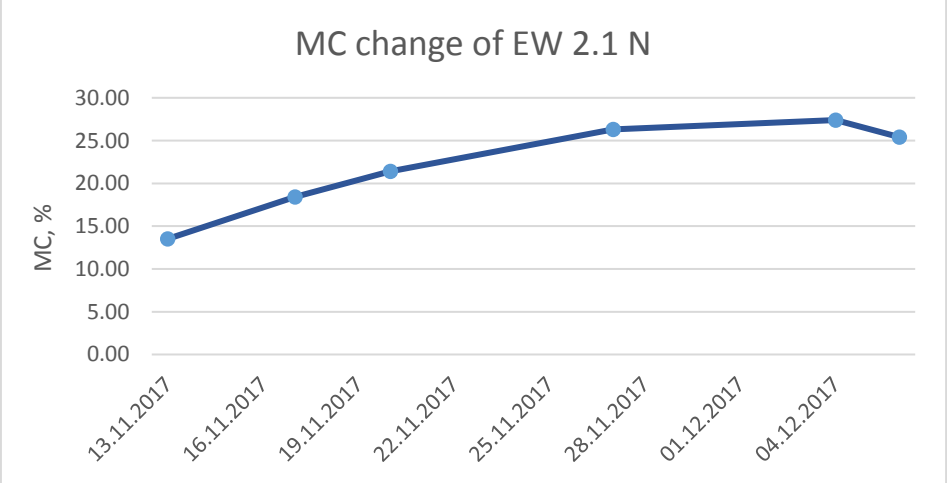

Figure 84. MC change of EW 2.1 N (Author's illustration)

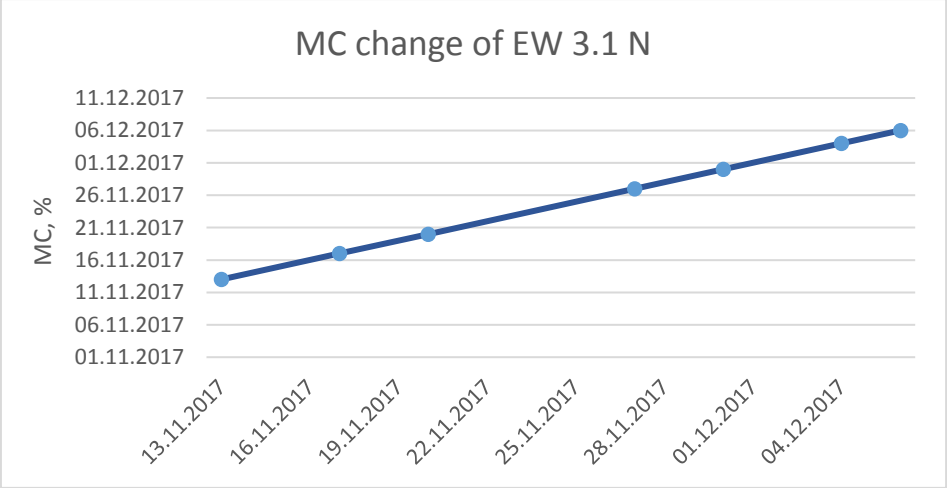

Figure 85. MC change of EW 3.1 N (Author's illustration)

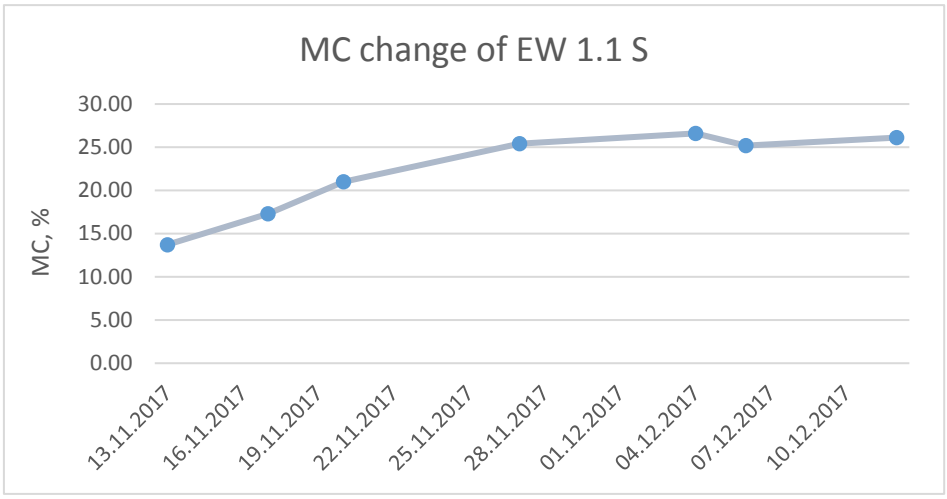

Figure 86. MC change of EW 1.1 S (Author's illustration)

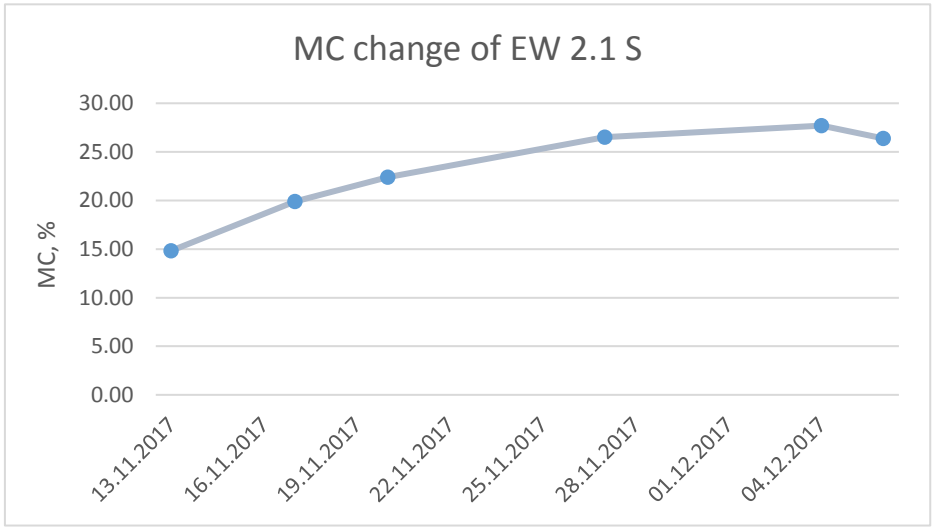

Figure 87. MC change of EW 2.1 S (Author's illustration)

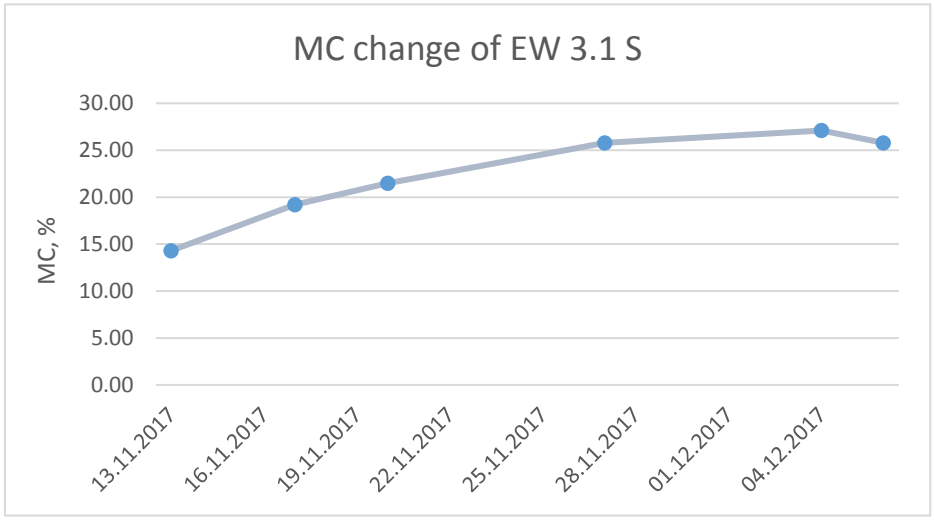

Figure 88. MC change of EW 3.1 S (Author's illustration)

Appendix 2 – Tables of differences

Table 4. Differences between calculated and measured data in wall type 1.

Wall, location	Average differences (Ave. diff. ± std. dev.)			
EW 1.1_N	T, °C	P_v, Pa	RH, %	q, W/m^2
L1	0.68±0.37	215.74±204	7.98±7.43	1.88±1.27
L2	0.84±0.36	215.96±267	8.57±10.32	
L3	1.41±0.53	114.71±83	3.91±3.05	
L4	1.56±0.68	104.06±114	8.73±6.23	
EW 1.2_N				
L1	0.49±0.27	89.96±81	3.41±2.84	1.95±2.41
L2	0.28±0.29	217.88±115	9.42±3.94	
L3	0.5±0.34	110.35±79	4.77±3.63	
L4	1.06±0.47	118.33±125	6.77±6.47	
EW 1.1_S				
L1	0.27±0.28	131.84±118	5.25±2.84	1.52±1.97
L2	0.35±0.29	162.85±140	6.70±4.19	
L3	0.55±0.36	143.41±107	6.06±4.69	
L4	1.3±0.65	156.69±189	8.54±5.98	
EW 1.2_S				
L1	0.81±0.37	160.69±76	7.41±2.02	1.84±2.01
L2	0.94±0.43	158.41±102	7.99±2.44	
L3	1.06±0.48	199.16±145	6.45±4.44	
L4	1.19±1.01	201.64±217	9.73±6.94	

Table 5. Differences between calculated and measured data in wall type 2.

Wall, location	Average differences (Ave. diff. ± std. dev.)			
EW 2.1_N	T, °C	P_v, Pa	RH, %	q, W/m^2
L1	0.39±0.31	130.36±139	5.40±4.59	1.89±2.22
L2	0.51±0.36	108.24±127	5.31±3.75	
L3	0.96±1.03	94.20±70	3.86±3.11	
L4	1.28±0.59	89.90±102	5.44±4.39	
EW 2.2_N				
L1	0.57±1.62	164.03±235	3.97±4.31	1.95±2.54
L2	1.00±1.40	134.21±100	7.28±4.16	
L3	1.30±1.92	104.84±118	5.81±4.79	
L4	0.52±0.36	79.23±89	6.19±5.93	
EW 2.1_S				
L1	0.22±0.28	104.13±129	3.80±2.96	1.65±1.87
L2	0.51±0.34	148.63±130	5.63±2.64	
L3	1.10±0.44	573.52±216	5.62±4.32	
L4	1.07±0.92	200.07±224	8.81±6.40	

EW 2.2_S				
L1	0.56±0.31	119.14±80	4.49±3.52	1.71±1.92
L2	0.73±0.31	146.88±81	7.11±2.19	
L3	0.98±0.88	191.87±90	6.50±3.79	
L4	1.00±0.55	188.30±205	8.75±6.11	

Table 6. Differences between calculated and measured data in wall type 3.

Wall, location	Average differences (Ave. diff. ± std. dev.)			
EW 3.1_N	T, °C	P_v, Pa	RH, %	q, W/m^2
L1	0.68±0.35	194.80±161	7.23±4.91	1.92±2.37
L2	1.42±0.58	438.71±210	12.93±5.68	
L3	1.63±0.64	682.16±279	22.64±10.96	
L4	1.13±0.37	125.90±147	7.83±6.71	
EW 3.2_N				
L1	0.33±0.30	158.47±147	5.95±5.25	1.93±2.39
L2	0.41±0.28	128.95±114	5.38±3.72	
L3	1.05±0.49	249.24±147	15.60±43.71	
L4	0.60±0.31	118.24±135	9.62±8.02	
EW 3.1_S				
L1	0.92±0.35	121.34±118	3.26±2.76	1.57±1.90
L2	1.18±0.49	225.40±123	4.92±2.32	
L3	1.67±0.78	790.97±337	27.94±12.53	
L4	1.00±0.47	178.96±224	9.88±7.32	
EW 3.2_S				
L1	0.73±0.29	73.12±75	3.29±2.11	1.61±1.98
L2	1.02±0.48	100.21±101	3.91±2.75	
L3	1.00±0.48	265.47±155	8.73±6.11	
L4	0.75±0.52	197.36±249	10.15±8.08	

Appendix 3 – List of terms

Definitions based on *Heat, Air and Moisture transfer terminology by Radu et.al.* (2012)

Adsorption – process when moisture is added or absorbed in material until steady state is reached.

Air Permeability – The density of air flow rate per unit gradient of air pressure in the direction of flow

Building envelope – A building element (e.g. walls, roofs) that separates the indoor environment from the outdoor environment.

Bulk density – mass divided by volume occupied by the material.

Capillary suction – result of differences in pore water pressure.

Condensation – phase change of water vapour into liquid water where the humidity by volume of air reaches the humidity by volume saturation (*RH*=100%).

Convection – moisture transfer process caused by air flows due to a difference in total pressure. Moving air always carries water vapour and may drag along water droplets or snow crystals.

Critical moisture content – Moisture content that corresponds to the lowest moisture content necessary to initiate moisture transport in liquid phase. Below this level, moisture is transported only in vapour phase.

Desorption – process when the material releases moisture to atmosphere and reaches a steady state.

Dew point temperature – temperature at which moist air becomes saturated at atmospheric pressure. Condensation occurs at any temperature below the dew point.

Diffusion – moisture transfer process occurring due to difference in vapour concentration, which results in a net transfer of water molecules to the region with the lowest concentration.

Equilibrium moisture content – moisture level in wood, where wood neither gains nor loses moisture, as it is in equilibrium with relative humidity of surrounding environment.

Fibre saturation point – point at which cell walls are completely saturated as bound water, while there is no water in cell lumen.

Gas permeability – product of the gas permeance and the perpendicular distance between surfaces of a flat layer of material.

Heat flux – rate of energy transferred through given surface.

Heat transfer – conduction – energy transferred when vibrating atoms collide and free electrons move collectively. Heat is transferred by conduction between solids at different temperature in

contact with each other, between points at a different temperature within the same solid, within fluids and in contact within fluids.

Heat transfer coefficient (U-value) **-** a rate of transfer of heat through a structure, divided by the difference in temperature across that structure.

Hygroscopic range – range of relative humidity in a material between 0 and 98% *RH.* In this range wood absorbs or desorbs water, respectively, swells or shrinks.

Moisture content – mass of water present in the open pores, divided by volume of dry material.

Moisture permeability/conductivity – ratio between the density of moisture flow rate and the suction gradient (capillary) in the direction of the moisture flow.

Moisture storage capacity – capacity of moisture amount which can be bound in pore structure of the material.

Mould index – describes the visible mould growth intensity on the surface of materials. The higher the index, more mould growth on the surface.

Relative humidity - the amount of water vapour present in air expressed as a percentage of the amount needed for saturation at the same temperature.

Thermal conductivity – material property that states its steady-state ability to conduct heat, calculated as density of a heat flow rate per one unit of thermal gradient in the direction of the flow. Its value depends on density, temperature and moisture content of the layer considered.

Thermal resistance - a value describing heat conductivity of a material, calculated as thickness divided by thermal conductivity (*λ)* of material in case the temperature is constant.

Thermal transmittance – value describing heat conductivity of a building envelope, calculated as a density of heat flow rate across a flat assembly in W/m^2, at a temperature difference of 1K between the surroundings of both surfaces. The reciprocal of the thermal transmittance is the total thermal resistance between surroundings on each side of the assembly.

Vapour barrier/retarder – material whose main function is to prevent/retard harmful diffusion of water vapour in or within a building component. It can also function as an air barrier.

Water vapour diffusion coefficient – thickness of a motionless air layer which has the same water vapour diffusion resistance as the material layer.

Water vapour partial pressure – part of the total atmospheric pressure exerted by water vapour.

Water vapour permeance – density of vapour flow rate across a layer per one unit of the vapour concentration or vapour pressure difference across the two parallel bounding surfaces under steady state conditions.

Water vapour resistance – inverse value of water vapour permeance.

Water vapour resistance factor – factor indicating how much larger the resistance of a porous material is against diffusion compared to an equally thick layer of stagnant air at the same temperature.

Wind pressure – in moisture transfer can force liquid water through cracks in the building envelope.